# MOLECULAR CHARACTERIZATION OF THE PLANT HYPERSENSITIVE RESPONSE AND MAIZE LESION MIMIC MUTANTS

by

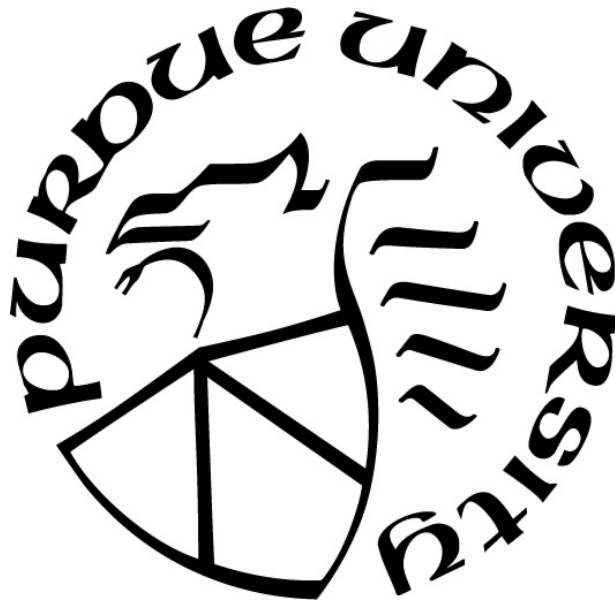**Ryan L. Benke**

**A Dissertation**

*Submitted to the Faculty of Purdue University*

*In Partial Fulfillment of the Requirements for the degree of*

**Doctor of Philosophy**



Department of Biochemistry

West Lafayette, Indiana

December 2022

# THE PURDUE UNIVERSITY GRADUATE SCHOOL
## STATEMENT OF COMMITTEE APPROVAL

**Dr. Brian Dilkes, Chair**

Department of Biochemistry

**Dr. Gurmukh Johal**

Department of Botany and Plant Pathology

**Dr. Sujith Puthiyaveetil**

Department of Biochemistry

**Dr. Joshua Widhalm**

Department of Horticulture and Landscape Architecture

**Dr. Jennifer Wisecaver**

Department of Biochemistry

**Approved by:**

Dr. Joseph Ogas

*I dedicate this dissertation to my parents, Larry and Connie Benke, and my sisters, Heidi Benke and Lori Skattum who have provided unconditional support every step of the way. In addition, I dedicate this dissertation to my loving girlfriend, Diana Salguero, who has become my rock and motivation as I complete this journey and I start my next.*

# ACKNOWLEDGMENTS

# TABLE OF CONTENTS

# LIST OF TABLES

# LIST OF FIGURES

# LIST OF ABBREVIATIONS

| | |
|---|---|
| avr | Avirulance |
| BC | Back cross |
| CC | Coiled coil |
| CCM | Chlorophyll content meter |
| DHBA | Dihydroxy benzoic acid |
| ETI | Effector triggered immunity |
| FC | Fold change |
| GWAS | Genome wide association study |
| HR | Hypersensitive Response |
| ICS | Isochorismate synthase |
| LC-MS | Liquid chromatography-mass spectrometry |
| Les | Lesion |
| LMM | Lesion mimic mutant |
| LRR | Leucine rich repeat |
| *m/z* | mass-to-charge ratio |
| NCC | Non chlorophyll containing catabolite |
| NLR | NBS-LRR |
| NBS | Nucleotide binding site |
| PAL | Phenylalanine ammonia lyase |
| PAMPs | Pathogen associated molecular patterns |
| PTI | PAMP-triggered immunity |
| ROS | Reactive oxygen species |
| SA | Salicylic acid |
| SNP | Single nucleotide polymorphism |
| TIR | Toll-interleukin receptor |
| TMV | Tobacco mosaic virus |
| VIGs | Virus-induced gene silencing |

# ABSTRACT

The rapid localized cell death at and around sites of attempted pathogen infection, termed the hypersensitive response (HR), is an immune response mechanism commonly utilized in plants. This cell death limits pathogens from accessing host nutrients which often leads to resistance. The interaction of pathogen signals and host receptors that are required for the HR are well studied; however, the processes that regulate cell death during the HR remain enigmatic. The plant lesion mimic mutants, which form spontaneous lesions and/or undergo autoactive cell death in the absence of infection or stress, are commonly used as model systems to study the HR. Some lesion mimic mutants are caused by autoactive alleles of the resistance genes that recognize pathogen signals and trigger the HR. These mutants have facilitated studies of the HR as they allow the study of the HR without the need to control for pathogen infection. Currently, the etiologies of most maize lesion mimic mutants are unknown. Lesion mimic mutants contain numerous metabolic perturbations, including the increased accumulation of salicylic acid (SA), phenylalanine, and intermediates in heme and chlorophyll biosynthesis and catabolism. Some of these perturbations are dependent on the cause of lesion formation. As such, the accumulation of any of these metabolites in a lesion mutant may infer the etiology of that mutant. This dissertation contains three projects related to the molecular characterization of HR and maize lesion mimic mutants. In the first project (Chapter 2), I compared the metabolite profile of 23 maize lesion mimic mutants. This work identified two major findings that were further explored in the other projects in this dissertation. The first major finding is that four of the 23 mutants have metabolic perturbations that are like those of the known HR lesion mutant, *Rp1-D21*. In project two (Chapter 3), I molecularly characterize, *Lesion10*, which is one of the mutants that has HR-like metabolic perturbations. Using genome-wide association studies, I identified a gene candidate that may modify *Lesion10* phenotypic severity. The second major finding from project one is that SA accumulates to higher than wild-type levels in most of the lesion mutants analyzed. In the third project (Chapter 4), I characterized how SA is synthesized in maize and if SA is necessary or sufficient for the formation of lesions during the HR in maize. Using untargeted metabolite analysis, stable isotope feedings, and enzyme assays, I provide evidence of both known SA biosynthetic pathways in maize and demonstrate that the two pathways are interdependent. In addition, I show that increased accumulation of SA is not required for the HR in maize.

# CHAPTER 1.  INTRODUCTION

## 1.1  The Hypersensitive Response

The plant hypersensitive response (HR) is the rapid localized cell death at and around sites of attempted pathogen infection, usually associated with resistance. The first descriptions of the HR were in the early 1900s (Ward, 1902; Gibson, 1904); however, the nomenclature of "plant hypersensitiveness" originated from work by Elvin Stakman in 1915, where he observed host cell death on cereal crops that were infected with *Puccinia graminis* (Elvin Stakman, 1915). The HR is a common plant defense mechanism and there are numerous studies of the HR in model systems such as *Arabidopsis thaliana* (Arabidopsis; Govrin et al., 2006; Huang et al., 2018), *Nicotiana tabacum* (tobacco; Karrer et al., 1998; Keller et al., 1999)*, and *Zea mays* (maize/corn; (Hu et al., 1998; Wang et al., 2015b; Olukolu et al., 2014).

The HR is part of a multilevel response to pathogen infection. An initial response happens at the cell surface where membrane-bound receptors recognize pathogen associated molecular patterns (PAMPs) that are specific to pathogens and foreign to the host. The detection of PAMPs by these receptors initiates a defense response known as PAMP-triggered immunity (PTI; Akira, 2009). PTI can lead to resistance (Lacombe et al., 2010; Zipfel, 2014), but does not trigger the HR. Pathogens can deliver effectors to plant cells that suppress PTI and promote pathogenesis (Akira, 2009). These effectors are recognized by host encoded resistance (R) genes, localized to the cytoplasm, which initiate an additional level of immune response called, effector-triggered immunity (ETI) which includes the HR (Akira, 2009; Balint-Kurti, 2019). The simplest model for the recognition of pathogen effectors by R genes is the "gene-for-gene" theory (Flor, 1971) in which both a host R gene and pathogen avirulance (avr) signal are necessary for the HR. If either the R gene or avr signal is mutated or missing, the HR does not initiate and disease results (Flor, 1971). The perception of avr signals by R genes can be through direct detection of proteins or components produced by pathogens or by indirect detection of host cellular changes in response to infection (Lo Presti et al., 2015).

The first R gene was cloned in 1992 (Johal and Briggs, 1992), and since then, hundreds of R genes have been identified and cloned in many plant systems (Bent, 1996; Ellis et al., 2000; Kourelis and van der Hoorn, 2018). While some R genes are associated with the HR, the

classification of R genes has been broadly applied to any genes associated with some level of resistance and is not dependent on the initiation of cell death. For example, membrane receptors that trigger PTI are often referred to as R genes (Kourelis and van der Hoorn, 2018) due to their resistance functionality (Lacombe et al., 2010; Zipfel, 2014); however, the perception of PAMPs by these receptors does not trigger cell death. The most common class of R genes associated with the HR encode proteins localized to the cytoplasm that contain both a nucleotide binding site (NBS) and leucine-rich repeat (LRR) domain, often referred to as NBS-LLR or NLR proteins. NLR proteins are further subdivided based on their N terminal structures. NLRs with toll-interleukin receptor (TIR) domains are specific to dicots, while NLRs with coiled coil (CC) domains are found in both monocots and dicots (Dangl and Jones, 2001; Balint-Kurti, 2019). These N-terminal structures play important roles in signaling the HR (Balint-Kurti, 2019; Kourelis and van der Hoorn, 2018). A surprisingly small number of NLRs, in relation to the number of detectable avr genes present across all pathogens, are present in the Arabidopsis genome (Dangl and Jones, 2001; The Arabidopsis Genome Initiative, 2000); however, some NLRs can recognize multiple avr genes (Rossi et al., 1998; Bisgrove et al., 1994).

Regulatory mechanisms controlling the HR are well studied. The HR needs to be tightly regulated as to not initiate run-away cell death (Chintamanani et al., 2010). In the absence of infection, the transcription of NLRs is low and upon infection there is a rapid increase in the expression of NLRs (Mohr et al., 2010). A common mechanism by which NLRs are regulated is intermolecular interactions between NLR domains. Expression of the N-terminal TIR or CC domains of NLRs without the corresponding NLR domains can initiate the HR (Wang and Balint-Kurti, 2015), indicating the NLR domains are inhibiting the HR functionality of the N-terminal domains. The functionality and regulation of NLRs seem to be dependent on numerous cellular proteins. NLRs are often found in oligomeric complexes with other proteins termed "helper" NLRs (Mestre and Baulcombe, 2006; Jubic et al., 2019) and these "helper" proteins are required for immunity and the HR (Wu et al., 2017).

It is still unknown how cell death initiates during HR. Multiple factors, including thermoregulation (Balint-Kurti, 2019), light dependence (Chandra-Shekara et al., 2006; Negeri et al., 2013), reactive oxygen species (ROS) formation (Delledonne et al., 2001), and the hormone salicylic acid (SA; Radojičić et al., 2018; Huang et al., 2018; Brodersen et al., 2005) have all been associated with regulation or the initiation of the HR. The mechanisms by which these factors

initiate cell death during the HR have not been fully demonstrated. As such, it still remains enigmatic if any of these factors are required for the HR.

In this dissertation, I present three projects related to the characterization of molecular signals regulating HR. In the first project (Chapter 2), I performed untargeted metabolite profiling on maize lesion mimic mutants of unknown etiology. This work identified two major findings. The first is that most maize lesion mimic mutants produce increased levels of SA compared to wild-type siblings. The second is that some uncharacterized lesion forming mutants have an overall metabolic syndrome like that of the HR mutant, *Rp1-D21*. These findings were further explored in projects two (Chapter 3) and three (Chapter 4). The second project encompasses the molecular characterization of *Lesion10*, a maize lesion mimic mutant that has an HR-like metabolic syndrome. The third project contains my work testing the function and biosynthesis of SA in maize during the HR. Additional background information related to these projects is summarized in the remainder of this introduction.

## 1.2    Lesion mimic mutants

The plant lesion mimic mutants (hereafter referred to as LMMs) are a diverse class of mutants that form spontaneous lesions and/or undergo cell death in the absence of observable infection or stress (Johal et al., 1995; Bruggeman et al., 2015). The first LMM was described by Rollins Emerson in 1923, where he observed a "blotched leaf" phenotype in maize that was heritable (Rollins Adams Emerson, 1923). The term "lesion mimic" was adopted to describe similar mutants due to their resemblance to leaves that had been infected by various pathogens (Neuffer and Calvert, 1975). LMMs have been described in numerous plant systems, including Arabidopsis (Bruggeman et al., 2015), *Oryza sativa* (rice; Undan et al., 2012), maize (Hu et al., 1996; Johal et al., 1995), and *Sorghum bicolor* (sorghum; Sindhu et al., 2018). Most molecular characterizations of LMMs have come from studies of Arabidopsis where more than 80 known LMMs have been identified (Bruggeman et al., 2015). Some of the proposed causal mechanisms of lesion formation in Arabidopsis LMMs include: misregulation of chlorophyll metabolism (Greenberg and Ausubel, 1993; Mach et al., 2001), increased lipid metabolism (Greenberg et al., 2000), disruption of intracellular trafficking (Kulich et al., 2013), ROS formation (Mateo et al., 2004), global transcriptional misregulation (Bruggeman et al., 2015), and constitutive activation of the HR and defense signaling (Rate et al., 1999). While these mechanisms encompass distinct

causes of lesion formation, LMMs of different etiologies may present more than one of the above syndromes. For instance, the formation of ROS is characteristic of both HR (Balint-Kurti, 2019) and chlorophyll biosynthetic mutants (Hu et al., 1998).

Mutants that present constitutive HR signaling are advantageous for the study of HR as they eliminate the need to control for pathogen infection and all measured molecular signals can be attributed to the biology of the plant. As such, these LMMs are often used as model systems to study the HR (Wang et al., 2015a; Wang and Balint-Kurti, 2016; Ge et al., 2021; Rate et al., 1999, 6). Identification of additional HR-like LMMs will increase the number of model systems to study the HR. In addition, it is likely that these mutants are encoded by genes involved in the HR or general defense response pathways and their characterization will likely improve our understanding of genes and molecular signals regulating the HR. A goal of this work was to identify uncharacterized LMMs in maize that have constitutive HR signaling.

Like Arabidopsis, many LMMs have been observed in maize. However, of the over 50 LMMs that have been phenotypically identified in maize, only five genes, *lethal leaf spot1* (*lls1*, (Zm00001d027656); Gray et al., 1997), *camouflage1* (*cf1*, (Zm00001d015366); Huang et al., 2009), *Lesion22* (*Les22*, (Zm00001d029074); Hu et al., 1998), *concentric ring1* (*conr1*, (Zm00001d003866); Kim et al., 2020), and *Rp1-D21* (Hu et al., 1996) encoding maize LMMs have been published. *lls1* is orthologous to Arabidopsis *Accelerated Cell Death1* (*ACD1*; Greenberg and Ausubel, 1993) and sorghum *dropdead1* (*ded1*; Sindhu et al., 2018) and encodes *pheophorbide a* oxygenase which catalyzes the oxygenation of pheophorbide *a*, an essential step in chlorophyll breakdown (Gray et al., 1997). *cf1* encodes *porphobilinogen deaminase* which catalyzes the conversion of porphobilinogen to hydroxymethyl-bilane upstream of chlorophyll and heme biosynthesis (Huang et al., 2009). *Les22* encodes *uroporphyrinogen decarboxylase* which converts uroporphyrinogen to coproporphyrinogen also upstream of chlorophyll and heme biosynthesis (Hu et al., 1998). *conr1* encodes a protein of unknown function that is annotated as a putative metal transporter involved in the suppression of defense response (Kim et al., 2020). *Rp1-D21* encodes a constitutively active NLR that originated from an intragenic recombination at the *Rp1* locus, which encodes a set of tandemly repeated NLR proteins that mediate resistance to the common rust fungus, *Puccinia sorghi* (Hu et al., 1998). *Rp1-D21* mutants present a non-attenuating HR phenotype that becomes more severe with plant age. *Rp1-D21* is frequently used

as a model system to study the HR in maize (Olukolu et al., 2014; Wang et al., 2015a; Wang and Balint-Kurti, 2016).

I am interested in identifying LMMs that are affected in genes involved in HR or defense response pathways. These mutants will provide additional model systems for studies of the HR in maize, and may be encoded by novel genes that regulate or modify HR. Multiple uncharacterized maize LMMs accumulate proteins (Morris et al., 1998) and transcripts (Mu et al., 2021) that accumulate during the HR. While not every LMM is an HR-like mutant, the large number of uncharacterized maize LMMs indicates a high probability that additional HR-like mutants exist in maize. In Chapter 2 of this dissertation, I explore using untargeted metabolomics as a high throughput means of identifying maize LMMs that have an HR-like metabolic syndrome.

## 1.3    Untargeted metabolite profiling

The plant LMMs present many known metabolic perturbations. Maize *Rp1-D21* mutants have increased accumulation of SA, DHBAs, phenylalanine, and numerous phenylalanine-derived compounds such as anthocyanins (Ge et al., 2021). Arabidopsis *acd1* (Greenberg et al., 2000) and *acd2* (Mach et al., 2001) mutants are deficient in chlorophyll breakdown and accumulate pheophorbide and red chlorophyll catabolites, respectively. The *Les22* mutant of maize accumulates a uroporphyrin intermediate (Hu et al., 1998). Dysregulation of lipid metabolism is also a known etiology of Arabidopsis LMMs (Bruggeman et al., 2015). Some of these metabolic perturbations are shared among numerous lesion mimics. For instance, increased accumulation of SA is also found in numerous autoimmune mutants of Arabidopsis (Bruggeman et al., 2015), including the *acd6* mutant (Rate et al., 1999). However, there are numerous lesion mutants that do not accumulate increased levels of SA (Bruggeman et al., 2015). Likewise, the chlorophyll biosynthetic intermediates would not be expected to be accumulated in LMMs that are not encoding enzymes involved in these pathways. The presence of common metabolic perturbations in some LMMs that are not present in others indicates that comparing metabolic perturbations of unknown LMMs with those of known etiology may be used as a first-line prediction of the etiology of unknown mutants.

While individual metabolites can be analyzed in a targeted manner, recent advances in untargeted metabolite profiling have facilitated the detection of thousands of metabolites using a single analysis (Li et al., 2014; Simpson et al., 2021b, 2021a). Programs, such as XCMS (Smith et

al., 2006) allow the high throughput extraction of all chromatogram information, including the mass-to-charge ratio (*m/z*) and the peak intensity of all detected metabolites. The accumulations of these detected features represent thousands of phenotypic values that can be compared amongst all samples analyzed. The identities of these metabolites can be deduced by running authentic standards under the same chromatography conditions, MS/MS fragmentation, or stable isotope flux analysis (Simpson et al., 2021a, 2021b; Li et al., 2014). Chapter 2 of this dissertation explores the possibility of predicting the etiology of uncharacterized lesion mutants by comparing their accumulation of thousands of metabolic features to a mutant of known etiology.

## 1.4    Salicylic acid function

SA (2-hydroxy benzoic acid) is an important plant hormone that functions in PTI (DebRoy et al., 2004), ETI (Delaney et al., 1994), and systemic acquired resistance against numerous pathogen infections (Vlot et al., 2009). The function of SA in immune response and defense signaling was initially proposed after the observation that tobacco cultivars that are resistant to tobacco mosaic virus (TMV) accumulate increased levels of SA following infection (Malamy et al., 1990). The increased levels of SA also coincided with increased transcription of pathogenesis-related genes (Malamy et al., 1990). Since then, increased accumulation of SA has been a common hallmark observed in most plants following pathogen infection (Vlot et al., 2009; Radojičić et al., 2018). SA can act as a defense signaling compound to induce transcriptional activation of defense-related genes by two distinct mechanisms (Ding et al., 2018). In one mechanism, SA directly binds NONEXPRESSOR OF PATHOGENESIS-RELATED GENES1 (NPR1) inducing transcription of immune response genes (Ding et al., 2018). Alternatively, SA can induce transcription of defense-related genes by binding and inhibiting the activities of NPR3/4, which act as transcriptional suppressers.

The HR is often associated with increased accumulation of SA (Radojičić et al., 2018; Ge et al., 2021). The function of SA during HR has been extensively tested in Arabidopsis and multiple observations have indicated that SA is necessary and sufficient for the HR in this species. Transient expression of *NahG*, an SA hydroxylase that severely reduces SA levels, suppresses the HR in Arabidopsis (Weymann et al., 1995; Rate et al., 1999; Brodersen et al., 2005; Huang et al., 2018). In addition, the HR can be initiated in Arabidopsis through external application of SA (Dietrich et al., 1994). The genetic resources to manipulate SA levels, that are well developed in

in Arabidopsis (Lawton et al., 1995; Gaffney et al., 1993; Wildermuth et al., 2001; Garcion et al., 2008), are lacking in most plant systems. As such, SA functionality, most notably the requirement of SA for the HR, has not been thoroughly tested in plant systems besides Arabidopsis. Recently, it was shown that HR severity and SA levels are highly correlated in maize *Rp1-D21* mutants in different genetic backgrounds (Ge et al., 2021) indicating that SA may be required for HR in maize; however this has yet-to-be tested. In Chapter 4 of this dissertation, I investigate the necessity and sufficiency of SA for inducing the HR in maize.

## 1.5    Biosynthesis of salicylic acid

How SA is synthesized in maize is explored in Chapter 4 of this dissertation. SA biosynthesis has only been characterized in a few plant systems. From this work, it has been demonstrated that SA can be synthesized from two known pathways. In one pathway, commonly referred to as the ICS-dependent pathway, chorismate is converted to isochorismate by ISOCHORISMATE SYNTHASE (ICS; Wildermuth et al., 2001; Garcion et al., 2008; Gross et al., 2006). Isochorismate is then converted to isochorismoyl-glutamate by the enzyme encoded by *avrPphB SUSCEPTIBLE3* (*PBS3*) and isochorismoyl-glutamate is spontaneously and/or enzymatically cleaved to form SA (See Chapter 4 Figure 4.1; Torrens-Spence et al., 2019; Rekhter et al., 2019). In the other pathway, SA is synthesized from phenylalanine by a yet-to-be determined synthesis pathway.

The complete ICS-dependent pathway has only fully been demonstrated in Arabidopsis and SA biosynthesis has not been explored in most plant systems. *ICS* genes are highly conserved in angiosperms (Yuan et al., 2009); however, ICS is required for the biosynthesis of phylloquinone (Garcion et al., 2008; Qin et al., 2019), an essential component of Photosystem I (PSI). and therefore, the conservation of *ICS* genes alone does not necessarily indicate a conservation of the ICS-dependent pathway of SA biosynthesis in plants. In Arabidopsis, there is a strong correlation between the accumulation of SA and *ICS* expression (Wildermuth et al., 2001); however, this is not the case for other tested systems. In tobacco, following pathogen infection, SA levels increased but *ICS* expression was unchanged (Ogawa et al., 2006). In pathogen-infected soybean and maize *Rp1-D21* mutants, which both accumulated increased levels of SA, *ICS* expression was significantly decreased (Shine et al., 2016; Olukolu et al., 2014). In tobacco, maize, and soybean, increased accumulation of SA is coincident with increased *PAL* expression (Shine et al., 2016;

Olukolu et al., 2014; Ogawa et al., 2006, 2). These findings indicate that, unlike in Arabidopsis, the ICS-dependent pathway may not have as substantial a contribution to SA biosynthesis in other plant systems.

The entire biosynthetic pathway of phenylalanine to SA has not been fully elucidated; however, labeled isotope flux analyses (Pallas et al., 1996; Coquoz et al., 1998) indicate the requirement of PHENYLALANINE AMMONIA LYASE (PAL), which deaminates phenylalanine to *trans*-cinnamic acid, and that benzoic acid is an intermediate in the pathway (Klämbt, 1962; Yalpani et al., 1993).

There is genetic evidence of both the ICS-dependent and PAL-dependent pathways in Arabidopsis; however, the contribution of each pathway to the total levels of SA seems to be disproportionate. Knockout of *ICS1* in Arabidopsis resulted in more than a 90% reduction in basal and pathogen-induced SA (Wildermuth et al., 2001; Huang et al., 2010). Conversely, genetic disruption of the four *PAL* genes in Arabidopsis decreased basal and pathogen induced SA by 50% (Huang et al., 2010). Since the combined decrease in SA accumulation when targeting either the ICS-dependent or PAL-dependent pathways in Arabidopsis exceeds 100% it seems likely that the two SA biosynthetic pathways are interdependent. This interdependency has also been observed in *Glycine max* (soybean) were SA accumulation was decreased by 90% when *ICS* was targeted by virus induced gene silencing (VIGS) and by 95% when PAL was targeted by VIGS (Shine et al., 2016).

SA is a precursor in the biosynthesis of numerous metabolites. SA can be converted to 2,3-dihydroxy benzoic acid (DHBA) and 2,5-DHBA by 3'- (Zhang et al., 2013) and 5'-hydroxylases (Zhang et al., 2017), respectively. Both SA and DHBAs can be conjugated with glucose by glucosyltransferases (Klämbt, 1962; Song et al., 2008; Huang et al., 2018). While free and conjugated SA are detectable from plant leaves (Klämbt, 1962; Wildermuth et al., 2001), 2,3-DHBA and 2,5-DHBA are only detected in the conjugated forms (Huang et al., 2018; Ge et al., 2021). Another common SA derivative is methyl salicylic acid (Park et al., 2007). Like SA, SA glucoside, methyl SA, 2,3-DHBA glucoside, and 2,5-DHBA glucosides increase in accumulation after pathogen infection and have been proposed to play critical functions in defense response (Klämbt, 1962; Park et al., 2007; Huang et al., 2018; Vlot et al., 2009).

## 1.6 Evolution of the ICS-dependent SA biosynthetic pathway

In plants, ICS activity is encoded by either a multifunctional gene *PHYLLO*, or by a stand-alone *ICS* gene. All Viridiplantae contain a *PHYLLO* gene that was formed from a fusion of genes homologous to the first four bacterial genes, *MenF* (ICS), *MenD* (Enzyme Commission Number ((E.C.) 2.2.1.9), *MenC* (E.C. 4.2.1.113), and *MenH* (E.C. 4.2.99.20) required for the biosynthesis of phylloquinone (See Chapter 4 Figure 4.1; Gross et al., 2006). The *PHYLLO* gene of angiosperms has lost the chorismate binding sequence of the *ICS* domain and no longer encodes ICS activity (Gross et al., 2006). Angiosperms instead encode a stand-alone ICS gene that is necessary for the biosynthesis of isochorismate and in turn phylloquinone (Garcion et al., 2008; Qin et al., 2019).

It still remains enigmatic when the chorismate binding domain of *PHYLLO* was lost and when a stand-alone *ICS* gene originated. It has been proposed that development of and *ICS* gene, separate from *PHYLLO*, allowed isochorismate to be utilized by plants for synthesis of SA (Gross et al., 2006). If that is true, then understanding the evolutionary history of *ICS* genes may provide insights as to the origins of SA biosynthesis from the ICS-dependent pathway in plants. Due to the necessity of phylloquinone in plants, the sub functionalized duplication of *PHYLLO*, that gave rise to an *ICS* gene, had to have proceeded the loss of the *PHYLLO* chorismate binding sequence. All angiosperms that are part of the Phytozome database (Goodstein et al., 2012) encode a *PHYLLO* gene that is missing sequence in the chorismate binding domain and at least one stand-alone *ICS* gene, indicating the origin of an *ICS* gene proceeded the origin of angiosperms. The *PHYLLO* genes of all non-seed producing Viridiplantae, present in the Phytozome database, are not missing the chorismate binding sequence in the *ICS* domain, and no stand-alone *ICS* gene is annotated in these species (Goodstein et al., 2012) indicating the sub functionalized duplication of *PHYLLO*, and the loss of chorismate binding sequence, happened prior to the divergence of seed plants.

# CHAPTER 2.    USING UNTARGETED METABOLOMIC ANALYSES TO PREDICT THE ETIOLOGIES OF UNCHARACTERIZED MAIZE LESION MIMICS

## 2.1    Introduction

Plant lesion mimic mutants (LMMs) undergo programmed cell death and/or form visible lesions in the absence of observable infection of stress. First discovered in *Zea mays* (maize) in 1923 (Rollins Adams Emerson, 1923), the leaves of many LMMs resemble the hypersensitive response (HR), the rapid, localized cell death at and around sites of pathogen infection. LMMs have been identified in many plant systems, including: *Sorghum bicolor* (sorghum; Sindhu et al., 2018), *Oryza sativa* (rice; Takahashi et al., 1999)*, Arabidopsis thaliana* (Arabidopsis; Mach et al., 2001)*, and maize (Johal et al., 1995). Most molecular characterizations of LMMs have been done in Arabidopsis (Bruggeman et al., 2015). From these works, multiple mechanisms that induce lesion formation, including misregulation of chlorophyll metabolism, increased lipid metabolism, disruption of intracellular trafficking, reactive oxygen species (ROS) production, global transcriptional misregulation, and constitutive activation of defense responses, have all been associated with one or more known LMMs (Bruggeman et al., 2015).

The phenotypes of LMMs make them an ideal model system to study programmed cell death and defense responses in plants; however, the use of LMMs in maize research is hindered by not knowing the causes of lesion formation in most mutants. In maize, over 50 LMMs have been phenotypically identified; however, only five genes encoding LMMs: *Lesion22* (*Les22*; Hu et al., 1998), *camouflage1* (*cf1*; Huang et al., 2009), *lethal leaf spot1* (*lls1*; Gray et al., 1997), *concentric ring1* (*conr1*; Kim et al., 2020) and *Rp1-D21* (Hu et al., 1996), have been published. *Les22* encodes *uroporphyrinogen decarboxylase*, which catalyzes the conversion of uroporphyrinogen to coproporphyrinogen (G. H. Elder and A. G. Robers, 1995)*. Les22* mutant accumulates high levels of a phototoxic porphyrin intermediate involved in chlorophyll and heme biosynthesis (Hu et al., 1998). *cf1* encodes *porphobilinogen deaminase* which catalyzes the conversion of porphobilinogen to hydroxymethyl-bilane. The leaf-patterning of *cf1* mutants is proposed to be from reduced ROS scavenging capacity (Huang et al., 2009). *lls1* encodes *pheophorbide a oxygenase* which catalyzes the oxygenation of pheophorbide *a* in chlorophyll breakdown (Gray et al., 1997). *conr1* encodes a protein of unknown function that is proposed to be a metal transporter

involved in the suppression of defense response (Kim et al., 2020). *Rp1-D21* is a constitutively active HR mutant that originated from an intragenic recombination at the *Rp1* locus, which encodes a set of tandemly repeated nucleotide-binding site leucine-rich repeat proteins that mediate resistance to the common rust fungus, *Puccinia sorghi* (Hu et al., 1996).

Numerous metabolic perturbations have been detected in previously characterized LMMs. The *Rp1-D21* mutant has increased accumulation of the defense response hormone salicylic acid (SA), SA-derived dihydroxy benzoic acids (DHBAs), and the aromatic amino acid phenylalanine (Ge et al., 2021). High accumulation of SA is a hallmark of many characterized Arabidopsis LMMs (Bruggeman et al., 2015). The *lls1* mutant of maize and the *accelerated cell death2* (*acd2*) mutant of Arabidopsis accumulate phototoxic catabolites in chlorophyll degradation (Mach et al., 2001; Gray et al., 1997). The *Les22* and *cf1* mutants of maize accumulate intermediates in chlorophyll and heme biosynthesis (Hu et al., 1998; Huang et al., 2009). The numerous metabolic perturbations of LMMs have led us to hypothesize that the etiology of uncharacterized LMMs can be predicted through metabolite profiling. For instance, LMMs that accumulate high levels of SA and phenylalanine are likely HR-like LMMs. Whereas accumulation of metabolites in chlorophyll synthesis or degradation may indicate those LMMs are encoded by enzymes involved in the biosynthesis or catabolism of these metabolites. Recent advances in untargeted metabolite profiling by liquid chromatography-mass spectrometry (LC-MS; Simpson et al., 2021a; Strauch et al., 2015; Simpson et al., 2021b) facilitate the characterization of thousands of metabolites from a single analysis. Common metabolic perturbations amongst uncharacterized and known LMMs may indicate a common mechanism of lesion formation in these mutants.

In this work I performed untargeted metabolite profiling of upper and lower leaves from 23 maize LMMs using LC-MS. I demonstrated that these mutants contain thousands of metabolic perturbations, including differential accumulation of SA, aromatic amino acids, and chlorophyll breakdown products. Using hierarchal clustering I have identified a subset of the 23 mutants whose metabolic perturbations are strongly positively correlated with the HR mutant *Rp1-D21*.

## 2.2 Materials and Methods

### 2.2.1 Plant material and growth conditions

All plant material was grown by Dr. Gurmukh Johal (Purdue University) and his lab during the 2018 field season at the Purdue Agronomy Center for Research and Education in West Lafayette, Indiana (40.4700° N, 86.9917° W). Material was planted in 3.84 m plots with 0.79 m of interrow spacing and 0.79 m of alley spacing between plots. Conventional pest and weed control practices for growing maize in Indiana were followed. Mutants in isogenic backgrounds had been introgressed for multiple generations by repeated backcrossing of a heterozygous mutant with an inbred wild-type plant from those specific backgrounds. All mutants included in this analysis were planted in two plots and were segregating 1:1 for mutant and wild-type siblings. The grow outs for dominant mutants in isogenic backgrounds were from a cross of a heterozygous mutant with an inbred wild-type plant. The grow outs for recessive mutants in isogenic backgrounds were from a sibling mate of two heterozygous mutants or from self-pollination of a nearly isogenic heterozygous mutant that had been introgressed into the background by backcrossing for multiple generation. Dominant mutants in a mixed genetic background were maintained by sibling mating a heterozygous mutant and a wild-type plant. Recessive mutants in a mixed genetic background were maintained by sibling mating two heterozygous mutants. Due to the nature of these crosses, the wild-type siblings for recessive mutants were heterozygous for the recessive mutation. The crossing scheme and genetic background information for each mutant are presented in Table 2.1.

### 2.2.2 Tissue collection, metabolite extractions, and LC-MS processing

All leaves were harvested at the V10 plant stage prior to anthesis. The upper leaf samples were samplings from leaves seven or eight and the lower leaf samples were samplings from leaves three or four. For all harvestings, a 5 x 5 cm piece of leaf tissue was excised from the plant 5-10 cm inward from the leaf tip. Four biological replicates, each containing leaves from two different plants were collected. Both upper and lower leaves in mutant and wild-type siblings were collected for a total of 16 samples per segregating mutant and sibling wild-type set. Individual biological replicates were placed in labeled shoot-bags, flash-frozen in liquid nitrogen, and stored on dry ice for the duration of collection. After collection, samples were stored at -80°C until processing.

Prior to metabolite processing, the two leaves of each biological replicate were transferred to a 50-mL Falcon tube. Tubes were flash-frozen in liquid nitrogen and the tissue was ground in the tubes using a pestle. The leaf midribs remained intact after this grinding and were removed prior to metabolite extraction. Soluble metabolites were extracted in 1:1 methanol:water (V/V) at a concentration of 100 mg of tissue per 1 mL of extraction solvent. Samples were incubated at 65°C for 2 h and vortex agitated every 30 min. After incubation, plant material was pelleted at 10,000 x $g$ for 10 min and 500 µL of supernatant was transferred to a new tube. Samples were dried completely in a speed vacuum at room temperature and the pellet was redissolved in 50 µL of 1:1 methanol:water (V/V). Samples were sonicated for 15 min, and non-soluble material was pelleted by centrifugation at 14,000 x $g$ for 10 min. 40 µL of supernatant was transferred to a LC-vial and stored at -20°C until processing.

Samples were analyzed at the Metabolite Profiling Facility at Purdue University similar to a previously described method (Simpson et al., 2021a) using an Agilent 1100 HPLC system (Agilent Technologies, Palo Alto, CA, USA) and a Shimadzu Shim-pack XR-ODS (3.0 × 75 mm × 2.2 µm) separation column and a mobile phase of 0.1% aqueous formic acid (V/V) and solvent B was 0.1% formic acid (V/V) in acetonitrile at a flow rate of 0.6 mL min$^{-1}$. For all analyses, 5 µL of sample was injected, and an initial solvent A:B ratio of 98:2 was held for 1 min. Metabolites were eluted by linear gradients to 94:6 at 5 min, 54:46 at 15 min, 5:95 at 21.5 min, and a 5:95 hold for 2 min. The column was then re-equilibrated by returning to 98:2 over 1 min and holding for 4 min prior to loading of the next sample. The column was maintained at 40°C during all steps. Mass spectrometry across a mass-to-charge ($m$/z) range of 80 – 1,100 amu was carried out on the column effluent via negative electrospray ionization (ESI) using an Agilent 6210 time-of-flight mass spectrometer at a capillary voltage of 3.2 kV; $N_2$ gas temperature of 325°C; drying gas flow rate of 9 L min$^{-1}$; nebulizer gas pressure of 55 psi; fragmentary voltage of 130 V; skimmer voltage of 45 V; octopole RF of 750 V. Mass accuracy was enhanced by infusing Agilent Reference Mass Correction Solution (G1969-85001) throughout each run. Samples were run in a random order with all the lower leaf samples being analyzed first followed by all the upper leaf samples.

The resulting Agilent MassHunter raw data (".d" directories) were visualized and converted to ".mzdata" files using Agilent MassHunter Qualitative Analysis software (v10.0). The conversion was performed using the options to centroid data, remove common +1 and +2 isotopes, and retain features that are above 100 counts in each mass scan. Peak picking, retention time

corrections, and extraction of the integrated peak areas of mass features were performed using XCMS (Smith et al., 2006) and a custom R script. The parameters used for feature detection were method = "centWave", ppm = 10, peakwidth = c(5,30), snthresh = 5, prefilter = c(3,150), and integrate = 1, mzdiff = -0.01. The parameters used for retention time correction were method = "obiwarp" and profStep =1. The parameters used for integration of mass features were method = "density", bw = 5, mzwid = 0.025, minfrac = 0, minsamp =4, and max = 100. All other parameters were default settings. Both non-filled and peak-filled output files were generated.

All additional data wrangling was performed using Microsoft Excel. Detected features in each sample were determined using the non-filled XCMS output file. The reproducibly detectable features were identified as those that accumulated in all replicates of at least one of the mutants or one of the wild-type siblings. The reproducibly detected features were then identified in the peak-filled output file and this file was used for all future analysis. The $\log_2$ FC accumulation of each feature across the mutants was determined by calculating the average peak area of the wild-type siblings of each mutant and then calculating the $\log_2$ FC of each mutant replicate relative to these wild-type averages.

### 2.2.3  Individual compound comparisons

All standards were obtained from Sigma-Aldrich. The amino acids used were part of the L-Amino Acids Kit (LAA-21) and SA was obtained as CAS 69-72-7. All compounds were dissolved in 1:1 methanol:water (V/V) and analyzed by the same LC-MS method as described above. The identity of SA glucoside was determined by the expected spontaneous fragmentation pattern of *m/z*: 299.077 → 137.024 → 93.035 amu and by the response of this feature to foliar application of SA (See Ch. 4 Figure 4.16). The putative NCC1 and NCC2 metabolites were identified by comparison to published *m/z* values (Berghold et al., 2006). The values presented in the individual metabolite graphs were calculated as the average $\log_2$ FC of each of these metabolites for the four biological mutant replicates in relation to the average value of the wild-type siblings. Metabolite accumulations that were statistically different in mutants compared to wild-type siblings were determined by comparing the raw count values of features in mutant and wild-type samples using Student's T-test and a *p*-value cutoff of $< 0.05$. All correlation analyses were performed in Excel using the "Regression" function in the data analysis package.

### 2.2.4 Hierarchal clustering

All clustering was performed using the "ward" method (Murtagh, Fionn, 2014) and JMP Professional V15. The 368-sample clustering was performed using the peak-filled values for the 22,732 features that were deemed reproducibly detected in either upper or lower leaves. The clustering of the 23 mutants was performed using the average $\log_2$ FC accumulation, that were calculated as described for the individual compounds, for the 13,339 features that were deemed reproducibly detected in upper leaves. Correlation of these values in *Rp1-D21* compared to the other 22 mutants were calculated using Excel and the "Correlation" function of the data analysis package.

## 2.3 Results

### 2.3.1 The maize lesion mimic mutants included in this study contain thousands of metabolic perturbations

I performed untargeted metabolite analyses on leaves of 23 different maize LMMs. The mutants included in this study were: *Lesion1* (*Les1*), *Lesion1-like* (*Les1-like*), *Lesion6* (*Les6*), *Lesion9* (*Les9*), *Lesion9-like* (*Les9-like*), *Lesion10* (*Les10*), *Lesion11* (*Les11*), *Lesion12* (*Les12*), *Lesion15* (*Les15*), *Lesion17* (*Les17*), *Lesion18* (*Les18*), *Lesion23-like* (*Les23-like*), *lesion24* (*les24*), *Lesion101* (*Les101*), *Lesion102* (*Les102*), *lesion2014* (*les2014*), *Rp1-D21*, *Bella-Fleck1* (*Bfl1*), *Lesion-Mop1* (*Les-Mop1*), *Florida-Lesion* (*FL-Les*), *lesion-E27* (*les-E27*), and *Lesion-EC91* (*Les-EC91*). These mutants present multiple different lesion types and severities (Figure 2.1). Each mutant was segregating 1:1 for mutant and wild-type siblings in either a mixed or isogenic B73, W22, Mo17, or Mo20W genetic background. The previous generation crossing scheme and genetic background for each mutant are presented in Table 2.1. All mutants that comprised this experiment were in a single genetic background except *Les9*, which was analyzed in both a B73 and Mo20W isogenic genetic background. All dominant mutants (denoted by a capital letter at the beginning of the lesion name) were analyzed as heterozygous individuals and all recessive mutants (denoted by a lower-case letter at the beginning of the mutant name) were analyzed as homozygous mutants. All metabolite profiling was performed on leaves form V10 stage plants. As lesion severity of LMMs varies with leaf age, I analyzed tissue from lower leaves (leaves 3 or 4) and upper leaves (leaves 7 or 8). I extracted metabolites from four biological

replicates of both lower and upper leaves from mutant and wild-type siblings for each of the LMMs included in this analysis for a total of 368 metabolite samples.

Leaf metabolites soluble in 50% methanol were analyzed by reverse-phase liquid chromatography-mass spectrometry (LC-MS). Mass features present in each sample were determined using XCMS (Smith et al., 2006). I detected a total of 38,473 different mass features that were present in any one of the 368 samples. To limit my future analysis to reproducibly detectable mass features, I trimmed the list of 38,473 features to only include features that were detectable in all four replicates of at least one mutant or wild-type condition (e.g., the feature was detected in all four replicates of the upper leaf samples from *Rp1-D21/+* mutants). This trimming retained 19,452 features for the lower leaf samples, 13,339 features for the upper leaf samples, and a total of 22,732 reproducibly detected features when considering both lower and upper leaf samples. The total number of detected features for each mutant is presented in Table 2.2. The range in the number of features detected for each mutant was 3,600-5,300 for lower leaf samples and 3,100-4,400 for upper leaf samples. For 21 of the 23 mutants, there was a higher number of features detected in lower leaf samples as compared to upper leaf samples. In addition, 22 of the 23 mutants had a higher proportion of features that were differentially accumulated in mutant vs. wild-type samples (T-test, $p < 0.05$) in lower leaf samples as compared to upper leaf samples. The detection of more mass features in lower leaf as compared to upper leaf samples was also reflected by the detection of higher total ion counts in lower leaf samples (Figure 2.2). For all 23 mutants, the total ion counts of reproducibly detectable features were higher in upper leaf than lower leaf samples.

### 2.3.2 Most maize lesion mimic mutants included in this study accumulate high levels of the defense response hormone salicylic acid

Salicylic acid (SA) is a known defense response hormone that has been shown to accumulate in lesion mimic mutants that are a result of autoactive HR-signaling (Ge et al., 2021). I identified SA (M137.024_T533) in my list of 22,732 features by comparison to an authentic standard and compared the accumulation of SA across the 23 mutants for both lower (Figure 2.3A) and upper leaf samples (Figure 2.3B). A total of 16 mutants when considering upper leaf samples and 15 mutants when considering lower leaf samples accumulated higher than wild-type sibling levels of SA. *Les1*, *Les6*, *Les9:B73*, *Les9:Mo20W*, *Les10*, *Les12*, *Les17*, *Les23-like*, *Les102*, *les-E27*, *Les-Mop1*, *Rp1-D21*, and *Bfl1* mutants accumulated higher than wild-type levels of SA in

both lower and upper leaf samples. Despite most of the mutants accumulating higher than wild-type SA levels, the degree of increased SA accumulation was highly variable amongst these mutants. The fold change (FC) accumulation of SA in mutant compared to wild-type samples for the mutants that accumulated higher than wild-type levels of SA ranged from 1.5 to 60 in lower leaf samples and from 1.5 to 123 in upper leaf samples. Consistent with previous reports(Ge et al., 2021) and with being an autoactive HR lesion mutant (Hu et al., 1996), *Rp1-D21* mutants accumulated 60- and 73-fold more SA than wild-type siblings in lower and upper leaves, respectively. *Les6*, *Les10*, *Les12*, *Les17*, *Les23-like*, *Les102*, and *Bfl1* all accumulated distinctly higher levels of SA ($\log_2$ FC > 4) in either upper or lower leaves than the other SA-accumulating mutants and *Bfl1* mutants had a higher FC increase in SA than *Rp1-D21* mutants for the upper leaf samples. Accumulation of SA in *Les1-like*, *Les9-like*, *Les18*, *les24*, and *Les101* mutants was indistinguishable from wild-type siblings for both upper and lower leaves. *Les11*, *Les15*, and *les2014* mutants accumulated higher than wild-type levels of SA in upper leaf samples only while *FL-Les* mutants only accumulated higher than wild-type SA levels in lower leaf samples. None of the mutants included in this analysis accumulated significantly lower than wild-type levels of SA. There was a strong positive correlation ($r = 0.88$, $p < 3.8E^{-8}$) between SA FC accumulation in upper and lower leaves for the 23 mutants.

In plants, free SA can be conjugated with glucose to form SA-glucoside (Klämbt, 1962; Song et al., 2008). I compared SA-glucoside (M299.078_T316; see methods for compound identification) accumulation across these 23 mutants compared to wild-type siblings (Figure 2.4). Eight mutants when considering upper leaf samples and 16 mutants when considering lower leaf samples accumulated higher than wild-type levels of SA glucoside. *Les1*, *Les9:B73*, *Les10*, *Les17*, *Les23-like*, *les-E27*, *Rp1-D21*, and *Bfl1* mutants accumulated higher than wild-type levels in both upper and lower leaves. *Les6, Les12*, *Les9:Mo20W*, *Les18*, *Les102*, *Les-Mop1*, *Les-EC91*, and *FL-Les* only accumulated higher than wild-type levels in lower leaves. Unlike free SA, where no mutant accumulated less than wild-type levels, *les2014* mutants accumulated significantly lower than wild-type levels of SA glucoside in upper leaf samples. I calculated the correlation coefficients between SA and SA glucoside accumulation across these 23 mutants and found that accumulation of these two metabolites were highly positively correlated in both upper ($r = 0.91$, $p < 5E^{-9}$) and lower ($r = 0.94$, $p < 4E^{-11}$) leaves.

### 2.3.3 Aromatic amino acid levels are elevated in lower leaves of most of the lesion mimic mutants included in this analysis.

I next evaluated aromatic amino acid accumulation in the lesion mutants included in this analysis. Phenylalanine (M164.072_T103), tryptophan (203.083_T214), and tyrosine (M180.066_T59) were all identified from my analysis by comparison to authentic standards. Phenylalanine accumulation was significantly higher than wild-type levels in upper leaves for eight lesion mutants (Figure 2.5A) and in lower leaves for 19 mutants (Figure 2.5B). *Les1-like*, *Les9:Mo20W*, *Les10*, *Les17*, *Les23-like*, *Les102*, *Bfl1*, and *Rp1-D21* mutants all accumulated higher than wild-type levels of phenylalanine in both upper and lower leaves. *Les1*, *Les6*, *Les9:B73*, *Les11*, *Les12*, *Les15*, *Les18*, *les24*, *Les101*, *les2014*, and *les-E27* only accumulated higher than wild-type levels of phenylalanine in lower leaves. None of the mutants included in this analysis accumulated higher than wild-type levels of phenylalanine in only upper leaves or accumulated lower than wild-type levels of phenylalanine in either upper or lower leaves. The FC accumulation of phenylalanine across these lesion mutants was less variable than that of SA and SA glucoside. The phenylalanine FC accumulation in mutant compared to wild-type samples for mutants that accumulated higher than wild-type levels of phenylalanine ranged from 1.9 to 5.3 in upper leaves and from 1.5 to 9 in lower leaves. There was not a significant correlation ($p > 0.12$) between the FC accumulation of phenylalanine in upper and lower leaves across these 23 mutants.

Tryptophan accumulation was significantly higher than wild-type levels in upper leaves for three mutants (Figure 2.6A) and in lower leaves for 18 mutants (Figure 2.6B). *Les23-like*, *Les101*, and *Rp1-D21* mutants accumulated higher than wild-type levels of tryptophan in both lower and upper leaves. *Les1*, *Les1-like*, *Les6, Les9:B73*, *Les9:Mo20W*, *Les10*, *Les11*, *Les12*, *Les17*, *Les18*, *les24*, *Les102*, *les2014*, *Les-EC91*, and *Les-Mop1* mutants accumulated higher than wild-type levels of tryptophan in only lower leaves. The *Bfl1* mutant accumulated significantly less than wild-type levels of tryptophan in upper leaf samples. The tryptophan FC in mutant vs. wild-type samples for mutants that accumulated higher than wild-type levels of tryptophan ranged from 1.3 to 3.3 in upper leaf leaves and from 1.5 to 6.8 in lower leaves. The *Bfl1* mutant accumulated approximately 60% of wild-type tryptophan levels. There was a positive correlation ($r = 0.55$, $p < 0.007$) between tryptophan FC accumulation in upper and lower leaves across these 23 mutants.

Tyrosine accumulation was significantly higher than wild-type levels in upper leaves for 10 mutants (Figure 2.7A) and in 22 mutants for lower leaves (Figure 2.7B). *Les9:B73*, *Les9:Mo20W*,

*Les9-like*, *Les10*, *Les15*, *Les17*, *Les23-like*, *les-E27*, *Bfl1*, and *Rp1-D21* mutants accumulated higher than wild-type levels of tyrosine in bother lower and upper leaves. *Les1*, *Les1-like*, *Les6*, *Les11*, *Les12*, *Les18*, *les24*, *Les101*, *Les102*, *les2014*, *Les-EC91*, and *Les-Mop1* mutants accumulated higher than wild-type levels of tyrosine in only lower leaves. No mutants accumulated lower than wild-type levels of tyrosine in either upper or lower leaves. The tyrosine FC accumulation in mutant vs. wild-type samples in mutants that accumulated higher than wild-type levels of tyrosine ranged from 1.2 to 7.7 in upper leaves and from 1.4 to 16.1 in lower leaves. There was a positive correlation ($r = 0.55$, $p < 0.006$) between tyrosine FC accumulation in upper and lower leaves across these 23 mutants.

To determine if the aromatic amino acids accumulated similarly across these 23 lesion mutants I calculated the correlation coefficients between the FC accumulation of phenylalanine, tryptophan, and tyrosine for both upper and lower leaves. There were positive correlations between the FC accumulation of phenylalanine and tryptophan ($r = 0.66$, $p < 7E^{-4}$), phenylalanine and tyrosine ($r = 0.83$, $p < 1.5E^{-6}$), and tryptophan and tyrosine ($r = 0.69$, $p < 3E^{-4}$) in upper leaves across these mutants. There were also positive correlations in lower leaves between the FC accumulation of phenylalanine and tryptophan ($r = 0.56$, $p < 0.006$), phenylalanine and tyrosine ($r = 0.70$, $p < 2E^{-4}$), and tryptophan and tyrosine ($r = 0.66$, $p < 5E^{-4}$).

### 2.3.4 Chlorophyll breakdown products predominantly only accumulate to higher than wild-type levels in the lower leaves of the lesion mutants included in this analysis

The last metabolites I compared across these mutants were the chlorophyll breakdown products, non-chlorophyll containing catablolite1 (NCC1) and non-chlorophyll containing catabolite2 (NCC2), which have been shown to accumulate in senescing maize leaves (Berghold et al., 2006). I identified mass features, from the metabolite analysis of the 23 mutants, consistent with the predicted mass-to-charge (*m/z*) ratio expected for NCC1 (M805.033_T716) and NCC2 (M839.336_T593).

NCC1 accumulation was significantly higher than wild-type levels in three mutants when considering upper leaves (Figure 2.8A) and 15 mutants when considering lower leaves (Figure 2.8B). *Les9:B73*, *Les23-like*, and *Rp1-D21* mutants accumulated higher than wild-type levels of NCC1 in both upper and lower leaves. *Les1*, *Les1-like*, *Les6*, *Les9:Mo20W*, *Les10*, *Les15*, *Les17*, *Les18*, *les24*, *Les102*, *les2014*, and *Bfl1* mutants only accumulated higher than wild-type levels of

NCC1 in lower leaves. *Les-Mop1*, *FL-Les*, and *les-E27* mutants accumulated lower than wild-type levels of NCC1 in upper leaves. No mutants accumulated lower than wild-type levels of NCC1 in lower leaves. The FC accumulation of NCC1 for the mutants that accumulated higher than wild-type levels of NCC1 ranged from 5 to 9 in upper leaves and from 1.9 to 25.3 in lower leaves. The FC decrease in accumulation of NCC1 for the three mutants that accumulated less than wild-type levels of NCC1 in upper leaves ranged from -7.3 to -12.1. There was a positive correlation ($r$ =0.5, $p$ < 0.01) between the FC accumulation of NCC1 in upper and lower leaves for the 23 mutants.

NCC2 accumulation was significantly higher than wild-type levels in three mutants when considering upper leaves (Figure 2.9A) and 18 mutants when considering lower leaves (Figure 2.9B). *Les1*, *Les9:B73*, and *Les23-like* mutants accumulated higher than wild-type levels of NCC2 in both upper and lower leaves. *Les1-like*, *Les6*, *Les9:Mo20W*, *Les9-like*, *Les10*, *Les15*, *Les17*, *Les18*, *les24*, *Les102*, *Bfl1*, *Rp1-D21*, *Les-Mop1*, *Les-EC91*, and *FL-Les* mutants accumulated higher than wild-type levels of NCC2 in only lower leaves. Despite accumulating higher than wild-type levels in lower leaves, *Les15*, *Les-Mop1*, and *FL-Les* mutants accumulated significantly lower than wild-type levels of NCC2 in upper leaves. The other mutant to accumulate lower than wild-type levels of NCC2 in upper leaves was the *les-E27* mutant. The FC accumulation of NCC2 for mutants that accumulated higher than wild-type levels of NCC2 ranged from 4.2 to 4.8 for upper leaves and from 3.5 to 16.6 for lower leaves. The FC decrease in accumulation for NCC2 for the four mutants accumulated less than wild-type levels of NCC2 in upper leaves ranged from -2 to -5.1. There was a positive correlation ($r$ = 0.56, $p$ < 0.005) between the FC accumulation of NCC2 in upper and lower leaves for the 23 mutants.

Since NCC1 and NCC2 are both breakdown products of chlorophyll, I hypothesized that their accumulation across these 23 mutants should be similar. To test this, I calculated the correlation coefficients between NCC1 and NCC2 accumulation in upper and lower leaves for these 23 mutants. As expected, there was a strong positive correlation between NCC1 and NCC2 accumulation in both upper ($r$ = 0.95, $p$ < $4E^{-12}$) and lower leaves ($r$ = 0.83, $p$ < $9E^{-7}$).

### 2.3.5   Metabolic similarity is influenced by leaf age

I next identified lesion mutants with common metabolic perturbations by performing hierarchal clustering of the 23 lesion mutants using metabolite accumulations. The first clustering I performed considered the raw count values of the 22,732 reproducibly detected features across

all 368 samples (Figure 2.10). The samples included in this analysis clustered into two large clades that each contained approximately an equal number of samples. One clade contained all the lower leaf samples, the upper leaf samples of *Bfl1* mutants, and the upper leaf samples of the wild-type siblings of *FL-Les* mutants. The other clade contained all the other upper leaf samples.

To assess if samples that should have similar metabolite profiles were grouped in this clustering analysis, I compared the positions of the wild-type sibling samples for mutants in the B73 genetic background and those in a mixed genetic background (Figure 2.10). In the lower leaf samples, wild-type siblings in the B73 genetic background clustered in a single clade that excluded any other samples. This trend was also observed for the lower leaf samples for the wild-type siblings in a mixed genetic background. For upper leaves, the clade that encompassed all the wild-type sibling samples in the B73 genetic background also contained the respective mutant samples. This pattern was also present for upper leaf samples for mutants and wild-type siblings in a mixed genetic background.

### 2.3.6  There is a subset of maize lesion mutants whose metabolite profile is like that of *Rp1-D21*

For the next clustering, I utilized the $\log_2$ FC accumulation of mass features in mutants compared to their respective wild-type siblings. There were moderately strong correlation coefficients in these $\log_2$ FC values between the biological replicates of each mutant (Table 2.3), ranging from 0.55 to 0.89 in lower leaves and from 0.27 to 0.74 in upper leaves. Since leaf age had a stronger influence on metabolite similarity than lesion formation (Figure 2.10) I focused my clustering analysis to only consider upper leaf samples. The upper leaves of the lesion mutants had a lower proportion of metabolic perturbations than lower leaves (Table 2.2) and I hypothesized that the observed perturbations in upper leaves are more likely a result of the initial responses to lesion formation in each mutant and less likely a result of secondary effects of cell death and leaf aging. Since I only utilized upper leaves for this analysis, I limited the metabolites I considered to the 13,339 features that were reproducibly detected in upper leaves. The average $\log_2$ FC accumulations for each metabolite were calculated for the 23 mutants and used in this analysis.

The output of this clustering sub-divided the lesion mutants into 6 arbitrary groupings (Figure 2.11A). The first group contained *Les9:Mo20W*, *Les9-like*, *Les18*, *les24*, *Les101*, *Les-EC91*, and *Les-Mop1*. The second group contained *Les6*, *Les11*, *Les12*, *les2014*, and *les-E27*. The

third group contained *Les1 and Les9:B73*. The fourth group contained *Les1-like*, *Les15*, and *Les102*. The fifth group contained only *FL-Les*. The sixth group contained *Les10*, *Les17*, *Les23-like*, *Bfl1*, and *Rp1-D21*. The mutants contained in group one, two, three, four, and five were all contained in a clade distinct from the mutants in group six.

The mutants that clustered with *Rp1-D21* were of interest because *Rp1-D21* is an autoactive HR mutant and the only LMM included in this analysis that has a publish etiology (Hu et al., 1996). To further explore the similarity of these mutants to *Rp1-D21*, I calculated the correlation coefficients between the $\log_2$ FC accumulation (mutant/wildtype) of the 13,339 mass features between *Rp1-D21* and each of the other 22 mutants. These correlation coefficients are presented in Figure 2.11B. Consistent with their clustering with *Rp1-D21*, the mutants with the strongest correlation to *Rp1-D21* were *Les10*, *Les17*, *Les23-like*, and *Bfl1*. These correlation coefficients were all over 0.5, indicating the clustering of these mutants was a result of strong metabolic similarity between these mutants and *Rp1-D21*. These four mutants are the best candidates to be HR-like mutants or to be mutated in genes associated with defense response. If that were the case, then I predicted that the correlation coefficients between *Rp1-D21* and these four mutants should increase if I only considered the mass features whose levels were significantly impacted by *Rp1-D21*. Consistent with his prediction, the correlation coefficient between *Rp1-D21* and all four mutants increased by at least 0.11 when considering this subset of features compared to when considering all features (Figure 2.11B). The correlation coefficients between *Rp1-D21* and *Les9:B73*, *Les102*, *Les12*, and *Les9:Mo20W*, and *Les6* also increased to a similar magnitude when considering the subset of *Rp1-D21* affected feature. These findings indicated these mutants also have similar metabolic perturbations as *Rp1-D21*, albeit to likely weaker degrees. The correlation coefficients between *Rp1-D21* and the other mutants included in this analysis changed very little when considering the subset of *Rp1-D21* affected features, further indicating they are not HR-like or defense response mutants.


## 2.4    Discussion, Conclusions, and Future Directions

In this work, I performed untargeted metabolite profiling on 23 maize LMMs. The first metabolite I compared amongst the mutants was the defense response hormone SA. High accumulation of SA is often associated with HR and autoimmune LMMs (Morris et al., 1998; Bruggeman et al., 2015; Radojičić et al., 2018), and foliar treatment of Arabidopsis leaves with

SA can induce HR (Dietrich et al., 1994). In addition, increased catabolism of SA via overexpression of *NahG*, an SA hydroxylate enzyme, can suppress lesion formation and cell death in Arabidopsis (Weymann et al., 1995; Rate et al., 1999; Brodersen et al., 2005; Huang et al., 2018). Over half of the mutants sampled accumulated higher than wild-type levels of SA in upper or lower leaves (Figure 2.3). Consistent with the strong correlation between SA FC accumulation in upper and lower leaves, 13 of the 23 mutants accumulated higher than wild-type levels of SA in both upper and lower leaves.

The only mutant included in this analysis with a known etiology was the HR-mutant *Rp1-D21* (Hu et al., 1996). Consistent with previous reports of *Rp1-D21* (Ge et al., 2021), there was a 60-fold and 73-fold increase in SA accumulation in *Rp1-D21* mutants compared to wild-type siblings in lower leaves and upper leaves, respectively. If SA accumulation in *Rp1-D21* can be used as a benchmark of the expected SA response during HR, there were four mutants, *Les17* (51-fold), *Les23-like* (78-fold), and *Bfl1* (123-fold) that had similar to *Rp1-D21* increases in SA levels in mutant compared to wild-type siblings in upper leaves and four mutants, *Bfl1* (45-fold), *Les23-like* (49-fold), *Les12* (56-fold), and *Les102* (60-fold) that had similar to *Rp1-D21* increases in SA levels in mutant compared to wild-type siblings in lower leaves. While there are numerous biotic and abiotic mechanisms known to induce SA accumulation (Vlot et al., 2009), the commonality of SA accumulation and the presence of leaf lesions in these mutants indicates they may induce SA by mechanisms present in *Rp1-D21*. This is most evident for *Bfl1* and *Les23-like*, which had *Rp1-D21-like* SA responses in both upper and lower leaves.

Despite 16 and 15 mutants accumulating higher than wild-type levels of SA in upper and lower leaves, respectively (Figure 2.3), most of these mutants had a drastically lower FC in SA accumulation than *Rp1-D21*. The lower FC accumulation of SA in these mutants compared to a known HR mutant indicates that these mutants are likely not HR or defense response mutants. Nonetheless, the higher than wild-type accumulation of SA in these mutants, many in both upper and lower leaves, indicates that SA is likely associated with multiple different LMMs and not just those caused by HR or autoimmunity.

Accumulation of SA in *Les1-like*, *Les9-like*, *Les18*, *les24*, and *Les101* mutants was indistinguishable from wild-type levels in both upper and lower leaves. There are numerous Arabidopsis LMMs that do not accumulate SA (Bruggeman et al., 2015) and these findings indicate there are some maize mutants that do the same. While it is possible these mutants are

defective in SA biosynthetic enzymes, the lack of SA accumulation in these mutants suggests the cause of their lesion formation is likely not HR or autoimmunity.

A common trend for most maize LMMs is that lesion severity positively correlates with leaf age(Johal et al., 1995). This was true for 22 of the 23 LMMs I profiled with the exception being the *Bfl1* mutant which has more noticeable lesions on upper than lower leaves. Despite the differences in lesion severity in upper and lower leaves in maize LMMs, the FC accumulations of SA in these tissues were comparable in magnitude (Figure 2.3). Due to characterizations of SA function in Arabidopsis (Bruggeman et al., 2015; Rate et al., 1999; Brodersen et al., 2005), SA is often proposed as a cause or requirement for HR and/or lesion formation; however, the differences in lesion severity and similarity in SA accumulation of upper and lower leaves within LMMs of maize indicate SA is likely not a primary cause of lesion initiation or severity in maize. For some mutants, lesion severity was negatively correlated with SA FC accumulation. *Les10*, *Les17*, *Les23-like*, and *Rp1-D21* mutants all had a higher FC accumulation of SA in upper leaves, which contain less lesions, that lower leaves, which contain more lesions. These findings demonstrate that SA can be accumulated without the progression of lesion severity.

High accumulation of SA is thought to be toxic to cells and as such, SA is often rapidly conjugated with glucose and stored in a more biologically inactive form (Enyedi et al., 1992). I measured the FC accumulation of SA-glucoside amongst these 23 mutants (Figure 2.4) and found almost a perfect correlation between SA and SA-glucoside accumulation in upper and lower leaves indicating SA is readily converted to SA glucoside in maize. The magnitude in the FC accumulation of SA and SA glucoside were similar in the highest SA accumulating mutants, such as *Rp1-D21*, indicating these mutants maintain a similar proportion of free SA and SA-glucoside. Due to the proposed toxicity of SA, the similarity of SA and SA glucoside in these leaves is unexpected. SA can be converted to other catabolites such as 2,3-dihydroxybenzoic acid (Zhang et al., 2013), 2,5-dihydroxybenzoic acid (Zhang et al., 2017), and methyl SA (Song et al., 2008) and it is possible SA toxicity is relieved through hyper-conversion of SA to these catabolites. It also may be that maize cells can tolerate large amounts of SA without adverse effects. Complete analyses of SA and SA-derived catabolites coupled with cellular integrity assays are needed to discern the SA threshold maize cells can tolerate.

Another set of metabolites I focused on in this analysis were the aromatic amino acids, phenylalanine (Figure 2.5), tryptophan (Figure 2.6), and tyrosine (Figure 2.7). In maize, both

phenylalanine and tyrosine can serve as precursors to the phenylpropanoid pathway from which lignin is synthesized (Morrison and Buxton, 1993). Reinforcement of cellular barriers against pathogen attack through increased accumulation of lignin is a plant defense response during HR (Menden et al., 2007). Previously characterizations of *Rp1-D21* mutants identified that they accumulate elevated levels of phenylalanine (Ge et al., 2021) and a retroactive review of an *Rp1-D21* RNA-seq experiment (Olukolu et al., 2014) has identified that numerous enzymes involved in phenylalanine metabolism and catabolism are elevated in *Rp1-D21* mutants. Tryptophan serves as a precursor in the biosynthesis of benzoxazinoids (Tipton et al., 1973), which have antifungal properties (Hashimoto and Shudo, 1996). Nearly every mutant sampled had increased accumulation of all three aromatic amino acids in older leaves when compared to wild-type samples. The only mutant that did not have increased accumulation of any one of these amino acids was *FL-Les*. All three aromatic amino acids are synthesized from common precursors indicating the similar accumulation of these compounds amongst the mutants may be from increased flux from a shared upstream pathway such as the shikimate pathway. The differential accumulation of these compounds in mutant vs. wild-type siblings was not as common in upper leaf samples. For all three amino acids, less than half the mutants showed increased accumulation of either compound in upper leaves. These findings suggest that accumulation of these amino acids is induced as mutants age and lesion severity increases. The accumulation of these amino acids in *Bfl1* stands out. In upper leaf samples, *Bfl1* accumulated higher than wild-type levels of phenylalanine and tyrosine but lower than wild-type levels of tryptophan. In the biosynthesis of these amino acids, chorismate is converted to anthranilate, a precursor for tryptophan, or prephenate, a precursor for phenylalanine or tyrosine. The accumulation of these amino acids in *Bfl1* mutants indicates there is an inhibition in tryptophan biosynthesis after the conversion of chorismate to anthranilate.

The last individual compounds I analyzed were the chlorophyll breakdown products NCC1 (Figure 2.8) and NCC2 (Figure 2.9). As expected for lesion mutants, there were elevated levels of NCC1 and NCC2 in lower leaves of nearly all mutants compared to wild-type controls. The accumulation of these compounds in upper leaves across the mutants was less uniform. Three mutants, *les-E27*, *Les-Mop1*, and *FL-Les* accumulated significantly less than wild-type levels of NCC1 and NCC2 in upper leaves. Any deficiencies in chlorophyll biosynthesis or catabolism would likely also result in decreased accumulation of NCC1 and NCC2. While the enzymatic

mechanisms have not been fully elucidated in maize, NCC1 and NCC2 are seemingly the expected products of the reactions catalyzed by LLS1 in maize (Simmons et al., 1998) (ACD1 in Arabidopsis (Greenberg et al., 2000)) and the gene homologous to Arabidopsis ACD2 (Mach et al., 2001). *lls1, acd1,* and *acd2* mutants are known lesion mutants that accumulate phototoxic breakdown products. Thus, lesion formation in *les-E27*, *Les-Mop1*, and *FL-Les* may be caused by a similar mechanism. There was a strong positive correlation between accumulation of NCC1 and NCC2 in both upper and lower leaves indicating they are likely synthesized from a common chlorophyll breakdown pathway.

A goal of this work was to identify lesion mutants with common metabolic perturbations. my first comparison using all 368 samples (Figure 2.10) demonstrated that leaf age had a significant influence on metabolite accumulation as the samples clustered into nearly a perfect bifurcation of upper and lower leaf samples. A previous report found that the metabolite profile of a maize leaf varies from the base of the leaf to the tip (Zhou et al., 2019). My findings demonstrate a large variation in metabolism between upper and lower leaves. While this might be expected for wild-type plants, my clustering indicates the metabolite profile of a lower leaf from any lesion mutant was more like that of a lower leaf from a wild-type plant than to that of an upper leaf from that same lesion mutant. These finding caution that standardized tissue harvesting practices should be observed when comparing metabolomes across different samples.

The comparison of the FC accumulation of features in the 23 mutants identified four mutants, *Les10*, *Les17*, *Les23-like*, and *Bfl1*, whose metabolite profiles were like that of the known HR-mutant *Rp1-D21* (Figure 2.11A). Dr. Rajdeep Khangura has recently identified the causal gene of *Bfl1* as a yet-to-be characterized glutamate receptor. *Les10* and *Les17* mutants hyperaccumulate pathogenesis-related genes consistent with them being HR-like or autoimmune LMMs (Morris et al., 1998; Mu et al., 2021) as indicated by the similarity of their metabolic perturbations to those of *Rp1-D21*. I have prioritized the characterization of *Les10* and *Les17* and I have ongoing projects working with both mutants. Chapter 3 of this dissertation contains my work characterizing *Les10*.

The *Les9* mutant was included in this analysis in two genetic backgrounds. Despite both mutants containing the same mutant allele, the *Les9:B73* and *Les9:Mo20W* samples did not cluster together in the metabolite analysis (Figure 2.11A). This finding questions the validity of any of the groupings, as the same mutant did not cluster together. Genetic background affects lesion severity and metabolite accumulation in *Rp1-D21/+* mutants (Ge et al., 2021) indicating the non-

clustering of *Les9:B73* and *Les9:Mo20W* samples may be due to genetic background. In this clustering, metabolite levels were normalized to a sibling wild-type sample; however, this correction would not account for any metabolite that accumulates in one genetic background and not in the other. With this in mind, it is likely that this clustering analysis would be improved by introgressing every mutant into the same genetic background.

Evaluation of the success of the clustering analysis will come after determining the underlying genetic cause of more mutants included in this analysis. A limitation of my clustering analyses was the lack of known mutants. The arbitrary clusters (Figure 2.11A) that contain only uncharacterized mutants were not as informative about the etiology of those mutants as the cluster of mutants with *Rp1-D21*. Identifying a single mutant from any of these clusters will immediately direct the molecular characterization of the other mutants in that cluster.


## 2.5    Declaration of collaborate work

All field grown material was maintained by Dr. Gurmukh Johal (Purdue University) and his laboratory. Leaf tissue was harvested with assistance from Dr. Bong-Suk Kim (Purdue University). LC-MS analysis was performed by Dr. Bruce Cooper (Purdue University). Results interpretation and writing was performed in consultation with my advisor, Dr. Brian Dilkes (Purdue University), and my dissertation advisory committee members, Dr. Johal, Dr. Sujith Puthiyaveetil (Purdue University), Dr. Joshua Widhalm (Purdue University), and Dr. Jennifer Wisecaver (Purdue University).

## 2.6    Figures and Tables
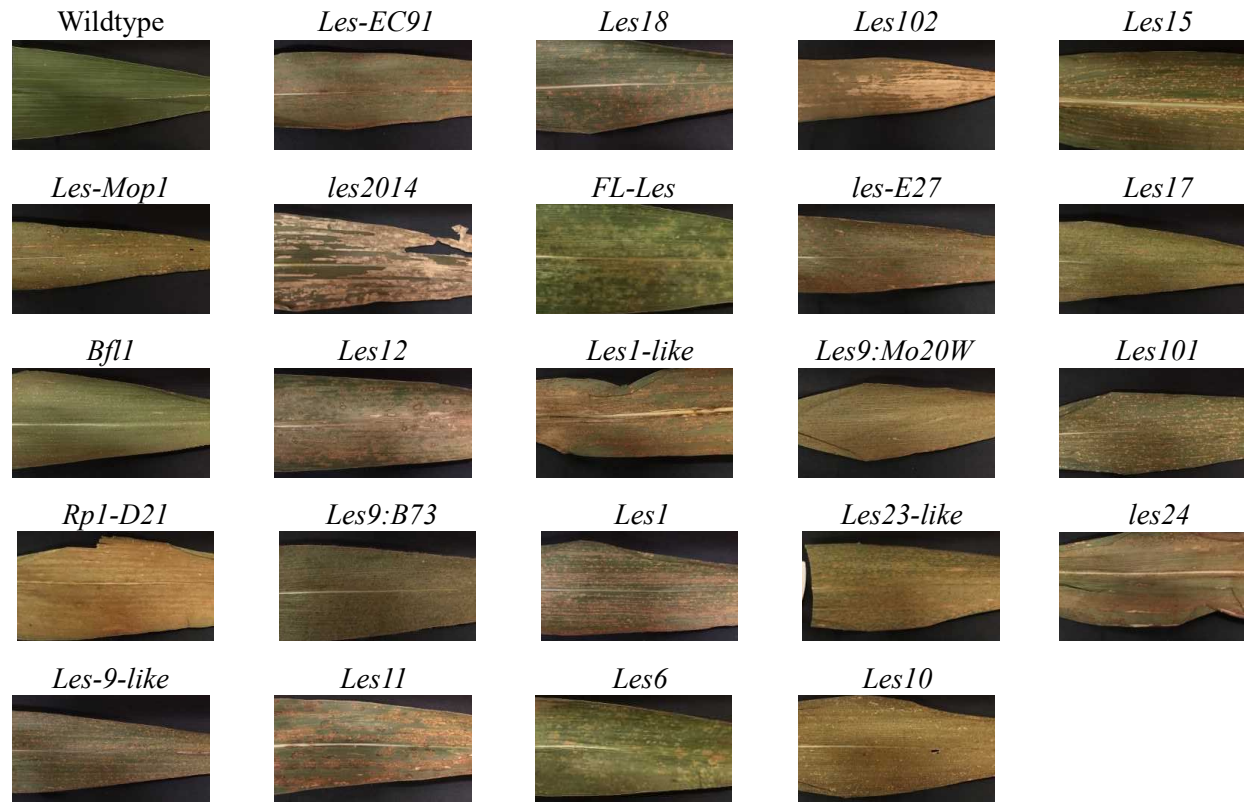
**Figure 2.1: Diversity of the maize lesion mimic mutants used in this study.**

Representative leaves a wild-type plant and the 23 different lesion mimic mutants that were metabolically analyzed.

**Table 2.1: Crossing information and genetic background of the lesion mutants included in this analysis.**

| Lesion mutant | Ear Parent | Pollen Parent | Background |
|---|---|---|---|
| *Les-EC91* | B73 | *Les-EC91/+:B73* | B73 |
| *FL-Les* | W22 | *FL-Les/+:W22* | W22 |
| *Bfl1* | Mo17 | *Bfl1/+:Mo17* | Mo17 |
| *les-E27* | *les-E27/+* | *les-E27/+* | Mixed |
| *Les9-like* | B73 | *Les9-like/+:B73* | B73 |
| *Les-Mop1* | Mo20W | *Les-Mop1/+:Mo20W* | Mo20W |
| *Les1* | B73 | *Les1/+:B73* | B73 |
| *Les1-like* | B73 | *Les1-like/+:B73* | B73 |
| *Les10* | B73 | *Les10/+:B73* | B73 |
| *Les101* | B73 | *Les101/+:B73* | B73 |
| *Les102* | B73 | *Les102/+:B73* | B73 |
| *Les11* | Wt-Sib | *Les11/+* | Mixed |
| *Les12* | Wt-Sib | *Les12/+* | Mixed |
| *Les15* | Wt-Sib | *Les15/+* | Mixed |
| *Les17* | B73 | *Les17/+:B73* | B73 |
| *Les18* | Wt-sibling | *Les18/+* | Mixed |
| *les2014* | *les1014/+:Mo17* | *les2014/+:Mo17* | Mo17 |
| *Les23-like* | B73 | *Les23/+:B73* | B73 |
| *Les6* | Wt-sibling | *Les6/+* | Mixed |
| *Les9:B73* | B73 | *Les9/+:B73* | B73 |
| *Les9:Mo20W* | Mo20W | *Les9/+:Mo20W* | Mo20W |
| *les24* | *les24/+:B73* | Self-pollinated | B73 |
| *Rp1-D21* | H95 | *Rp1-D21/+:H95* | H95 |

**Table 2.2: Number of mass features reproducibly detected for each lesion mutant.**

| Lesion Mutant | Lower Leaves | | Upper Leaves | |
|---|---|---|---|---|
| | Detected Features | Differentially Accumulated | Detected Features | Differentially Accumulated |
| Les-EC91 | 4,547 | 2,075 | 3,973 | 330 |
| FL-Les | 4,259 | 1,837 | 3,401 | 1,401 |
| Bfl1 | 4,686 | 2,192 | 4,360 | 2,025 |
| les-E27 | 4,153 | 2,348 | 4,209 | 640 |
| Les9-like | 4,670 | 1,024 | 3,818 | 316 |
| Les-Mop1 | 4,076 | 832 | 3,568 | 577 |
| Les1 | 4,468 | 1,887 | 3,501 | 339 |
| Les1-like | 4,256 | 2,617 | 3,738 | 1,037 |
| Les10 | 5,174 | 2,890 | 3,558 | 851 |
| Les101 | 5,054 | 1,044 | 4,050 | 249 |
| Les102 | 4,710 | 3,105 | 3,410 | 643 |
| Les11 | 4,228 | 1,633 | 3,264 | 306 |
| Les12 | 4,184 | 1,765 | 3,175 | 474 |
| Les15 | 3,854 | 1,518 | 3,648 | 1,025 |
| Les17 | 3,924 | 2,143 | 3,604 | 956 |
| Les18 | 3,682 | 1,310 | 3,596 | 429 |
| les2014 | 4,689 | 1,612 | 3,702 | 766 |
| Les23-like | 3,896 | 1,957 | 4,007 | 1,411 |
| Les6 | 4,604 | 1,280 | 3,268 | 368 |
| Les9:B73 | 5,202 | 3,086 | 4,062 | 1,012 |
| Les9:Mo20W | 4,856 | 2,870 | 3,360 | 539 |
| les24 | 4,538 | 1,332 | 3,925 | 522 |
| Rp1-D21 | 5,255 | 3,539 | 3,975 | 1,735 |
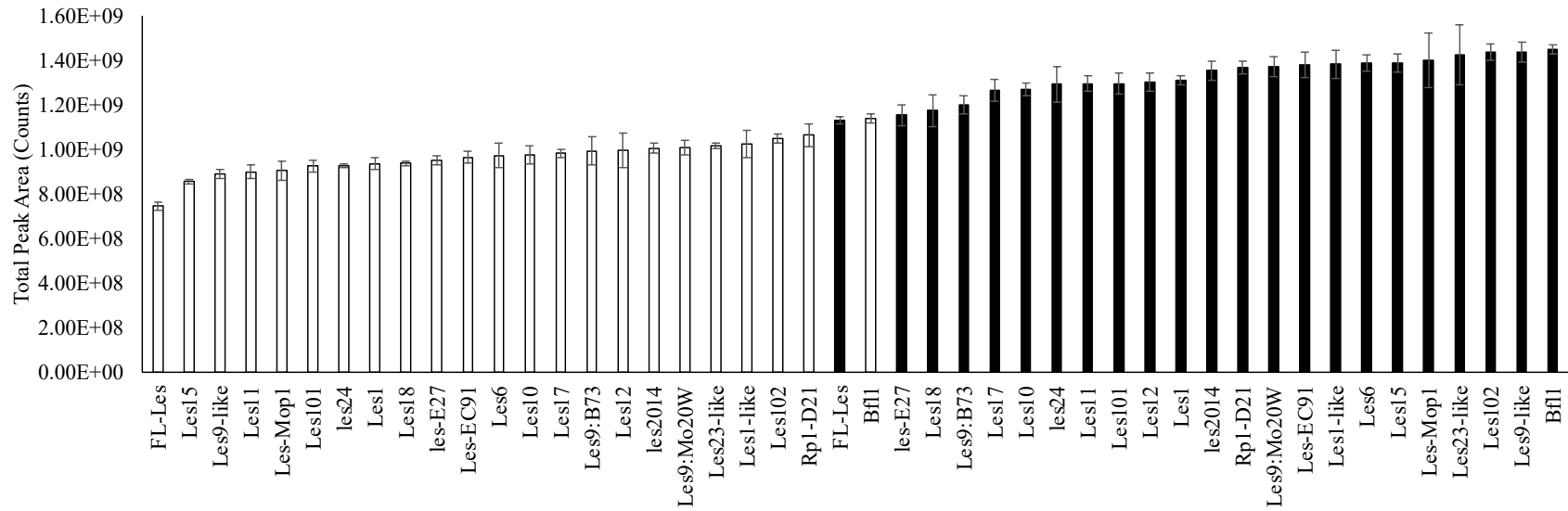
**Figure 2.2: Lower leaf samples have more total ion count than upper leaf samples.**

Average total ion count for all 22,732 detected mass features for lower leaf (black bars) and upper leaf (white bars) samples across the lesion mutants included in this analysis. Data presented are means $\pm$ standard errors (n = 4).
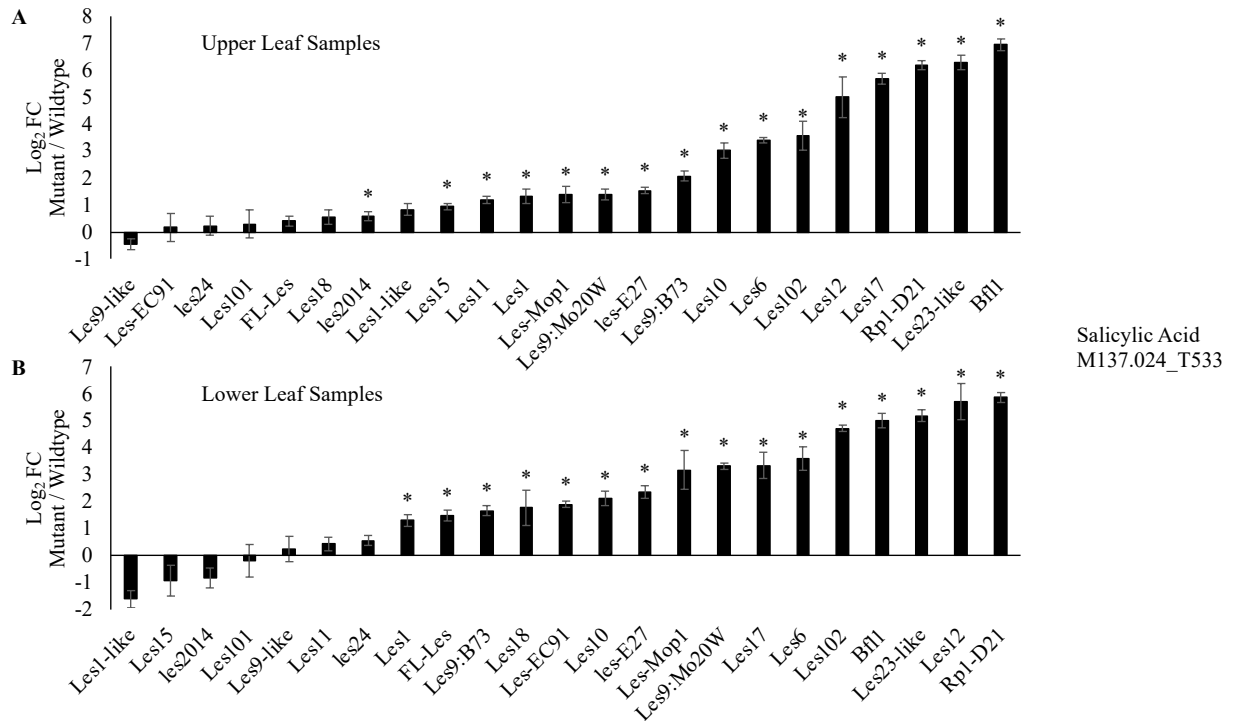
**Figure 2.3: Most lesion mutants included in this analysis accumulate high levels of salicylic acid.**

Average $\log_2$ FC (mutant/wildtype) of salicylic acid for (A) upper leaf and (B) lower leaf samples from each mutant. Values presented are means $\pm$ standard errors. Stars above bars represent significantly different accumulation between mutant and wild-type siblings (Student's T-test, $p < 0.05$).
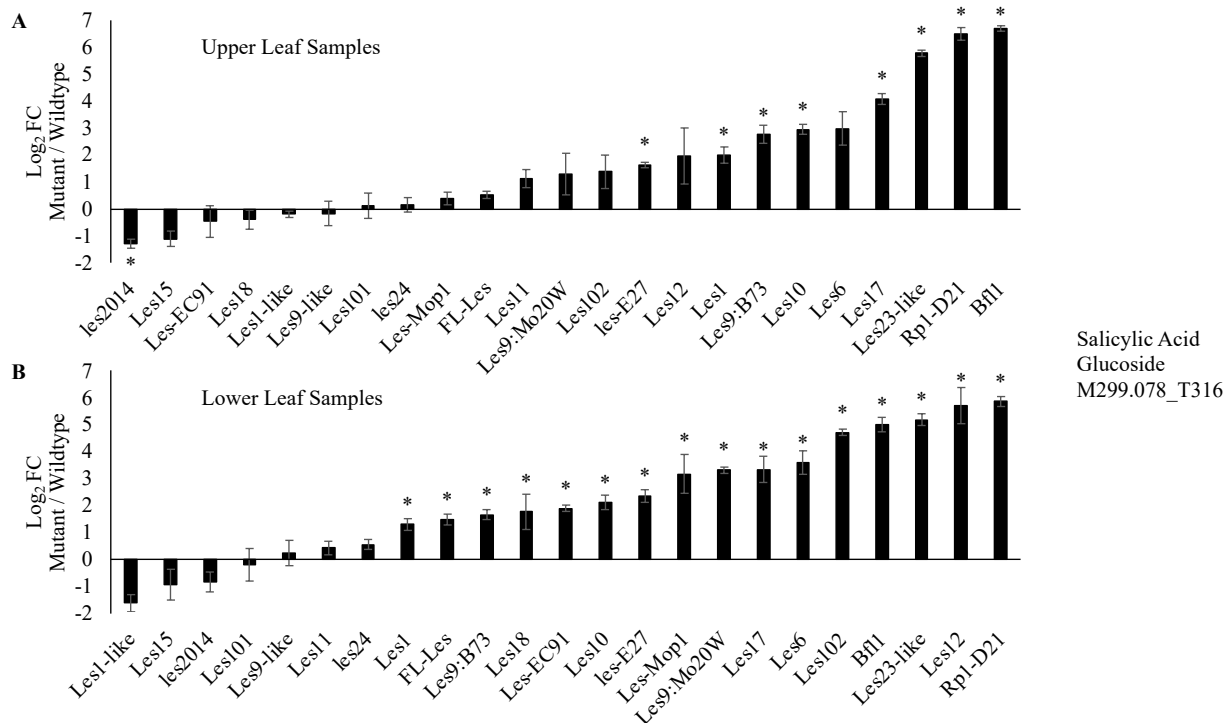
**Figure 2.4: Salicylic acid is abundantly converted to salicylic acid glucoside in maize lesion mutants.**

Average $\log_2$ FC (mutant/wildtype) of salicylic acid glucoside for (A) upper leaf and (B) lower leaf samples from each mutant. Values presented are means $\pm$ standard errors. Stars above bars represent significantly different accumulation between mutant and wild-type siblings (Student's T-test, $p < 0.05$).
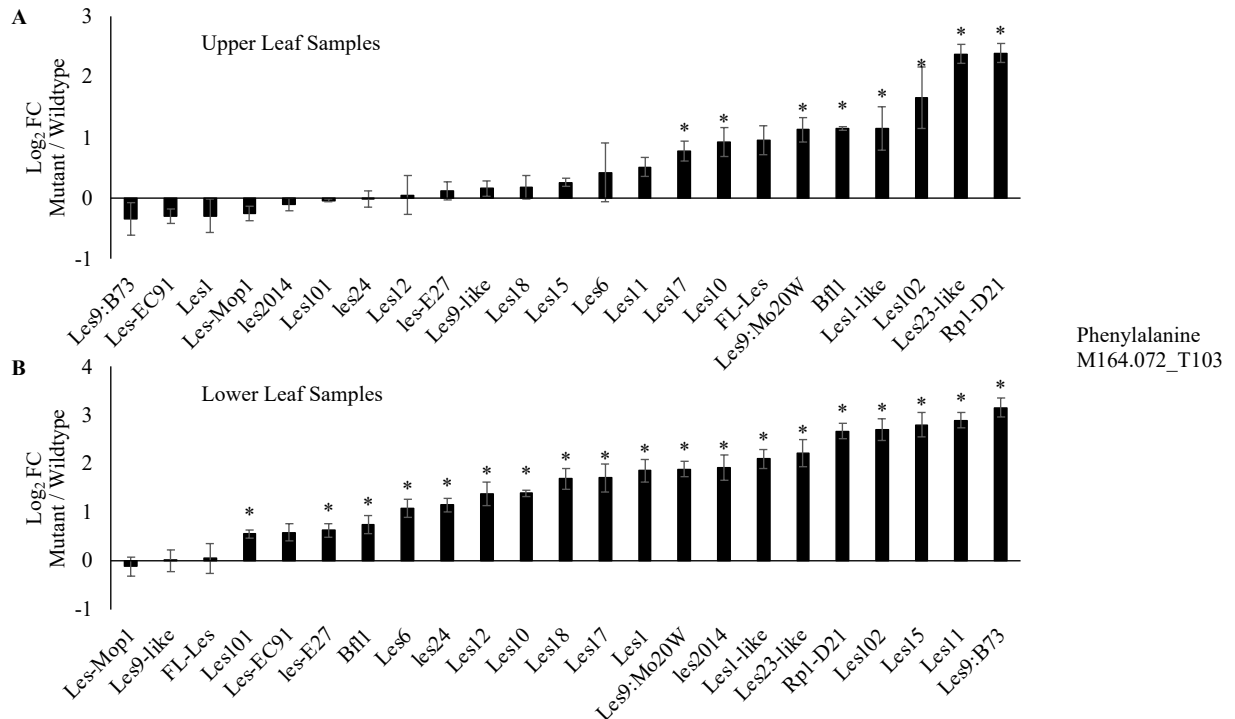
**Figure 2.5: Phenylalanine accumulation is elevated in lower leaves of most maize lesion mutants included in this analysis.**

Average log$_2$ FC (mutant/wildtype) of phenylalanine for (A) upper leaf and (B) lower leaf samples from each mutant. Values presented are means $\pm$ standard errors. Stars above bars represent significantly different accumulation between mutant and wild-type siblings (Student's T-test, $p < 0.05$).
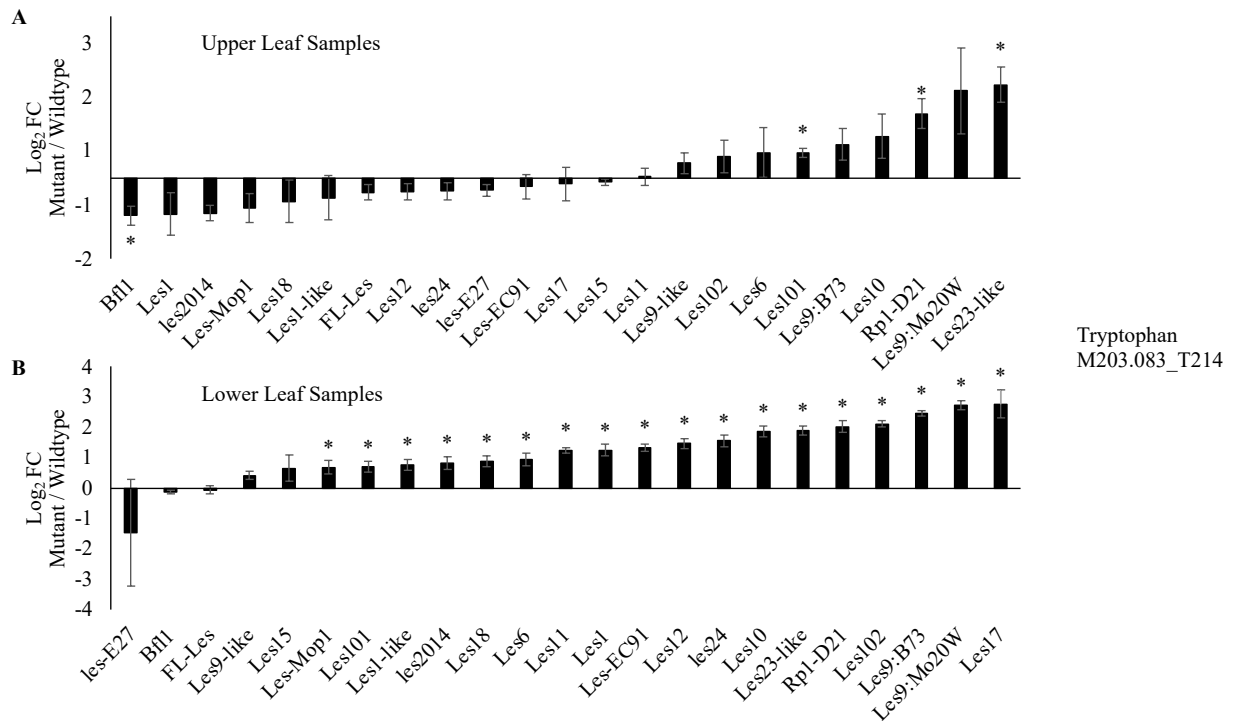
**Figure 2.6: Tryptophan accumulation is elevated in lower leaves of most maize lesion mutants included in this analysis.**

Average log2 FC (mutant/wildtype) of tryptophan for (A) upper leaf and (B) lower leaf samples from each mutant. Values presented are means + standard errors. Stars above bars represent significantly different accumulation between mutant and wild-type siblings (Student's T-test, $p < 0.05$).
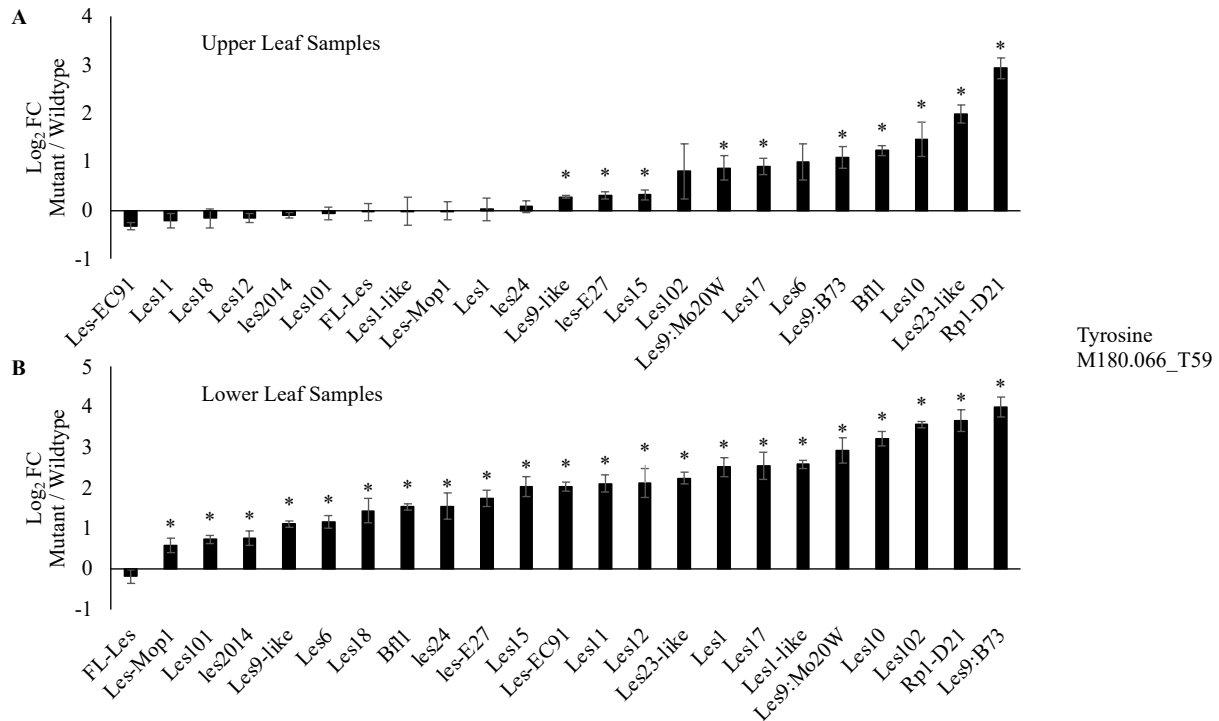
**Figure 2.7: Tyrosine accumulation is elevated in lower leaves of most maize lesion mutants included in this analysis.**

Average log$_2$ FC (mutant/wildtype) of tyrosine for (A) upper leaf and (B) lower leaf samples from each mutant. Values presented are means $\pm$ standard errors. Stars above bars represent significantly different accumulation between mutant and wild-type siblings (Student's T-test, $p < 0.05$).
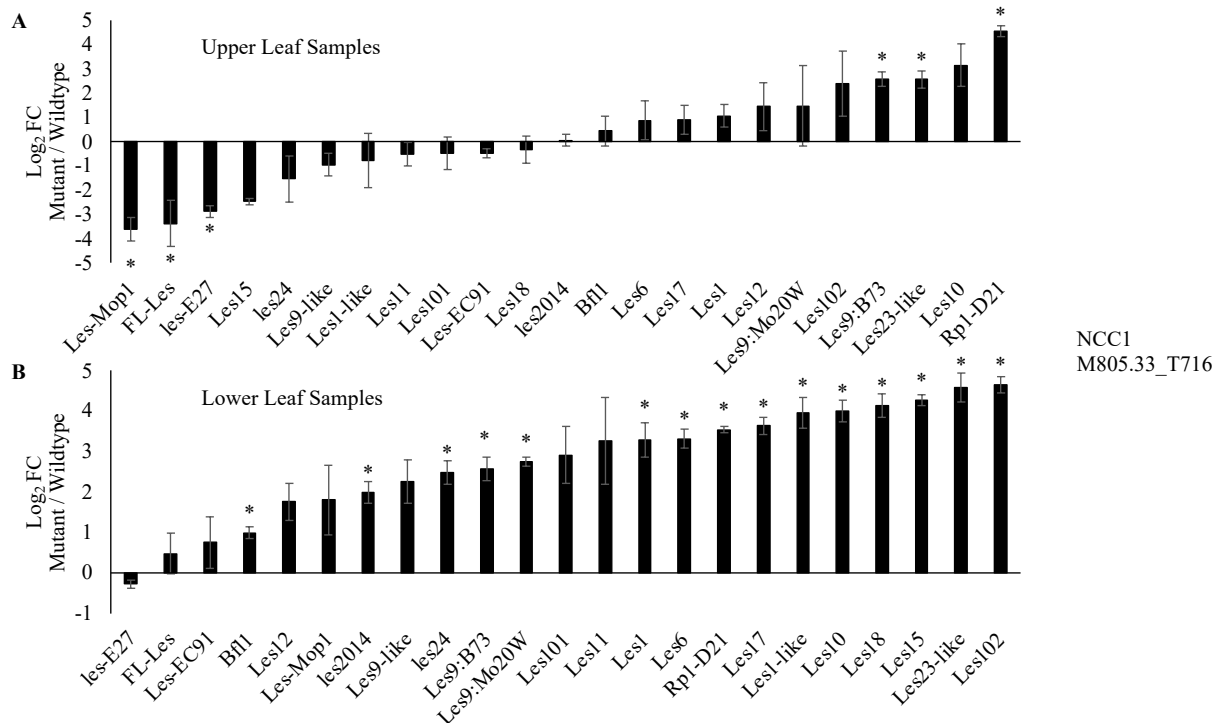
**Figure 2.8: NCC1 accumulation is elevated in lower leaf samples of most lesion mutants included in this analysis.**

Average $\log_2$ FC (mutant/wildtype) of NCC1 for (A) upper leaf and (B) lower leaf samples from each mutant. Values presented are means $\pm$ standard errors. Stars above bars represent significantly different accumulation between mutant and wild-type siblings (Student's T-test, $p < 0.05$).

**A** Upper Leaf Samples

**B** Lower Leaf Samples
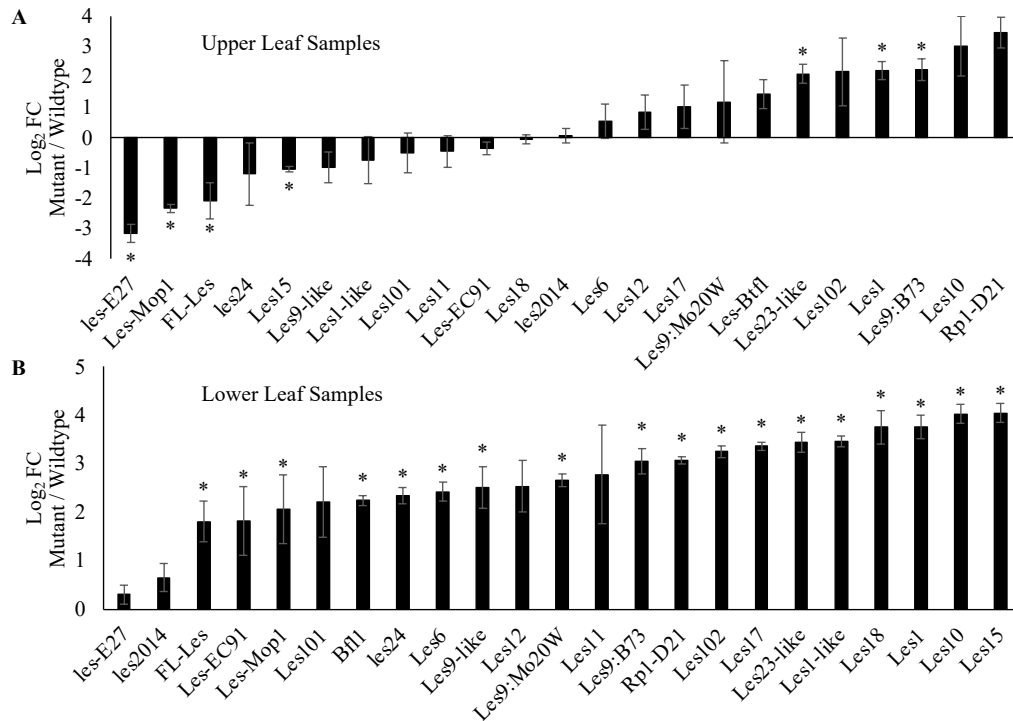
NCC2
M839.336_T593

**Figure 2.9: NCC2 accumulation is elevated in lower leaf samples of most lesion mutants included in this analysis.**

Average $\log_2$ FC (mutant/wildtype) of NCC2 for (A) upper leaf and (B) lower leaf samples from each mutant. Values presented are means $\pm$ standard errors. Stars above bars represent significantly different accumulation between mutant and wild-type siblings (Student's T-test, $p < 0.05$).
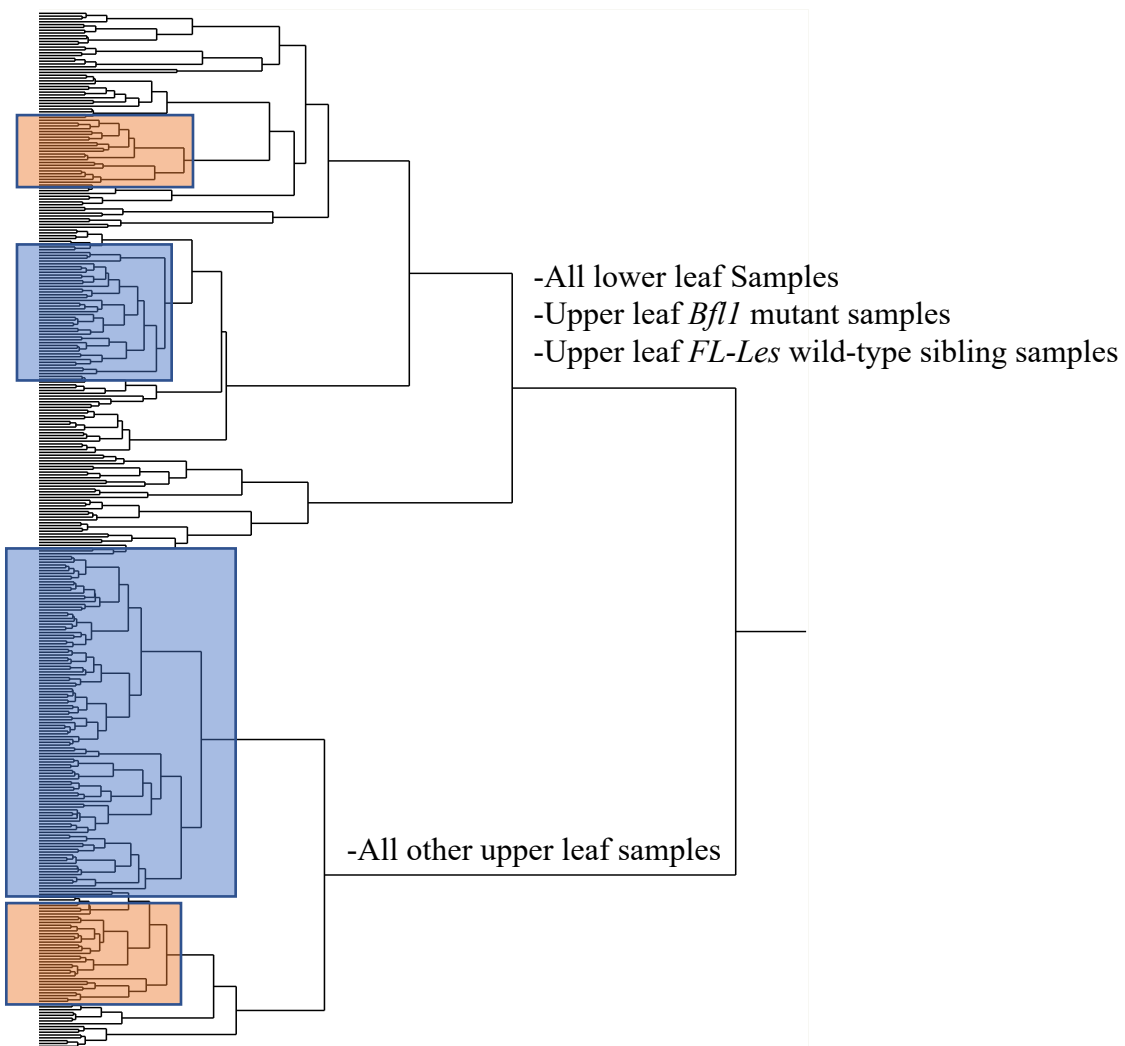
**Figure 2.10: Leaf age has a strong influence on metabolic similarity**.

Hierarchal clustering of all 368 metabolite samples using the raw ion counts of the 22,732 reproducibly detectable mass features. Samples were clustered using the Ward method. Shaded boxes span the clades that contain the wild-type sibling samples from the B73 (blue boxes) and mixed (orange boxes) genetic backgrounds.

**Table 2.3: Correlation coefficients of biological replicates of each lesion mutant.**

| Lesion Mutant | Correlation coefficient between the log$_2$ FC (mutant/wildtype) of biological replicates | |
|:---:|:---:|:---:|
| | Lower leaves | Upper leaves |
| *Les-EC91* | 0.76 $\pm$ 0.01 | 0.32 $\pm$ 0.02 |
| *FL-Les* | 0.66 $\pm$ 0.03 | 0.75 $\pm$ 0.01 |
| *Bfl1* | 0.68 $\pm$ 0.02 | 0.74 $\pm$ 0.01 |
| *les-E27* | 0.81 $\pm$ 0.01 | 0.54 $\pm$ 0.02 |
| *Les9-like* | 0.53 $\pm$ 0.01 | 0.42 $\pm$ 0.02 |
| *Les-Mop1* | 0.51 $\pm$ 0.05 | 0.52 $\pm$ 0.03 |
| *Les1* | 0.84 $\pm$ 0.01 | 0.61 $\pm$ 0.03 |
| *Les1-like* | 0.86 $\pm$ 0.01 | 0.55 $\pm$ 0.01 |
| *Les10* | 0.85 $\pm$ 0.01 | 0.55 $\pm$ 0.07 |
| *Les101* | 0.58 $\pm$ 0.03 | 0.27 $\pm$ 0.04 |
| *Les102* | 0.85 $\pm$ 0.01 | 0.35 $\pm$ 0.06 |
| *Les11* | 0.77 $\pm$ 0.02 | 0.28 $\pm$ 0.03 |
| *Les12* | 0.79 $\pm$ 0.01 | 0.36 $\pm$ 0.05 |
| *Les15* | 0.77 $\pm$ 0.01 | 0.72 $\pm$ 0.01 |
| *Les17* | 0.79 $\pm$ 0.03 | 0.44 $\pm$ 0.04 |
| *Les18* | 0.71 $\pm$ 0.05 | 0.37 $\pm$ 0.02 |
| *les2014* | 0.65 $\pm$ 0.03 | 0.51 $\pm$ 0.03 |
| *Les23-like* | 0.77 $\pm$ 0.02 | 0.63 $\pm$ 0.01 |
| *Les6* | 0.58 $\pm$ 0.01 | 0.38 $\pm$ 0.04 |
| *Les9:B73* | 0.87 $\pm$ 0.00 | 0.36 $\pm$ 0.05 |
| *Les9:Mo20W* | 0.84 $\pm$ 0.02 | 0.40 $\pm$ 0.06 |
| *les24* | 0.55 $\pm$ 0.02 | 0.36 $\pm$ 0.01 |
| *Rp1-D21* | 0.89 $\pm$ 0.00 | 0.71 $\pm$ 0.01 |
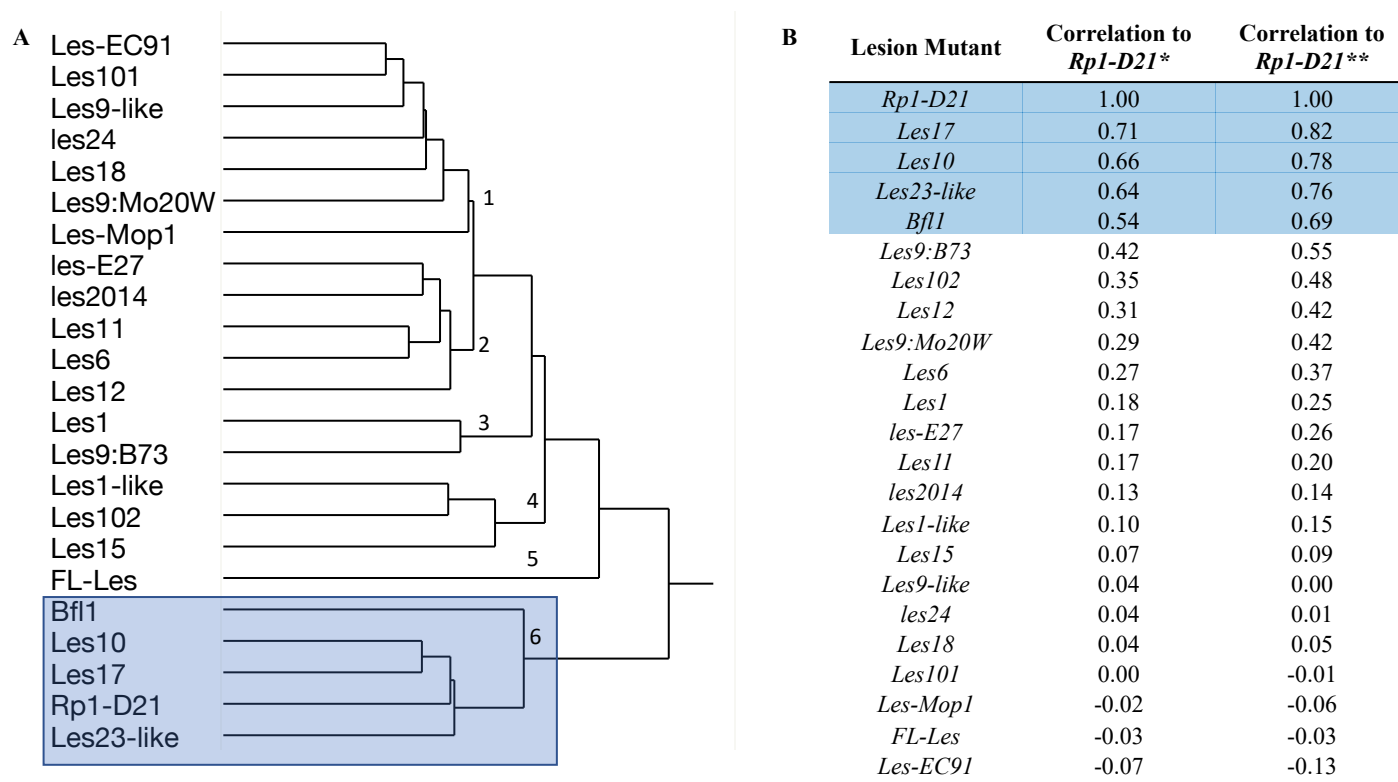
**Figure 2.11: There are a subset of lesion mutants whose metabolite profiles are like that of *Rp1-D21*.**

(A) Hierarchal clustering of the 23 lesion mutants using the log$_2$ FC accumulation (mutant/wildtype) of the 13,339 mass features that were reproducibly detected in upper leaf samples. Mutants were clustered using the Ward method. The shaded box spans the clade that contains *Rp1-D21*. Groupings as mentioned in results section 2.3.6 are denoted by numbers 1 through 6. (B) Correlation coefficients between the log$_2$ FC accumulation (mutant/wildtype) in *Rp1-D21* and the other 22 lesion mutants considering (*) all 13,339 reproducibly detectable mass features and (**) those features that significantly accumulate to different levels in *Rp1-D21/+* as compared to wild-type siblings. The mutants that cluster with *Rp1-D21* are shaded in blue.

# CHAPTER 3. GENETIC AND MOLECULAR CHARACTERIZATION OF THE MAIZE LESION MUTANT, LESION10

## 3.1 Introduction

The *Lesion10* (*Les10*, originally denoted as *Les\*-A607*) mutant was first identified in the early 1970s by Dr. Jerry Kermicle as a spontaneously arising mutant in an A632 stock that carried T-male sterile cytoplasm (personal communication with Dr. Kermicle). *Les10/+* mutants present small, round, chlorotic, and necrotic lesions on their leaf blades and leaf sheaths (Johal et al., 1995). Lesions are first visible on *Les10/+* mutants 10-14 days after sowing on the first leaf. Lesion severity increases as *Les10/+* mutants age, and there is a positive correlation between leaf age and the number of lesions on each leaf. Towards the end of the lifespan of *Les10/+* mutants, all leaves are completely covered with lesions resulting in early senescence compared to wild-type siblings. Outcrossing *Les10/+* heterozygous mutants with wild-type plants results in 1:1 segregation of lesion-forming plants to green plants in the F1-progenies and therefore, the *Les10* mutant has been regarded as dominant.

The gene encoding *Les10* is currently unknown; however, molecular studies of the mutant indicate it is likely encoded by a gene associated with plant immunity and/or defense response. Both *pathogenesis-related protein1* (*PR-1*) and *PR-5* are induced in *Les10/+* mutants, and the expression of both genes was positively correlated with *Les10* lesion severity (Morris et al., 1998). In addition, many genes associated with defense response are differentially expressed in *Les10/+* mutants(Mu et al., 2021). In Chapter 2 of this dissertation, I have shown that the metabolite profile of *Les10* is like that of the autoactive HR mutant, *Rp1-D21* (Figure 2.11), including the accumulation of SA (Figure 2.3), phenylalanine (Figure 2.5), and chlorophyll breakdown products associated with leaf senescence (Figures 2.8 and 2.9).

*Les10* has been mapped to chromosome 2; however, the physical position of *Les10* remains broad and enigmatic. *Les10* showed linkage with both *tassel seed1* and *white tip1* (David Hoisington, 1987); however, both genes are on the same side of *Les10*; therefore, this analysis did not provide a lower and upper bound of the region containing the *Les10* gene. A broad upper and lower bound for the region containing the *Les10* gene can be inferred from the moderate linkage of *Les10* with the translocation breakpoint stocks *waxy1* (*wx1)* T2-9b and *wx1* T2-9d (Gerald Neuffer, 1994). The exact physical positions of T2-9b and T2-9d have not been mapped; however,

considering other linkage analyses using these stocks, their positions are estimated to be at ~50,000,000 and ~200,000,000, respectively, in relation to the B73 version 4 (v4) assembly (Jiao et al., 2017) on chromosome two. The *Les10* gene is likely between these physical positions.

In this work, I provide a phenotypic and molecular characterization of *Les10/+* heterozygous and *Les10/Les10* homozygous mutants. I demonstrate that *Les10/+* heterozygous mutants are stunted and contain less chlorophyll than wild-type siblings. I show that these phenotypes are even more severe in *Les10/Les10* homozygous mutants and that *Les10/Les10* homozygous mutants completely suppress the formation of tassels, ears, and brace roots. I perform genome-wide association studies (GWAS) using variation in *Les10* trait severity in *Les10/+* hybrids to identify gene candidates that modify the *Les10* phenotype. Lastly, I discuss the prospect of using whole genome sequencing of *Les10/Les10* homozygous mutants and somatic wild-type revertant sectors of *Les10/+* heterozygous mutants to identify the gene encoding *Les10*.

## 3.2    Materials and Methods

### 3.2.1    Plant material and growth conditions

*Les10* mutants in three different genetic backgrounds were used for these experiments. The first *Les10* material was obtained from Dr. Gurmukh Johal (Purdue University) in which *Les10* had been introgressed into the B73 genetic background for eight generations by repeated backcrossing of B73 ear parents with *Les10/+* pollen parents. The second *Les10* material was obtained from Dr. Toni Kazic (University of Missouri) in which *Les10* had been introgressed into the Mo20W genetic background for five generations by repeated backcrossing of Mo20W ear parents with *Les10/+* pollen parents. The third *Les10* material was a B73/Mo20W hybrid generated by pollinating a B73 ear with pollen from a *Les10/+* mutant that had been backcrossed to the M020W background for five generations. All three sets of *Les10* material were segregating 1:1 for wild-type and lesion-containing plants.

The material segregating for *+/+*, *Les10/+,* and *Les10/Les10,* used for the degree of dominance tests and the sequencing of homozygous *Les10/Les10* mutants was generated by self-pollinating a *Les10/+* heterozygous mutant that had been backcrossed to the B73 genetic background for eight generations. For the GWAS, *Les10/+* mutants from the material from Toni Kazic were crossed to a panel of 378 inbred lines that included lines from the maize association

population (Flint-Garcia et al., 2005) and the Ames inbred panel (Romay et al., 2013). For all crosses, *Les10/+* pollen from multiple tassels was collected in tassel bags and bulk-combined in glassine wax bags. A small slit was made in the corner of the wax bag, and pollen was distrusted evenly onto an ear from each inbred line. This process was repeated daily over a two-week period to accommodate the differences in flowering time of the 378 inbred lines. Ears with viable seeds were recovered from 185 crosses.

All material was field grown at the Purdue Agronomy Center for Research and Education in West Lafayette, Indiana (40.4700° N, 86.9917° W). The material for the semi-dominance testing and GWAS was tractor planted in 3.84 m rows with interrow spacing of 0.79 m and alley spacing of 0.79 m. The material for the somatic sector analysis was jab-planted in one continuous row. Each F1-hybrid segregating for wild-type and *Les10/+* siblings was planted in two non-adjacent field plots containing 15 seeds. Supplemental irrigation was applied as needed and conventional fertilizer, pest control, and weed control practices for growing field maize in Indiana were followed.

### 3.2.2    Field phenotyping, data collection, and processing

Phenotyping of the material segregating for *+/+*, *Les10/+*, and *Les10/Les10* and the F1-hybrids from the GWAS were all performed the same way. All measurements other than lesion severity and chlorophyll content were made after plants had reached reproductive maturity. Lesion severity was scored at three different time points. For all time points, the severity score was determined visually considering each mutant within a plot. Early-season scoring was performed at 19-days after sowing using a 5-point severity scale. The middle-season and late-season scoring were performed 30- and 58-days after sowing using a 10-point severity scale. Chlorophyll content was measured on the middle of the second leaf below the flag leaf, on either side of the midrib, 31-days after sowing using a chlorophyll content meter (model CCM-200 plus; Opti-Sciences, Inc., Hudson, NH). Flag-leaf height and ear-height were measured using a 2" by 4" piece of wood that had been marked with centimeter spacing. Flag-leaf height and ear height were measured in centimeters from the base of the soil line to the auricle of the top leaf and from the base of the soil line to the node of the top ear, respectively. Number of tassel branches were determined by removing tassels and hand counting branches. Stalk width was measured in caliper units at the first ear node using a caliper. Number of ears-per-plant, number of above ground nodes with brace roots, and presence of *Ustilago maydis* (smut) were counted after visual inspection of plants.

### 3.2.3 Genome-wide association analysis

Lesion severity traits were the average score of the two separate plantings. Ears-per-plant values were generated by counting the total number of ears in mutant and wild-type siblings across both plantings and dividing by the total number of mutant and wild-type plants, respectively. The ears-per-plant trait was the ratio of these values in mutant divided by wild-type plants Flag-leaf height, chlorophyll content, stalk width, aboveground nodes with brace roots, and tassel branches traits were calculated by dividing the average value of these traits across three biological mutant replicates by the average value of these traits across three biological wild-type replicates.

The GWAS analysis was performed similarly to a previously described method (Khangura et al., 2019) with minor modifications. Briefly, approximately 83 million variant sites relating to the maize B73 reference genome v3 assembly were obtained from HapMap3 (Bukowski et al., 2018). Of the 185 inbred lines that I recovered ears from after crossing with *Les10/+*, 172 were genotyped as part of HapMap3. Each GWAS only considered hybrids that I had trait measurements for that were generated from crosses with these 172 genotypes. The 83 million variants were filtered using VCFtools (Danecek et al., 2011) and approximately 19 million variants that were present in more than 10% of lines with a minor allele frequency greater than 5% were considered for each GWAS. Each GWAS was performed using the R package "GAPIT" (Tang et al., 2016). Kinship and population structure values were calculated previously (Khangura et al., 2019) by using a subset of the 19 million SNPs. The Bonferroni statistical correction for multiple testing was determined by dividing 0.05 by the number of variants considered. The linkage tests were performed by incorporating each SNP as a reference allele or alternative allele as they corresponded to each line into the kinship matrix. Visualization of GWAS output was performed using R and Microsoft Excel.

### 3.2.4 Somatic sector generation

Approximately 400 seeds from the cross of a B73 ear parent by a *Les10/+*: Mo20W BC5 pollen parent were completely submerged in water containing 30 mM ethyl methanesulfonate for six hours in the dark. Seeds were rinsed eight times with water, patted dry using paper towers, and air dried for 12 hours in a fume hood with the door closed. Seeds were planted as described above. 14-days after emergence, all plants that did not present the *Les10* lesion phenotype were removed.

Plants were visually observed every five days, and any wild-type sectors in *Les10/+* mutants were tagged. After 60 days, the entire leaf containing each sector was harvested, photographed, and a portion of both the sector and mutant tissue was harvested from each leaf for DNA analysis.

### 3.2.5   DNA extraction and sequencing analysis

For all DNA extractions a 2 x 2 cm portion of plant tissue was placed in an Eppendorf tube, flash-frozen in liquid nitrogen, and stored at -80°C until processing. Before extraction, tubes were flash froze in liquid nitrogen again. Tissue was ground in the Eppendorf tube using a pipette tip. 600 µL of cetyltrimethyl ammonium bromide:2-mercaptoethanol solution (V:V – 40 mL:68 µL) was added, samples were vortexed for 10 seconds, and samples were incubated at 65°C for 45 minutes. 500 µL of 24:1 (V:V) chloroform:isoamyl alcohol was added and tubes were inverted five times until homogenous. Samples were centrifuged for 20 minutes at 16,550 x *g*, and the upper aqueous layer was transferred to a new tube. An equal volume of cold isopropanol was added to each sample and tubes were incubated at -20°C for at least one hour. Samples were centrifuged at 16,550 x *g* for 3 minutes and the entire liquid portion was pipetted away from the pellet. 150 µL of 70% aqueous ethanol (V:V) was added, samples were centrifuged at 16,550 x *g* for one minute, and all liquid was removed using a pipette. Samples were air-dried for 24 hours and resuspended in 50 µL of twice-distilled water. DNA concentrations and quality were determined and visualized using a Nanodrop and by gel electrophoresis, respectively. DNA from each sector was kept as an individual sample. DNA from nine *Les10/Les10* homozygous mutants was pooled before submitting for sequencing. All samples were stored at -20°C until sent for sequencing.

DNA sequencing was done by the Bindley Core for Genomics at Purdue University in West Lafayette, Indiana. Libraries were constructed from the submitted samples using the Illumina DNA Prep Kit. The resulting libraries were titered by adding a fixed volume of each to a pool and running that pool on an Illumina MiSeq cassette. Cluster counts for each library generated by the MiSeq run were used to create a normalized pool which was then run on a NovaSeq 6000 using S4 chemistry.

## 3.3    Results

### 3.3.1    *Les10* is semidominant

All previous studies of *Les10* have used *Les10/+* heterozygous mutants(Mu et al., 2021, 10; Morris et al., 1998), and there are currently no reports of homozygous *Les10/Les10* mutants. To generate and characterize *Les10/Les10* homozygous mutants I self-pollinated a *Les10/+:B73* heterozygous mutant. The F1-generation from this cross segregated for three phenotypes: green plants that resembled inbred B73 plants, moderately lesioned plants that resembled *Les10/+:B73* heterozygous mutants, and short plants that had numerous lesions and resembled a more severe *Les10* phenotype than *Les10/+* heterozygous mutants (Figure 3.1). The phenotypic segregation of green to *Les10/+:B73*-looking to *Les10*-severe plants in this F1-generation was 4:9:3 which is consistent with the 1:2:1 segregation of homozygous wildtypes to heterozygous mutants to homozygous mutants that would be expected for the progeny of a self-pollinated heterozygous mutant ($\chi^2$= 0.375, df = 2, *p* = 0.83). The segregation ratio of the F1-progeny and the increased phenotypic severity of the *Les10*-severe plants indicated that they are likely *Les10/Les10* homozygous mutants.

To further characterize the difference between *Les10/+* heterozygous and *Les10/Les10* homozygous mutants, I compared leaf chlorophyll content, flag-leaf height, first-ear height, number of tassel branches, number of ears-per-plant, and number of above ground nodes with brace roots in wildtype, *Les10/+* heterozygous mutants, and *Les10/Les10* homozygous mutants. Like lesion severity, chlorophyll content varied in heterozygous and homozygous *Les10* mutants. *Les10/+* mutants had 34% of wild-type chlorophyll levels while *Les10/Les10* mutants had only 7% of wild-type levels (Figure 3.2A). Plant height was also different between *Les10/+* and *Les10/Les10* mutants. *Les10/+* mutants were 15% shorter for flag-leaf height and 24% shorter for first-ear height than wild-type siblings (Figures 3.2B and 3.2C). The decrease in flag-leaf height was more severe for *Les10/Les10* mutants which were 59% shorter than wild-type siblings and 54% shorter than *Les10/+* siblings (Figures 3.1 and 3.2B). None of the *Les10/Les10* mutants produced an ear; therefore, I was unable to measure and compare their first-ear height to wild-type or *Les10/+* mutant siblings. There was no difference in the number of tassel branches in *Les10/+* mutants compared to wild-type siblings (Figure 3.2D). Like ears, none of the *Les10/Les10* mutants produced a tassel; therefore, I was unable to characterize how tassel branching in these mutants

varies from wildtype. All wild-type plants from this F1 population produced two ears. All *Les10/+* mutants produced one or two ears and the average number of ears-per-plant across the *Les10/+* mutants was 1.6 ± 0.15. As previously noted, none of the *Les10/Les10* mutants produced any ears (Figure 3.2E); thus, I was unable to compare the number of ears-per-plant in *Les10/Les10* mutants with that of wild-type or *Les10/+* mutant siblings. Lastly, there was a significant decrease in the number of aboveground nodes with brace roots in both *Les10/+* and *Les10/Les10* mutants. Wild-type plants had, on average, 4.0 ± 0.4 nodes with brace roots, while *Les10/+* mutants had only 1.4 ± 0.2 nodes with brace roots. No nodes with brace roots were observed for any *Les10/Les10* mutants (Figure 3.2F). In summary, *Les10/Les10* mutants had increased phenotypic severity compared to *Les10/+* mutants for lesion severity, chlorophyll content, and flag-leaf height. In addition, *Les10/Les10* mutants completely suppressed ear formation, tasseling, and generation of brace roots.

### 3.3.2  There is a modifier acting in cis located on chromosome 2 associated with *Les10* phenotypic severity

The severity of lesion mimic mutants can be influenced by genetic background and introgression of lesion mutants into some genetic backgrounds may suppress or enhance lesion formation (Johal et al., 1995; Gray et al., 1997). While there are no peer-reviewed reports of the influence genetic background has on *Les10* lesion severity, there are numerous photos on the Maize Genetics and Genome Database (MaizeGDB; www.maizegdb.org) that depict different lesion severities in *Les10/+* mutants that have been introgressed into different genetic backgrounds. If these differences in *Les10* lesion severity are under genetic control, I hypothesized that I could identify genes regulating *Les10* by GWAS and identifying genomic regions associated with variation in *Les10* phenotypic severity.

For this GWAS, *Les10/+* in a nearly isogenic Mo20W background was crossed as a pollen parent to an inbred association panel that consisted of 379 lines from the maize association population (Flint-Garcia et al., 2005) and the Ames inbred panel (Romay et al., 2013). I obtained viable seeds from 185 of these 379 crosses. These F1 populations segregated 1:1 for wild-type and *Les10/+* mutant siblings where all plants are hybrids for Mo20W and the genetic background of the inbred used for the cross. (Figure 3.3). Seeds from these 185 populations were planted in two field locations in 2020 at the Purdue University Agronomy Center for Research and Education in

West Lafayette, Indiana. Lesion severity was visually scored for each *Les10/+* hybrid at three time points: early-season, mid-season, and late-season. Severity scores were assigned using a 5-point (early-season; Figure 3.4A) or 10-point (mid-season and late-season) scale. There was a strong positive correlation between the lesion severity scores between duplicate plantings of each population in the early-season ($r = 0.72$, $p < 5E\text{-}31$), mid-season ($r = 0.78$, $p < 2E\text{-}39$) and late-season ($r = 0.51$, $p < 3E\text{-}13$) indicating that field position was likely not a significant factor influencing *Les10* lesion severity. The distribution in lesion severity for the early-season scoring was skewed-left, with most *Les10/+* hybrids having very minor lesion severity (Figure 3.4B). The distribution for mid-season scoring was slightly skewed-right, with most *Les10/+* hybrids having moderate lesion severity (Figure 3.4C). The distribution for late-season scoring was skewed-right, with most *Les10/+* hybrids having high lesion severity (Figure 3.4D). Like previously observed for *Les10/+* mutants in isogenic backgrounds, there was a general trend across these *Les10/+* hybrids of increased lesion severity as plants age. The average lesion severity of the early-season scoring was $1.94 \pm 0.07$, which increased to $2.71 \pm 0.06$ in the mid-season scoring, which further increased to $3.60 \pm 0.04$ for the late-season scoring.

To identify genetic loci associated with the variation in *Les10* lesion severity I performed GWAS using these scoring values as traits. HapMap3 genotype data was available for 172 of 185 inbred lines used to generate the F1 hybrids segregating for *Les10/+* mutants. For each of the three lesion scoring time points, the average lesion score between the two different plantings was calculated and used as the trait score for GWAS. The GWAS using the early-season scoring revealed a strong association on chromosome two (Figure 3.5A). Two single nucleotide polymorphisms (SNPs) on chromosome two, located at positions 135,041,479 and 133,848,291, in relation to the maize B73 v4 assembly (Jiao et al., 2017), passed the significance threshold for multiple test correction. The same strong association on chromosome two was also present in the GWAS using the mid-season scoring traits (Figure 3.5B). The same two SNPs, identified from the early-season scoring, also showed the most significant association in the mid-season scoring; albeit, for this scoring, the order of which SNP was most significant was reversed. There were no SNPs that passed the significance threshold for multiple test corrections in the late-season scoring GWAS; however, there was a moderately strong association in the same region of chromosome two as observed for both early-season and late-season scoring (Figure 3.5C). In the early-season scoring GWAS output, there were over 2,000 SNPs between positions 132,000,000 and

136,000,000 on chromosome two that passed a significance threshold of at least $p < 10^{-4}$. Many of many of these SNPs had a significance $p$-value close to that of the top SNP indicating this chromosomal region may have high linkage disequilibrium. If that were the case, then the presence of multiple significant SNPs at this location would likely be the result of linkage and not different loci associated with *Les10* severity. To determine if this region on chromosome two has linkage disequilibrium, I performed two separate GWAS that used the early-season scoring traits and considered the SNPs, 2-133,848,291 (Chromosome – Position relative to B73 v4 assembly) or 2-135,041,479, as cofactors. The SNPs between positions 132,000,000 and 136,000,000 that passed a significant threshold of $p < 10^{-4}$ association when only considering early-season lesion severity no longer passed that threshold when considering SNP 2-133,848,291 (Figure 3.5D) or 2-135,041,479 (Figure 3.5E) as cofactors. These findings indicate there is linkage disequilibrium in this region.

The most statistically significant SNP associated with early-season *Les10* lesion severity, SNP 2-135,041,479, is within the broad mapping window of *Les10*(Gerald Neuffer, 1994), indicating that this SNP may be a cis-acting polymorphism or is linked to a cis-acting modifier of *Les10*. To characterize gene candidates that may be associated with this polymorphism, I identified the gene that is closest in proximity to position 135,041,479 on chromosome two. This position is within an intron of an uncharacterized gene, Zm00001d004738 (Figure 3.6). The predicted protein sequence of this gene contains an ankyrin repeat domain and is 40% similar and 27% identical to Arabidopsis ACCELERATED CELL DEATH6 (ACD6). The Arabidopsis *acd6/+* mutant is a dominant gain-of-function defense response lesion mimic mutant (Rate et al., 1999).

Next, I compared how SNP 2-135,041,479 is associated with lesion severity and expression of genes in proximity. The most significant polymorphism is not always the cause of the observed variation, and often times the gene in closest proximity to the most significant polymorphism is not the causative gene (Baxter, 2020). The reference allele at position 135,041,479, present in the B73 inbred, is an adenine, and the alternative allele is a guanine. For the early-, mid-, and late-season scoring, the alternative allele was associated with an increase in *Les10/+* lesion severity (Figure 3.7). To determine if this polymorphism was associated with gene expression variation, I compared how each allele affects the expression of the five expressed genes, Zm00001d004734, Zm00001d004737, Zm00001d004738, Zm00001d004739, and Zm00001d004740 that are closest in proximity to this polymorphism using an available maize gene expression database (Kremling

et al., 2018). There was not a significant difference in the expression of Zm00001d004374, Zm00001d004737, or Zm00001d004740 for lines containing the alternate allele as compared to lines containing the reference allele at this position (Figure 3.7). Expression of Zm00001d004738 and Zm00001d004739 were differentially expressed in lines containing the alternate allele as compared to lines containing the reference allele at position 135,041,479; however, each gene was affected in the opposite direction. Zm00001d004738 was expressed to a lower extent in lines carrying the alternate allele while Zm00001d004739 was expressed at higher levels in these lines.

### 3.3.3   Lesion severity of *Les10/+* mutants negatively correlates with many *Les10* phenotypes

In addition to lesion severity, I measured chlorophyll content, stalk width, flag-leaf height, above ground nodes with brace roots, the number of ears-per-plant, and the number of tassel branches in these *Les10/+* hybrids compared to their wild-type siblings (Figure 3.8). The distribution in the ratio of chlorophyll content in mutant compared to wild-type siblings was skewed left with most mutants having less than 40% of wild-type chlorophyll levels (Figure 3.8A). The distribution in the ratio of stalk width in mutant compared to wild-type siblings was roughly normal centered around 0.7 (Figure 3.8B). The distribution in the ratio of flag-leaf height in mutant compared to wild-type siblings was skewed right (Figure 3.8C). The distributions in the ratio of above ground nodes with brace roots (Figure 3.8D) and ears-per-plant (Figure 3.8E) in mutant compared to wild-type siblings were skewed left. The distribution in the number of tassel branches in mutant compared to wild-type siblings was roughly normal centered around 0.9 (Figure 3.8F).

To determine how the variation in chlorophyll content, stalk width, flag-leaf height, aboveground nodes with brace roots, the number of ears-per-plant, and the number of tassel branches relate to *Les10/+* lesion severity, I calculated the correlation coefficients between the mid-season lesion scoring values and the ratio of these traits in mutant divided by wild-type siblings. *Les10/+* lesion severity was negatively correlated with chlorophyll content ($r = -0.78$, $p < 4E-38$), stalk width ($r = -0.65$, $p < 5E-23$), flag-leaf height ($r = -0.73$, $p < 2E-31$), above ground nodes with brace roots ($r = -0.56$, $p < 4E-31$), the numbers of ears-per-plant ($r = -0.67$, $p < 2E-47$), and the number of tassel branches ($r = -0.42$, $p < 3E-9$). These findings are consistent with my measurements of these traits in *Les10/+* and *Les10/Les10* mutants (Figure 3.2) and demonstrate that an increase in *Les10* lesion severity negatively correlates with plant development.

Due to the strong correlation between *Les10/+* lesion severity and chlorophyll content, stalk width, flag-leaf height, above ground nodes with brace roots, the number of ears-per-plant, and the number of tassel branches, I hypothesized that the SNPs identified from GWAS using lesion severity would also be associated with variation of these traits. To test this, I performed additional GWAS using each of these phenotypes as the traits (Figure 3.9). The same region on chromosome two associated with variation in *Les10/+* lesion severity (Figure 3.5) was associated with variation in chlorophyll content (Figure 3.9A), stalk width (Figure 3.9B), flag-leaf height (Figure 3.9C), aboveground nodes with brace roots (Figure 3.9D), and the number of ears-per-plant (Figure 3.9E). Despite the number of tassel branches negatively correlating with lesion severity, this region on chromosome two was not associated with variation in tassel branch number (Figure 3.9F).

### 3.3.4 *Les10* mutants are more susceptible to *Ustilago maydis* than wildtype siblings

Towards the end of the field season, there was increased pressure of corn smut caused by the fungus *Ustilago maydis* in the fields that contained the F1 hybrid populations. To determine if the susceptibility to corn smut was different in *Les10/+* mutants compared to wild-type siblings, I counted the number of infected mutant and wild-type plants in each plot and compared the proportion of infected plants. In replicate one, 128 of the 185 hybrids populations had smut on at least one mutant or wild-type sibling. In 95 of these 128 instances there was a higher proportion of mutant than wild-type plants that were infected by smut. In 65 of these 95 populations, smut was only detectable on mutant plants. For the 33 populations that had a higher proportion of wild-type than mutant plants infected by smut, smut was only detected on the wild-type plants in 24 instances. These proportions were similar for the second replicate planting where 123 of the 185 populations had detectable smut on at least mutant or wild-type sibling. In 92 instances, there was a higher proportion of mutant than wild-type plants that were infected by smut. In 61 of these 92 populations, smut was only detectable on mutant plants. For 31 populations, the proportion of wild-type plants infected with smut was greater than that of mutants. In 17 of these 31 instances, smut was only detectable on wild-type plants.

The duplicate planting of these hybrid populations allowed us to test if the susceptibility of *Les10/+* mutants to corn smut was consistent across the field. Of the 128 populations that had smut in replicate one and 123 populations that had smut in replicate two, 94 hybrid populations had

observable smut on at least one plant in both replicates. In 55 of these 94 hybrids, *Les10/+* mutant plants were infected with smut at a higher portion than wild-type siblings in both replicates. The proportion of wild-type plants with smut was higher than mutants in both replicates for only seven hybrids. In 17 and 14 hybrids, the proportion of mutants infected with smut was higher than wildtype for only rep one and rep two, respectively.

## 3.4    Discussion, Conclusions, and Future Directions

The majority of maize LMMs are dominant (Johal et al., 1995); however, the degree of dominance is unknown for most of these mutants. In this work I performed phenotypic characterization of *Les10/+* heterozygous and *Les10/Les10* homozygous mutants. Consistent with *Les10* being a semi-dominant mutant, the phenotypic severity of lesion formation (Figure 3.1), chlorophyll content (Figure 3.2A), flag leaf height (Figure 3.2A), suppression of ear formation (Figure 3.2E), and suppression of brace root formation (Figure 3.2F) was greater in *Les10/Les10* homozygous mutants than *Les10/+* heterozygous mutants. A similar analysis, as I have performed for *Les10,* of phenotypic severity in heterozygous and homozygous mutants of the other uncharacterized maize LMMs should be effective at determining their degree of dominance.

*Les10/Les10* homozygous mutants completely suppressed the formation of ears, tassels, and brace roots. The absence of ears (barren stalk phenotype; Gallavotti et al., 2011), formation of tassels (Wang et al., 2022), and formation of brace roots (Hostetler et al., 2021) all are under known genetic control. While the *Les10* gene is unknown, it is possible *Les10* is also involved in genetic regulation of these periphery. However, it is also possible that *Les10/Les10* mutants suppress ear, tassel, and brace root formation due to stress and sickness of the plant. Ear formation and tassel growth can be suppressed during stress (Danilevskaya et al., 2019), and the lack of these periphery in *Les10/Les10* homozygous mutants may be simply due to fitness consequences. This would be consistent with the overall height defects (Figures 3.1 and 3.2B) and leaf wilting (Figure 3.1) observed for *Les10/Les10* mutants compared to wild-type siblings. The identification of the *Les10* gene will provide insights into the possibility *Les10* directly regulates ear, tassel, and brace root formation.

Using GWAS, I identified a locus on chromosome two associated with variation in *Les10* lesion severity. Within this locus, is a gene, Zm00001d004738, whose predicted protein product contains an ankyrin repeat domain and is 40% similar and 27% identical to Arabidopsis

ACCELERATED CELL DEATH6 (ACD6). This gene is a strong candidate that may regulate *Les10* as a dominant gain of function *acd6* mutant in Arabidopsis also produces lesions and accumulates high levels of SA (Rate et al., 1999; Lu et al., 2003). In addition, natural variation in Arabidopsis *ACD6* leads to differences in immune response and plant growth (Todesco et al., 2014). Further testing is needed to determine if Zm00001d004738 directly regulates *Les10*. There was an association between differential expression of Zm00001d004738 and *Les10* lesion severity (Figure 3.7); however, these may be two phenomena that a linked to another factor.

Since Zm0001d004738 is within the broad mapping window or *Les10*, it is possible Zm00001d004378 is the gene encoding *Les10* and not just a putative modifier of *Les10*. In a similar GWAS analysis as I performed here, the most significant SNP associated with chlorophyll variation in hybrids of *Oil yellow 1-N1989* (*Oy1-N1989*), a gene involved in chlorophyll biosynthesis, was in the *Oy1* gene itself (Khangura et al., 2019), indicating this analysis can identify causative genes. Furthermore the phenotypes of *Les10/+* mutants are consistent with Arabidopsis *acd6/+* mutants (Rate et al., 1999; Lu et al., 2003) and the susceptibility to *Ustilago maydis* is consistent with a known ankyrin repeat containing mutant of maize (Zhang et al., 2019).

A clear limitation inhibiting the interpretation of these characterizations of *Les10* mutants is the lack of knowing what gene encodes *Les10*. I currently have ongoing projects focused on determining this gene. The phenotypes of some dominant gain-of-function LMMs are cell autonomous, and lesion formation can be completely suppressed on a cell-by-cell basis by mutating the gene causing lesion formation (Balint-Kurti, 2019). This can result in chimeric plants whose leaves are covered with lesions except for sectors of wild-type revertant tissue for which the causative gene has been knocked out (Balint-Kurti, 2019). I hypothesized that I could identify the causative polymorphism encoding *Les10* by generating multiple independent wild-type revertant sectors in *Les10/+* heterozygous plants and identifying a common gene that is mutated in every sector. In addition, since all these sectors would be from *Les10/+* plants carrying the *Les10* allele, the mutant alleles found in the sectors should all be in cis with the causative polymorphism of *Les10*. This technique was previously used to identify the causative mutation and the gene encoding *Bfl1* (Khangura et al., unpublished).

I have generated wild-type revertant sectors in *Les10/+* mutants by performing an ethyl methanesulfonate (EMS) mutagenesis of seeds segregating 1:1 for *Les10/+* mutants and wild-types siblings. EMS mutagenesis predominantly produces G/C to A/T transitions (Greene et al.,

2003). I have recovered seven independent wild-type revertant sectors out of 200 *Les10/+* mutants (Figure 3.10). Sectors 1, 2, 3, and 7 were in the middle of the leaf, and the wild-type revertant portion of the leaf was bordered by lesion-containing tissue on both its left and right sides. Sectors 4, 5, and 6 were on the edge of the leaves and only were bordered by lesion containing tissue on one side. Sector 1 still contained visible lesions within the sector while all other sectors were completely void of lesions. I have extracted DNA from each sector and have submitted for whole-genome sequencing along with a pool of DNA from *Les10/Les10* mutants. I will combine these sequencing results with fine mapping to identify a set of gene candidates that may be the *Les10* gene.

## 3.5    Declaration of collaborative work

All field grown material was maintained with the assistance of Dilkes laboratory members. *Les10* material used in this analysis was previously generated by Dr. Gurmukh Johal (Purdue University) and Toni Kazic (University of Missouri). Pollinations and trait measurements were performed with the assistance of Dr. Rajdeep Khangura (Purdue University) and Alyssa Nestor (Purdue University). Results interpretation and writing was performed in consultation with my advisor, Dr. Brian Dilkes (Purdue University), and my dissertation advisory committee members, Dr. Johal, Dr. Sujith Puthiyaveetil (Purdue University), Dr. Joshua Widhalm (Purdue University), and Dr. Jennifer Wisecaver (Purdue University).

## 3.6    Figures and Tables



**Figure 3.1: Lesion severity in *Les10/Les10* homozygous mutants is more severe than *Les10/+* heterozygous mutants.**

Representative (A) plants and (B) leaves of a wildtype (+/+), *Les10/+* heterozygous mutant, and *Les10/Les10* homozygous mutant 50-days post planting.
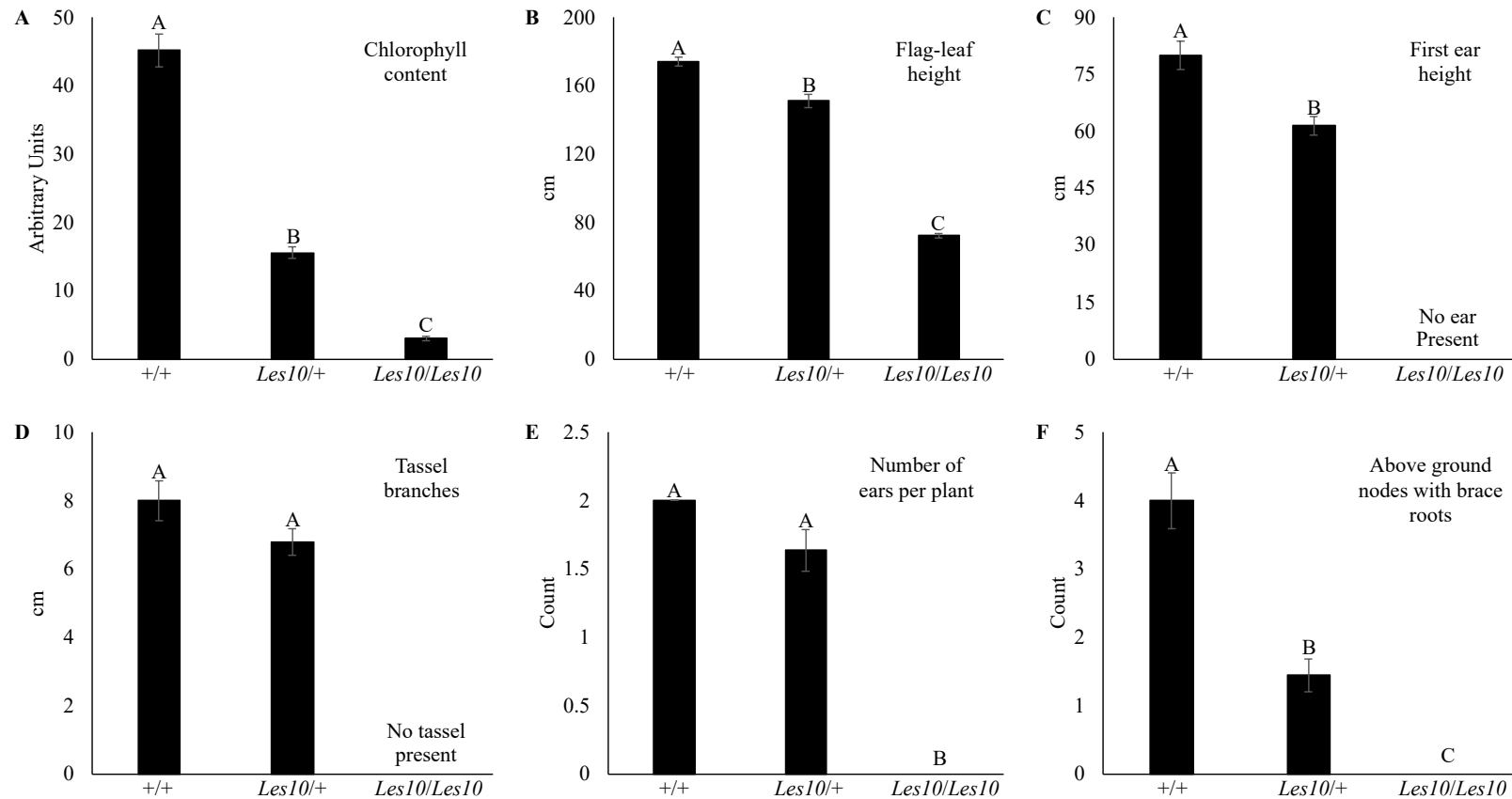
**Figure 3.2: Phenotypic severity of *Les10/Les10* homozygous mutants is more severe than *Les10/+* heterozygous mutants.**

(A) Chlorophyll content, (B) flag-leaf height, (C) first ear height, (D) tassel branch number, (E) number of ears-per-plant, and (F) above ground nodes with brace roots for wildtype (+/+), *Les10/+* mutants, and *Les10/Les10* mutants. Data presented are the mean values $\pm$ S.E. (n $\geq$ 4). Letters above bars represent statistically different measurements (paired sample Student's T-test $p < 0.05$).
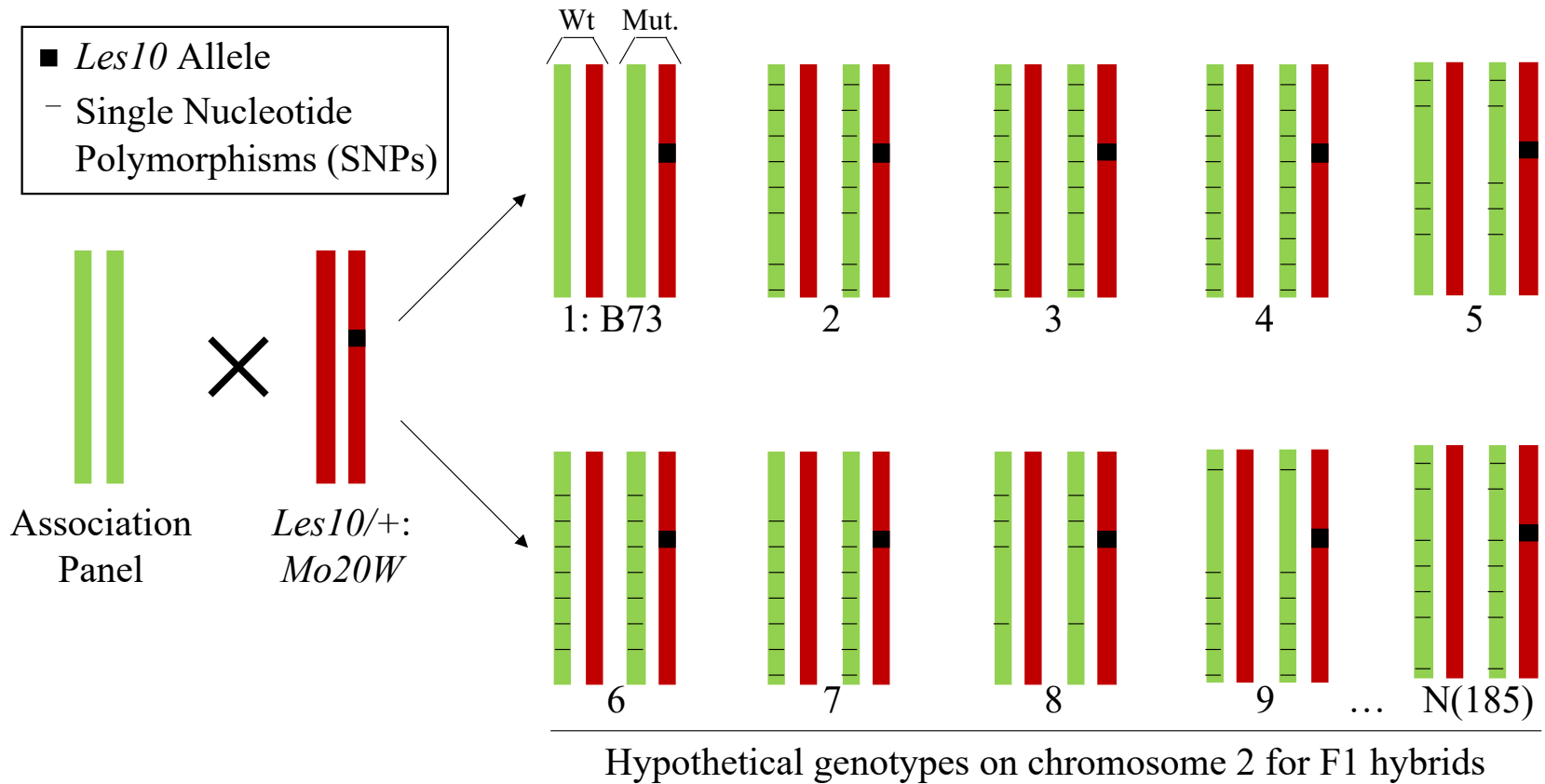
**Figure 3.3: Crossing scheme to test for modifiers of *Les10* phenotypic severity**

Green and red bars represent hypothetical second chromosomes for each inbred line and Mo20W, respectively. For each F1-hybrid the chromosomes for a hypothetical mutant and wild-type sibling are presented. The black box represents the hypothetical *Les10* mutation. Thin black lines that run horizontally across the chromosomes represent hypothetical SNPs in relation to the B73 reference gene.
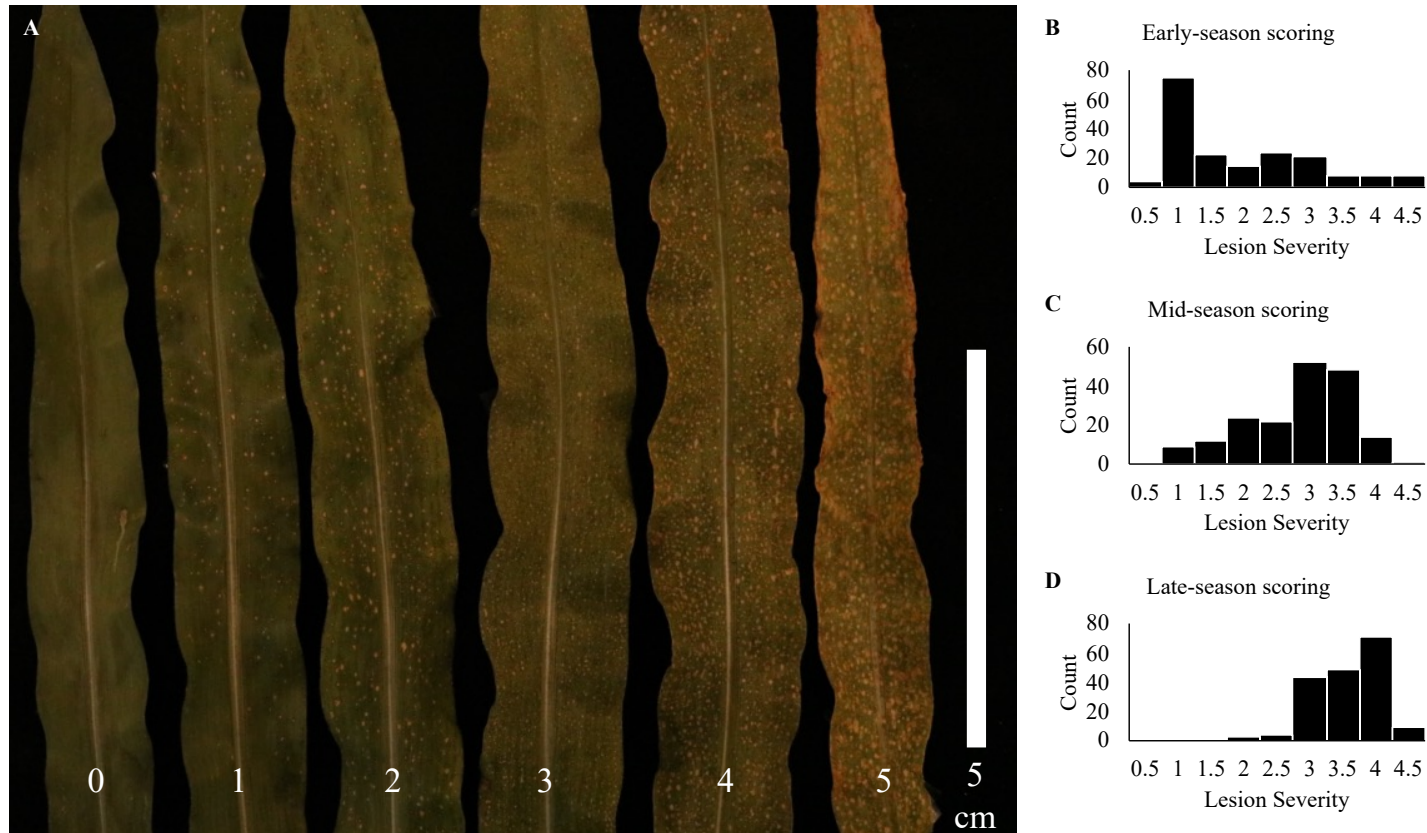
**Figure 3.4:** *Les10/+* **lesion severity is background dependent.**

(A) Representative leaves encompassing a 5-point scale of *Les10* lesion severity in 28-day old *Les10/+* mutants. The "0" score is a wild-type plant and the numbers "1-5" are *Les10/+* hybrids of Mo20W with the inbred lines (1) R168, (2) Va22, (3) PHP60, (4) LH51, and (5) CM105. White by provides a scale of 5 cm. Distribution of lesion severity in the *Les10/+* hybrids at (B) 19-days, (C) 30-days, and (D) 58-days after planting. Values for each hybrid are the average severity of the mutant planted in two field locations.
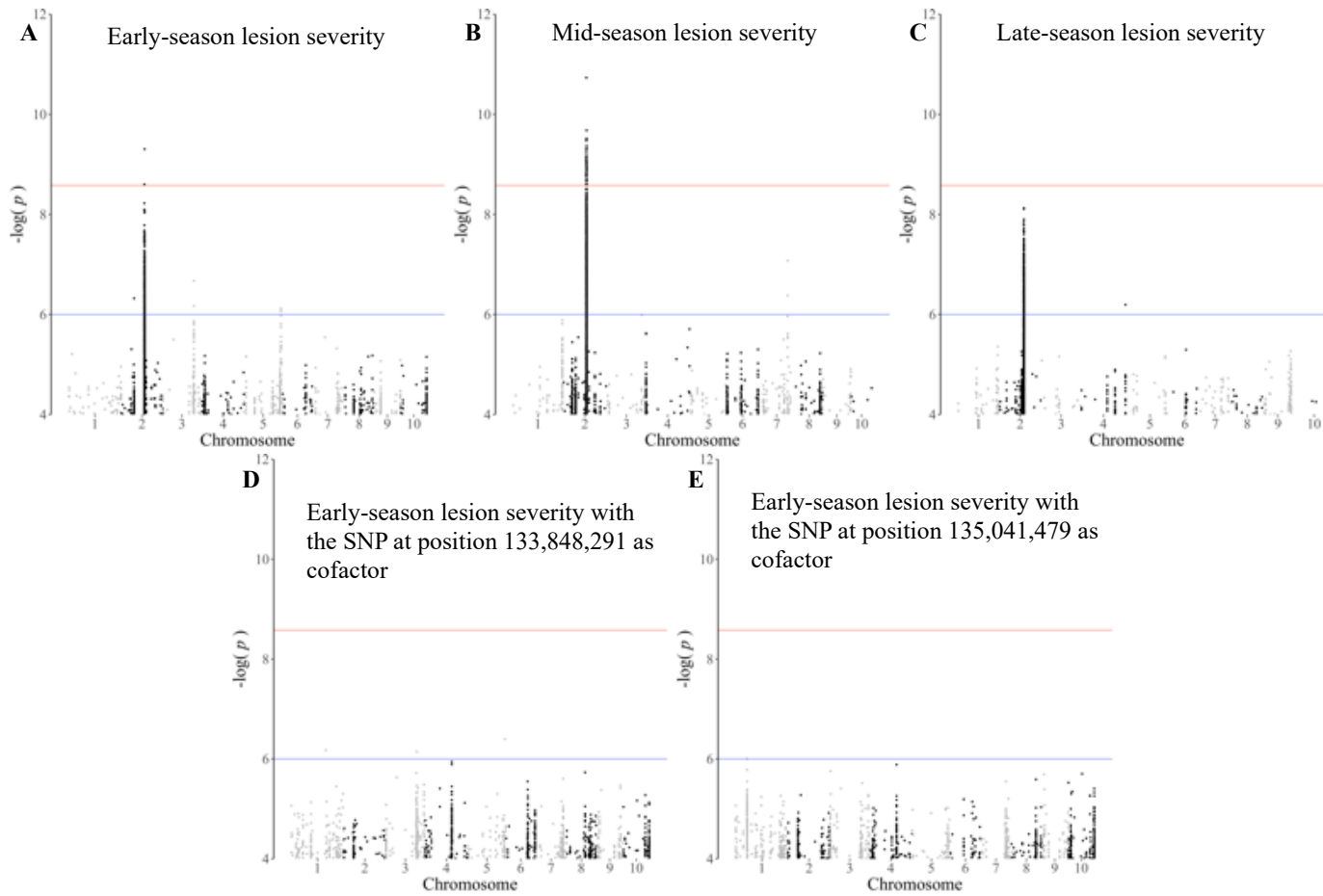
**Figure 3.5: There is a region on chromosome two associated with *Les10* Lesion severity**

Manhattan plots for (A) early-season scoring, (B) mid-season scoring, (C) late-season scoring, and early-season scoring with the SNPs at positions (D) 133,848,291 and (E) 135,041,479 considered as cofactors. The y-axes are the –log(p-value) for each SNP and the x-axes are the physical position of each SNP separated by chromosome. The thin blue and red line represent an arbitrary $p = 10^{-6}$ and a multiple test correction threshold, respectively. Only SNPs that passed a threshold of $p < 10^{-4}$ are plotted.
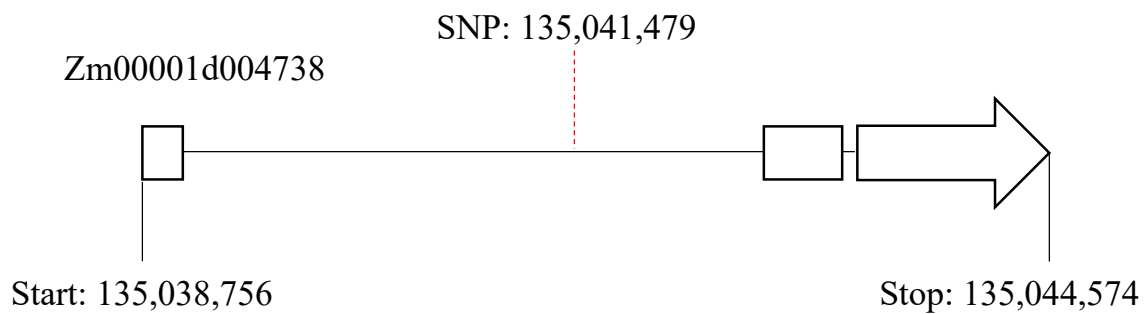
**Figure 3.6: The most significant polymorphism associated with early-season *Les10* lesion severity is within an uncharacterized ankyrin repeat containing maize gene.**

Exon/intron structure of Zm00001d004738. The exons are denoted by white boxes and the introns by thin lines. The position of the start and stop codons and the SNP with the strongest association to early-season *Les10* lesion severity are marked.
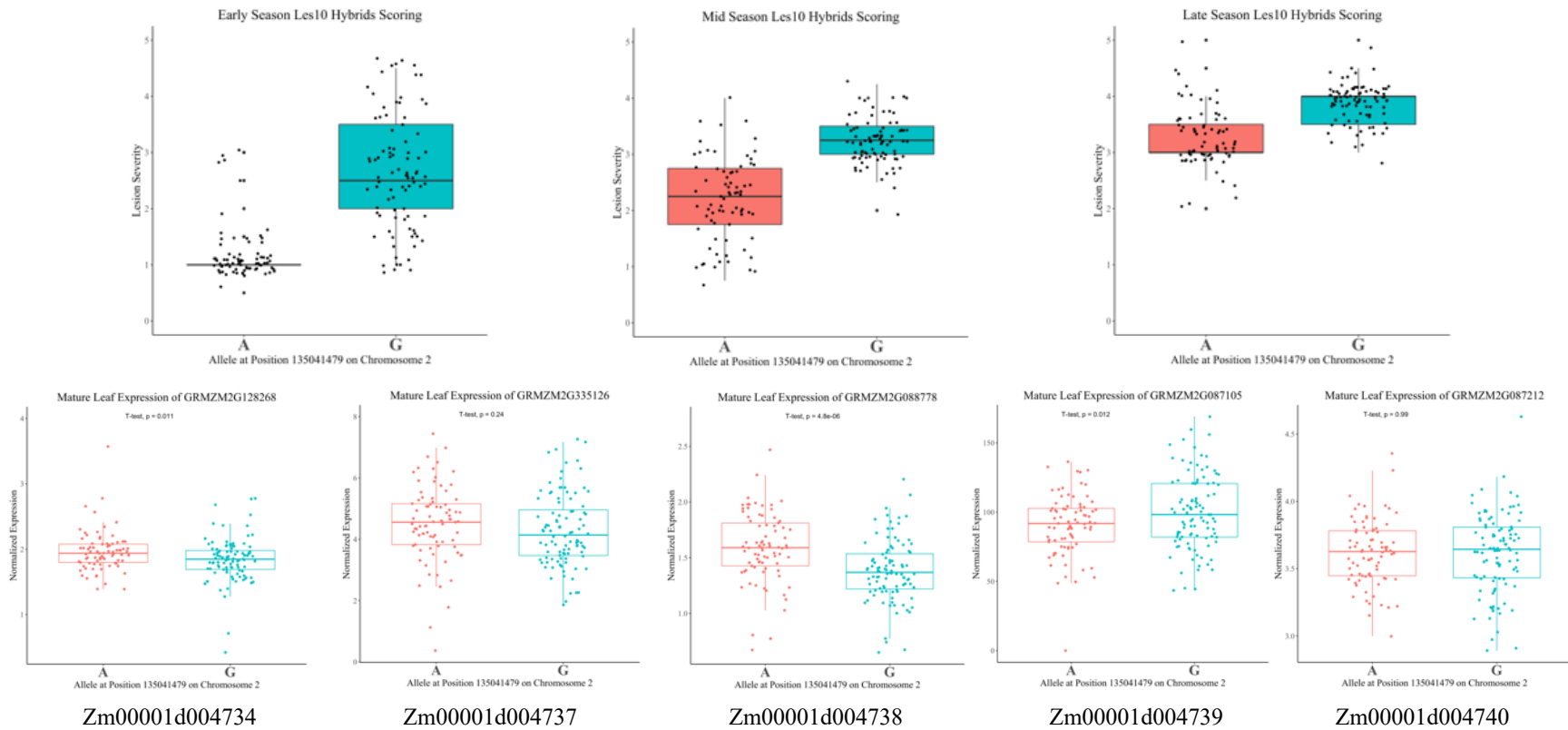
**Figure 3.7: The same polymorphism associated with variation in *Les10* lesion severity is associated with variation in expression of Zm00001d004738.**

(Top) Variation in lesion severity for early, mid, and late season scoring in relation to the reference adenine (A) and alternate guanine (G) allele at position 135,041,479 on chromosome two. (Bottom) Mature leaf expression of the five genes in closest proximity to position 135,041,479 on chromosome two in relation to the reference and alternate allele. Note: Zm00001d004736 and Zm00001d004735 were not expressed in mature leaves.
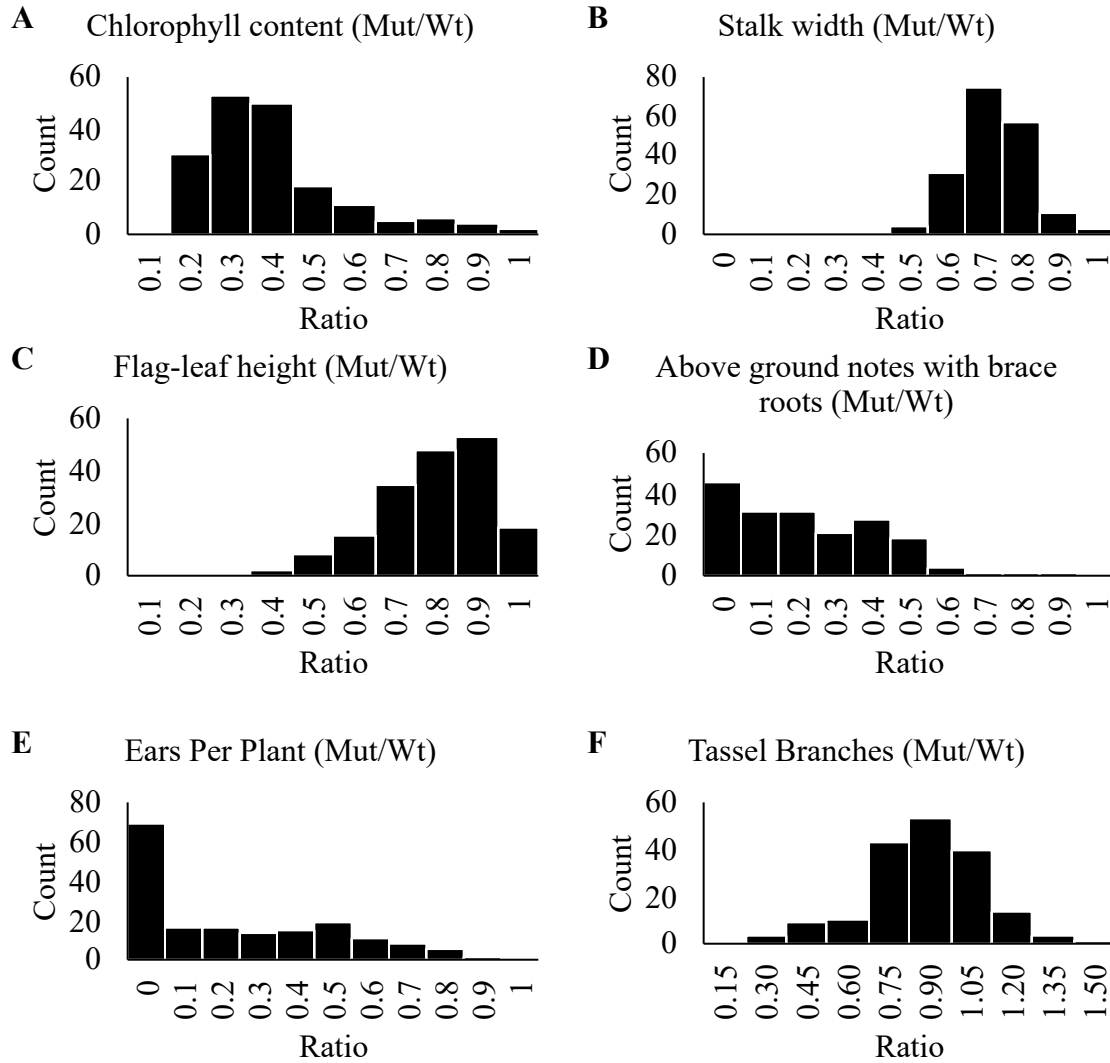
**Figure 3.8: Variation of other phenotypes in *Les10/+* mutants.**

Distribution of the ratio of (A) chlorophyll content, (B) stalk width, (C) flag-leaf height, (D) above ground nodes with brace roots, (E) ears-per-plant, and (F) tassel branches in the *Les10/+* hybrids compared to wild-type siblings.
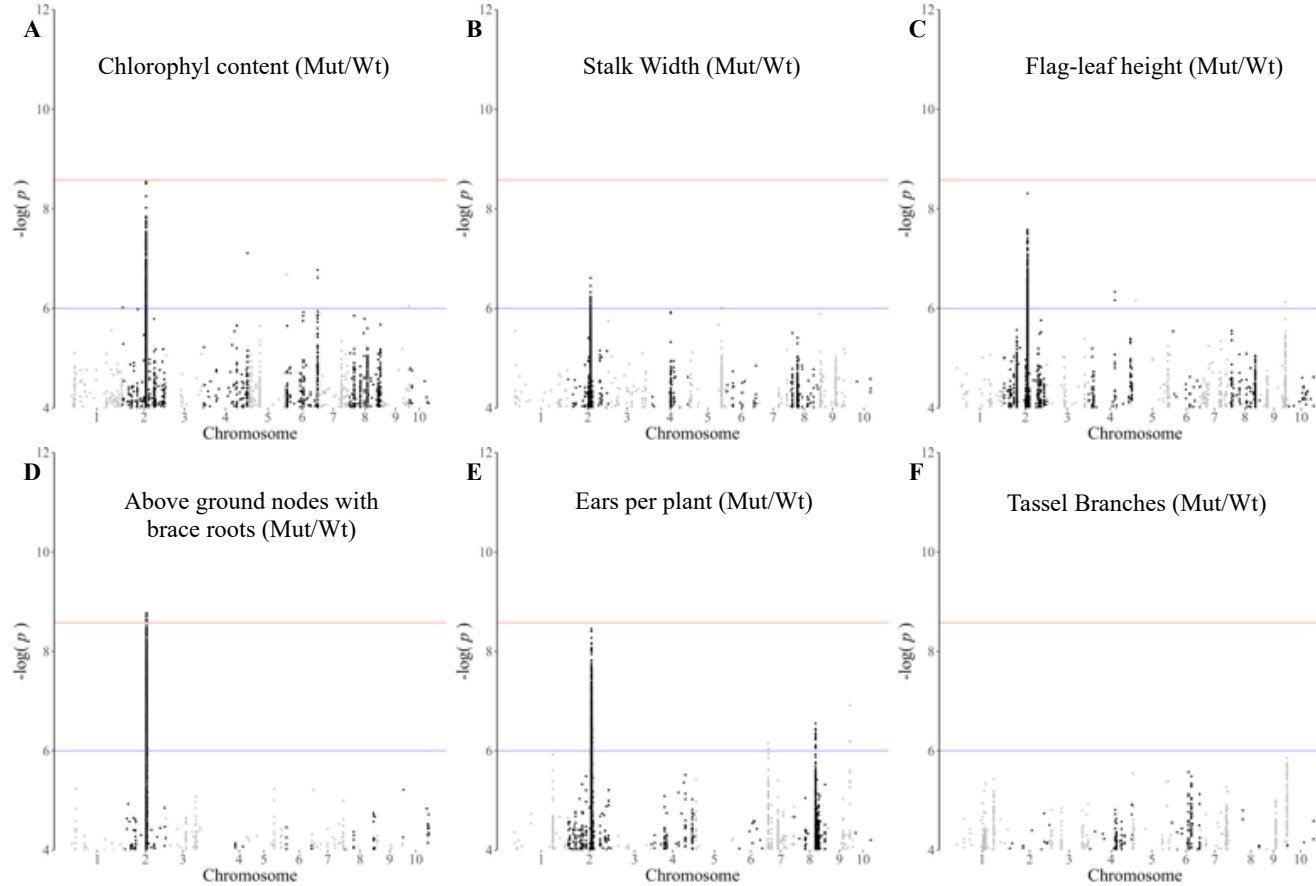
**Figure 3.9: The same region on chromosome two identified in the GWAS using lesion severity is also associated with variation in other *Les10* phenotypes.**

Manhattan plots using the ratio of (A) chlorophyll content, (B) stalk width, (C) flag-leaf height, (D) above ground nodes with brace roots, (E) numbers of ears-per-plant, and (F) number of tassel branches in *Les10/+* mutants (mut) compared to wild-type (Wt) siblings as traits., The y-axes are the –log(p-value) for each SNP and the x-axes are the physical position of each SNP separated by chromosome. The thin blue and red line represent an arbitrary $p = 10^{-6}$ and a multiple test correction threshold, respectively. Only SNPs that passed a threshold of $p < 10^{-4}$ are plotted.

Sector #1     Sector #2     Sector #3     Sector #4     Sector #5     Sector #6     Sector #7

**Figure 3.10: Wild-type revertant sectors isolated from *Les10/+* mutants.**

Leaves from seven different *Les10/+* mutants that have wild-type revertant sectors after seed mutagenesis with EMS.

# CHAPTER 4.    DISRUPTION OF ZEA MAYS ISOCHORISMATE SYNTHASE1 DECREASES PHENYLALANINE AMMONIA LYASE ACTIVITY AND SUPPRESSES HYPERSENSITIVE RESPONSE INDUCED METABOLISM

## 4.1    Preface

This chapter has been submitted to *The Plant Cell*. As of the deposit of this dissertation, it is currently under review. A preprint of this chapter is available on *bioRxiv* and can be accessed at https://doi.org/10.1101/2022.11.04.515247.

## 4.2    Introduction

ISOCHORISMATE SYNTHASE (ICS) catalyzes the reversible conversion of chorismate to isochorismate (Figure 4.1), an essential precursor in the biosynthesis of the Photosystem I (PSI) electron carrier phylloquinone (Gross et al., 2006; Garcion et al., 2008; Qin et al., 2019). Plants deficient in phylloquinone are pale, stunted in growth, and exhibit germination defects and seedling lethality (Garcion et al., 2008; Qin et al., 2019; Orcheski et al., 2015; Emonds-Alt et al., 2017). In plants, ICS activity is encoded by the multifunctional gene *PHYLLO* and/or by a stand-alone *ICS* gene. All Viridiplantae contain a *PHYLLO* gene derived from a fusion of genes homologous to bacterial *MenF* (ICS), *MenD* (Enzyme Commission Number (E.C.) 2.2.1.9), *MenC* (E.C. 4.2.1.113), and *MenH* (E.C. 4.2.99.20). In *Physcomitrella patens* and green algae, the tetra-fused PHYLLO is responsible for the first four steps in phylloquinone biosynthesis, including isochorismate synthesis. Angiosperms, however, encode two sub-functionalized duplicates of the multifunctional *PHYLLO* gene. One duplicate encodes the activities of MenD, MenH, and MenC, but a deletion within the MenF derived sequences removed the chorismate binding domain (Gross et al., 2006). The other duplicate, annotated as ICS, retained the MenF derived sequences but has lost the MenD, MenC, and MenH derived sequences and is necessary and sufficient for the biosynthesis of isochorismate (Garcion et al., 2008; Qin et al., 2019).

Isochorismate is also an intermediate in one of the two biosynthetic pathways for salicylic acid (SA) in plants. In the ICS-dependent SA pathway, isochorismate is converted to isochorismoyl-glutamate by the enzyme encoded by *avrPphB SUSCEPTIBLE3* (*PBS3),* and isochorismoyl-glutamate is spontaneously and/or enzymatically cleaved to form SA (Figure 4.1;

Rekhter et al., 2019; Torrens-Spence et al., 2019). The other route to synthesize SA in plants is from L-phenylalanine (Figure 4.1). Although the genes encoding all steps of the pathway from phenylalanine to SA have not been identified, both genetic evidence (Huang et al., 2010; Yuan et al., 2019) and isotope-labeling analyses (Pallas et al., 1996; Coquoz et al., 1998) indicate the requirement of PHENYLALANINE AMMONIA LYASE (PAL), which deaminates phenylalanine to *trans*-cinnamic acid. In multiple plant species, benzoic acid also serves as a precursor for SA in the PAL-dependent SA pathway (Klämbt, 1962; Yalpani et al., 1993).

Genetic evidence suggests that SA production from the ICS-dependent and PAL-dependent pathways is unequal. In Arabidopsis, knockout of *ics1* resulted in a greater than 90% decrease in pathogen-induced SA production (Wildermuth et al., 2001; Huang et al., 2010). As such, the PAL-dependent pathway has been treated as a minor contributor to SA biosynthesis in Arabidopsis. However, genetic disruption or virus-induced silencing of *PAL* genes in Arabidopsis, soybean, and maize resulted in a greater than 50% reduction in pathogen-induced SA accumulation (Huang et al., 2010; Shine et al., 2016; Yuan et al., 2019). Thus, these two pathways appear to be interdependent, as the combined decrease in SA accumulation when targeting either the PAL-dependent or ICS-dependent SA biosynthetic pathways in Arabidopsis (Huang et al., 2010) and soybean (Shine et al., 2016) exceeds one hundred percent.

Studies on the function of SA in plants have focused on its role in immune signaling and defense response. SA can act as a signaling molecule perceived by NONEXPRESSOR OF PATHOGENESIS-RELATED GENES1 (NPR1) or by NPR3/4. The binding of SA to NPR1 or NP3/4 results in transcriptional activation of pathogenesis-related genes by two distinct mechanisms (Ding et al., 2018). SA signaling plays functional roles in both effector- and pattern-triggered immunity, and SA is required for both local and systemic responses to numerous pathogens (Vlot et al., 2009). Much of our understanding of SA function in plants comes from work in tobacco and Arabidopsis, where the genetic resources to manipulate SA accumulation are well developed (Gaffney et al., 1993; Lawton et al., 1995; Wildermuth et al., 2001; Garcion et al., 2008). These resources are lacking for most plants, and the functions of SA in plant immunity responses have not been adequately tested in plants other than tobacco and Arabidopsis.

Accumulation of SA is a hallmark of the plant hypersensitive response (HR), the rapid localized cell death at and around the site of pathogen infection (Balint-Kurti, 2019). Studies of HR and HR-induced molecular signaling have been facilitated by lesion mimic mutants encoded

by autoactive alleles of resistance (R) genes and display constitutive HR-signaling and lesion formation in the absence of pathogen infection (Bruggeman et al., 2015). These mutants are advantageous for molecular studies of HR, as they eliminate the need to control for pathogen infection, and all measured molecular signals can be attributed to the biology of the plant. In maize, the most well-studied autoactive R-gene mutant is *Rp1-D21*. This mutant originated from an intergenic recombination at the *Rp1* locus, which encodes a set of tandemly repeated nucleotide-binding site leucine-rich repeat (NLR) proteins that mediate resistance to the common rust fungus, *Puccinia sorghi* (Hu et al., 1996)*. Rp1-D21* mutants accumulate high levels of SA (Ge et al., 2021), but a requirement of SA for lesion formation and HR-responsive molecular signaling in *Rp1-D21* mutants has yet to be tested.

In this work, I characterized a loss-of-function allele of the *ICS1* gene of maize and investigated the biosynthesis and function of SA. Using metabolite analysis, labeled isotope feedings, and enzyme-activity assays, I provide evidence for the existence of both the ICS-dependent and PAL-dependent SA biosynthetic pathways in maize. I demonstrate that the two pathways are not independent and that loss of ICS-activity in maize suppresses PAL-activity. This is coincident with increased accumulation of phenylalanine and decreased accumulation of phenylalanine-derived metabolites. Double mutants of *ics1-1* and *Rp1-D21#4* do not accumulate SA but do initiate lesions, demonstrating that SA hyperaccumulation is not required for this phenotype. Metabolite profiling shows that SA accumulation is also dispensable for the differential accumulation of most HR-responsive metabolic perturbations in maize.

## 4.3    Materials and Methods

### 4.3.1    Sequence similarity searches

The maize B73 reference genome (version 4; Jiao et al., 2017) was downloaded from www.maizegdb.org. The Arabidopsis *ICS1* and *ICS2,* and maize *ics1*, exons were obtained from the Phytozome v13 database (Goodstein et al., 2012). Similar sequences in the maize genome were identified using the amino acid sequences corresponding to each exon as queries and TBLASTN (Gertz et al., 2006) to search for a conceptual translation of ICS in the maize nucleotide genome. Genomic regions matching the exons were determined based on high sequence match and low expectation (E) scores. The conceptual translations corresponding to the full-length protein

sequences of Arabidopsis *ICS1*, Arabidopsis *ICS2*, and maize *ics1* were also used for similarity searches of the B73 reference genome (version 4) using TBLASTN and identified the same genomic regions as the single exon searches.

### 4.3.2 *ICS* phylogenetic analysis

All protein sequences with greater than 50% sequence similarity to Arabidopsis ICS1 (At1G74710) or ICS2 (At1G18870) were downloaded from the Phytozome v13 database (Goodstein et al., 2012). Sequences were aligned using Clustal Omega (Sievers et al., 2011). Sequences deemed partial or incomplete were identified and removed before proceeding with the phylogenic analysis by visualizing the alignments using the constraint-based alignment tool (COBALT) for multiple protein sequences (Papadopoulos and Agarwala, 2007). Phylogenetic trees were generated using IQ-TREE (Trifinopoulos et al., 2016). Ultrafast bootstrap approximations were used. The IQ-TREE parameters were: 1000 bootstrap alignments; 1000 maximum iterations; a minimum correlation coefficient of 0.99; 1000 replicates of the SH-aLRT branch test; perturbations strength of 0.5; and 100 as the IQ-TREE stopping rule. Phylogenetic Trees were visualized using FigTree v1.4.4 (https://github.com/rambaut/figtree/releases). Nodes indicating likely duplications were highlighted after visualization of tree.

### 4.3.3 Plant material and genotyping

The *ics1-1* mutant allele (mu1039765) was obtained from the UniformMu population (McCarty et al., 2013) in the W22 inbred background as stock UFMu-03865 from the Maize Genetics Co-Op (http://maizecoop.cropsci.uiuc.edu). Genotyping of the *ics1-1* allele was done using three primers, two complementary to *ics1*, ICS1FP 5'-TCTCAGGTACCATTTTGACGA-3' and ICS1RP 5'-CCCATTCAGGTTCAATCAATGT-3' that span the *Mu* insertion site and one complementary to the *Mu* terminal inverted repeat (TIR) 5'-GCCTCCATTTCGTCGAATCCC-3'. All PCR contained 4 μL buffer, 1.6 μL 25 mM MgCl$_2$, 0.4 μL 10mM dNTPs, 0.4 μL 10 μM of each primer, 0.1 μL GoTaq® Flexi DNA polymerase (Promega Corporation Ref: M8291), 12.1 μL water, and 1 μL template DNA. The PCR program consisted of an initial 2 min at 95°C followed by 10 cycles of 95°C for 30 s, 65°C for 30 s, decreasing the temperature by 1°C each cycle, and 72°C for 45 s, and then 25 cycles at 95°C for 30 s, 55°C for 30 s, and 72°C for 45 s, and

finally 5 minutes at 72°C. Wild-type alleles were detected as a ~450 bp amplicon using the two *ics1* primers and *ics1-1* alleles were detected as a ~250 bp amplicon using the *Mu* TIR and ICS1FP primers. After initial genotyping experiments, *ics1-1/ics1-1* homozygous mutants were identified by a yellow leaf phenotype visible by 14d after sowing. Two alleles of *Rp1-D21* were used, the reference *Rp1-D21* allele (Hu et al., 1996) and the *Rp1-D21#4* allele (Karre et al., 2021). Both alleles were maintained as heterozygotes in nearly isogenic B73 backgrounds. *Rp1-D21/+* and *Rp1-D21#4/+* mutants were identified by 14d after sowing due to lesion formation on the leaves. The *Oy1-N1989* mutants used were maintained as heterozygotes in a nearly isogenic B73 background as previously described (Khangura et al., 2019). *Oy1-N1989/+* mutants were identified by a yellow leaf phenotype after emergence. Material segregating 3:3:1:1 for wild type, *Rp1-D21#4/+*, *ics1-1*, and *Rp1-D21#4/+; ics1-1* was generated by crossing *Rp1-D21#4/+:B73* with *ics1-1/+:W22* and then crossing an F1 plant without lesions and heterozygous for *ics1-1* (*+/+; ics1-1/+*) with a sibling heterozygous for both *Rp1-D21#4* and *ics1-1* (*Rp1-D21#4/+; ics1-1/+*). Plants segregating 3:1 for wild type:*ics1-1* were generated by self-pollinating an *ics1-1/+* heterozygous plant from the F2 progeny of the above-mentioned sibling mating. Material segregating 1:1:1:1 for wild type, *Rp1-D21#4/+; Oy1-N1989/+*, and *Rp1-D21#4/+;Oy1-N1989/+* was generated by crossing an F2 *Rp1-D21#4/+* mutant from the above-mentioned sibling mating with an *Oy1-N1989/+:B73* mutant.

### 4.3.4 Growth conditions

Material for the phylloquinone analysis, plastoquinone analysis, labeled phenylalanine feeding, all untargeted metabolite profiling, and salicylic acid treatments were grown under greenhouse conditions (mogul-based high-pressure sodium lamps (1000 Watts) on a 16-hour light/8-hour dark cycle with the temperature set at 28°C-day and 20°C-night). Plants were sown in Berger BM2 Seed Germination and Propagation Mix in 36-cell 606 deep plastic flats with one seed per well. Flats were sub-irrigated with fertilizer water as needed, usually every third day after emergence, until tissue collection. All field material was tractor-planted and grown at the Purdue Agronomy Center for Research and Education in West Lafayette, Indiana (40.4700° N, 86.9917° W). Material was planted in 3.84 m rows with interrow spacing of 0.79 m and alley spacing of 0.79 m. Supplemental irrigation was applied as needed, and conventional fertilizer, pest control, and weed control practices for growing maize in Indiana were followed.

### 4.3.5 Foliar application and analysis of SA, 2,3-DHBA, and 2,5-DHBA effects

SA, 2,3-dihydroxy benzoic acid (2,3-DHBA), and 2,5-dihydroxy benzoic acid (2,5-DHBA) were dissolved in distilled water and 0.1% V/V Tween-20. 10-day-old plants were spray-treated every 24 hours for three days. For metabolite analyses, the second leaf was collected 24 hours after the last treatment from three plants per replicate.

Calculation of the correlation between SA levels and lesion severity in *Rp1-D21/+* mutants of different genetic backgrounds was performed by reanalysis of the data presented in (Ge et al., 2021). Total and free SA values were obtained by measuring the height of each bar from the graph in Figure 5A (Ge et al., 2021) using a ruler. Correlation analyses of SA accumulation means, and the lesion severity scores in Figure 5B for *Rp1-D21/+* in each genetic background, were performed using the "=correl()" equation in Microsoft Excel.

### 4.3.6 Phylloquinone and plastoquinone analysis

All steps were conducted in dimmed light to limit the photodegradation of quinones. Approximately 300 mg of flash-frozen ground maize leaf tissue, harvested 17-days after planting, was extracted overnight at 4°C in 3 mL methanol containing 2.7 nmol menaquinone-4 as an internal standard. Phylloquinone and plastoquinone were analyzed directly on an Agilent Infinity 1260 high-performance liquid chromatography (HPLC) system (Agilent Technologies, Palo Alto, CA, USA) coupled with diode array (DAD) and fluorescence (FLD) detectors using a method adapted from previous work (Block et al., 2013, 2014; McCoy et al., 2018). Before analysis, the methanolic extract was filtered using a 0.2 μm polytetrafluoroethylene (PTFE) syringe filter, and 100 μL was directly analyzed on a Zorbax SB-C18 column (4.6 x 250 mm x 5 μm) at 25°C and eluted in isocratic mode at 0.5 mL min$^{-1}$ for 30 minutes with 30% solvent A (60:40 (V/V) isopropanol:hexanes containing 10 mM ammonium acetate) and 70% solvent B (80:20 (V/V) methanol:isopropanol containing 10 mM ammonium acetate). Phylloquinone (retention time 11.8 min) and plastoquinone (23.0 min) were detected fluorometrically (at 238 nm excitation and 426 nm emission and 290 nm excitation and 330 nm emission, respectively). Fluorescence-based detection of phylloquinone was achieved by reducing it in line with a post-column chemical reactor (1.5 x 70 mm) packed with −100 mesh zinc (Sigma-Aldrich) placed between the DAD and FLD

modules (van Oostende et al., 2008). Phylloquinone and plastoquinone were quantified relative to external calibration standards and corrected for recovery using a menaquinone-4 internal standard.

### 4.3.7 Photosynthetic parameter analysis

The maximum quantum yield of photosystem II (PSII) was measured using a Hansatech pulse amplitude modulated (PAM) fluorescence monitoring system (FMS1) (Norfolk, England). Leaves were dark adapted for 30 min before measurement. Minimum fluorescence ($F_o$) was obtained by illuminating with measuring light ($\leqq 0.01$ µmol m$^{-2}$ s$^{-1}$). Maximum fluorescence ($F_m$) for the dark-adapted state was determined with a 0.8-second-long saturating pulse of white light (13000 µmol m$^{-2}$ s$^{-1}$). The actinic light was then switched on, and a second saturating pulse was applied after 6 minutes ($F'_m$). Fv/Fm was calculated as $\frac{F_m - F_0}{F_m}$, NPQ was calculated as $\frac{F_m - F'_m}{F_m}$, and ΦPSII as $\frac{F'_m - F_s}{F'_m}$. Fraction of reduced PQ-pool (1-qL) was calculated as $1 - \left( qP \frac{F'_0}{F_s} \right)$, where $qP = \frac{F'_m - F_s}{F'_m - F'_0}$. Electron transport rate through PSII (ETR) was calculated as PPFD x 0.84 x 0.5 x ΦPSII. The redox state of P700 was determined by difference absorption spectroscopy of the reaction center chlorophyll P700 using a JTS-10 spectrophotometer (Bio-Logic). The leaves were dark adapted for 30 min before measurement. PSI redox activity was determined by monitoring optical changes at 705 nm during 5 s of illumination with an actinic light peaking at 630 nm (940 µmol m$^{-2}$ s$^{-1}$) and 5 s of dark re-reduction. The amounts of PSI and PSII were determined by difference absorption spectroscopy as described in (McKenzie et al., 2020).

### 4.3.8 Untargeted metabolite analysis

Tissue was flash frozen in 15- or 50-mL Falcon tubes and ground in the Falcon tubes using a metal spatula. Soluble metabolites were extracted in 1:1 methanol:water (V/V) at a concentration of 100 mg tissue per 1 mL of extraction solvent. Samples were incubated at 65°C for 2 h and vortex agitated every 30 min. Samples were centrifuged at 10,000 x $g$ for 10 min and 500 µL of supernatant was transferred to a new tube. Samples were dried in a speed vacuum at room temperature and then redissolved in 50 µL 50% methanol. Samples were sonicated for 15 min and centrifuged at 14,000 x $g$ for 10 min. 40 µL of supernatant was transferred to a new tube and stored at -20° C prior to analysis. Metabolites were processed as described in Method 2.2.2. Linear model

analysis was performed using the "lm" function in R (https://www.rdocumentation.org/packages/stats/versions/3.6.2/topics/lm).

All standards were obtained from Sigma-Aldrich. The amino acids used were part of the L-Amino Acids Kit (LAA-21) and salicylic acid was obtained as CAS 69-72-7. Samples were dissolved in 50% methanol and analyzed by LC-MS using the same method as described above. The identity of SA glucoside was determined by the expected spontaneous fragmentation pattern of $m/z$: 299.077 → 137.024 → 93.035 amu and by the response of this feature to foliar application of SA. 2,5-DHBA glucoside and 2,3-DHBA glucoside were identified by the expected spontaneous fragmentation pattern of $m/z$: 315.072 → 151.019 → 109.029 amu and by the response of these features to the foliar application of 2,5-DHBA (CAS 490-79-9) and 2,3-DHBA (CAS 303-38-8) respectively.

### 4.3.9   $^{13}$C-ring labeled phenylalanine feeding

Phenylalanine feedings were performed similarly to the method of (Simpson et al., 2021b). Progeny from a sibling cross of wildtype x *Rp1-D21/+* segregating 1:1 for wildtype: *Rp1-D21/+* were sown in Turface Athletics MVP® (Profile Products LLC, Mfg. Number: BFMVP5004) for approximately 14 d under greenhouse conditions as described above. Three replicates of wildtype and *Rp1-D21/+* were fed 1 mM of phenylalanine (Sigma-Aldrich) or 1 mM $^{13}$C-ring labeled phenylalanine (Cambridge Isotope Laboratories, Tewksbury, MA. Cat No. CLM-1055) in Murashige and Skoog medium (PlantMedia SKU: 30630058-3). Potting media was washed off roots with water, and whole plants were placed into 120 mL specimen cups containing 30mL feeding media, which was enough to submerge the roots. After 24 h, the basal 2 cm of each plant was harvested and flash frozen in liquid nitrogen. Soluble metabolites were extracted and analyzed using the untargeted LC-MS method as described above.

Labeled features derived from $^{13}$C-ring labeled phenylalanine were identified as mass feature pairs that coeluted within 5 s and had an $m/z$ that increased by 6.02 $\pm$ 0.002 amu, as expected from ring-labeled phenylalanine. This was done by duplicating the XCMS output file and running a custom R script (Supplemental File S2) that uses the "fuzzyjoin" package (https://cran.r-project.org/web/packages/fuzzyjoin/index.html) to perform pairwise comparisons of retention times and $m/z$ of all detected features. The labeled compound list was trimmed to remove any features annotated as labeled compounds that were also detectable in non-label

treatments. This library was then used to annotate phenylalanine-derived metabolites in *Rp1-D21#4/+; ics1-1*. Because metabolite analyses were done at different times, mass features were paired based on a shared *m/z* ($\pm$ 0.05 amu) and a retention time difference of $\pm$ 15 s.

### 4.3.10  PAL assay

Leaf tissue from 15-d-old plants was flash frozen and ground to a fine powder using a mortar and pestle. Immediately after grinding, approximately 400 mg of tissue was transferred to a 1.7 mL Eppendorf tube, and 1.2 mL of extraction buffer (100 mM Tris-HCl pH 8, 10% glycerol, 5 mM dithiothreitol) was added. Tubes were kept on ice until all samples were processed and then centrifuged at 20,000 x *g* for 15 min at 4°C. The supernatants were transferred to new tubes and samples were desalted using Cytiva PD-10 Desalting Columns following the manufacturer's instructions. Protein concentrations were determined using the Bradford assay with bovine serum albumen as a standard (Bradford, 1976). Each PAL assay contained 190 µL of protein extract and 10 µL of 0.1 M phenylalanine for a total volume of 200 µL. Reactions were incubated for 90 minutes at 37°C. The reactions were quenched with 24 µL of glacial acetic acid and flash frozen in liquid nitrogen. Samples were centrifuged at 14,000 x *g* for 1 h at 4°C. Assay products were quantified by HPLC at 276 nm using cinnamic acid (Eastman Organic Chemicals) as a standard as previously described (Klempien et al., 2012; Wang et al., 2018). PAL activities are reported as the picokatals (pkat) per mg of protein where one pkat is the picomoles of cinnamate produced per second.

### 4.4    Results

### 4.4.1    Characterization of Zea mays isochorismate synthase

The *Zea mays* B73 version 4 reference genome contains a single annotated *ics* gene, which was previously named *isochorismate synthase like1* (*ics1;* Zm00001d020220). The predicted gene product of *ics1* contains a putative 21-amino acid N-terminal chloroplast signaling peptide (Emanuelsson et al., 1999), a chorismate binding domain motif (Pfam accession no. PF00425), and four amino acid residues conserved across all ICS enzymes and required for substrate binding and catalysis (Figure 4.2; Kolappan et al., 2007; Garcion et al., 2008). To determine if there are any other *ICS*-like genes in maize, I performed tBLASTn searches of the *Zea mays* B73 version 4

reference genome using the exon sequences of maize *ics1* and Arabidopsis *ICS1* and *ICS2* as query. The maize *ics1* gene was the only ICS homolog identified among these BLAST hits, indicating that the maize genome encodes a single isochorismate synthase gene.

Previously characterized plant *ICS* genes have 13, 14, or 15 exons with 15 exons representing the most likely ancestral *ICS* gene structure (Yuan et al., 2009). Maize *ics1* contains 14 exons and has lost intron two compared to the 15-exon structure (Figure 4.3). To determine when plant *ICS* genes underwent exon-intron boundary modifications and any gene duplications, a phylogenetic analysis of angiosperm *ICS* genes was overlayed with the gene structure changes and gene duplication events (Figure 4.3). Two *ICS* paralogs are present in *Brassicaceae* consistent with a duplication at the base of this lineage. Lineage-specific duplications, consistent with recent polyploidy events, are present in *Glycine max*, *Gossypium raimondii*, and *Arachis hypogaea*. The differences in gene structures of the *ICS* genes included in this phylogeny could be explained by four intron-loss events, relative to the 15-exon structure. The loss of intron five, a feature that distinguishes the Arabidopsis *ICS1* and *ICS2* paralogs, occurred within *Brassicaceae* after the divergence of *Eutrema salsugineum* from the other species analyzed. The *ICS1* gene from Arabidopsis has further undergone a lineage-specific loss of intron three. Intron two was lost twice, once at the base of the *Fabaceae* lineage and once within the panicoid grasses. The 14-exon maize *ics1* gene structure is consistent with the gene structure present in other panicoid grasses.

### 4.4.2   *Zea mays ics1* is required for phylloquinone biosynthesis

To test the function of maize *ics1*, I obtained a mutant, *ics1-1* (mu1039765), that contained a *Mutator* transposable-element (*Mu*) insertion in exon 14 of *ics1* (Figures 4.2 and 4.3). This mutation was inherited as a single recessive trait (wildtype:*ics1-1* - 51:17 in an F2 family resulting from a self-pollinated *ics1-1/+* heterozygous individual, $\chi^2 = 0$, df = 1, $p = 1$). The *ics1-1* mutants were visually indistinguishable from wild-type sibling plants at emergence and did not show a yellow or stunted growth phenotype until 12-14 days after sowing (Figure 4.4). The yellow and stunted phenotype of the maize *ics1-1* mutant (Figures 4.4 and 4.5) was similar to that described previously for loss-of-function *ics* mutants in Arabidopsis and barley (Garcion et al., 2008; Qin et al., 2019). No recombinants were detected between the yellow leaf phenotype and the *Mu* insertion in *ics1-1* (76 green homozygous wild-type or heterozygous plants: 22 yellow homozygous mutants). The coloration of *ics1-1* mutants was consistent as the plants aged; however, the stunted

growth phenotype became more severe (Figure 4.5A). The penetrance of the *ics1-1* mutant was extremely variable. Most *ics1-1* mutants died prior to reproduction or were sterile but rare individuals survived to maturity and produced viable pollen. To determine the consequence of *ics1* disruption on phylloquinone biosynthesis, I measured the amount of phylloquinone in leaves of wild-type and *ics1-1* mutant plants. The *ics1-1* mutants accumulated approximately 10% of wild-type phylloquinone levels (Figure 4.6A).

### 4.4.3    The *ics1-1* mutant is deficient in electron transport and has decreased amounts of Photosystem I

We next evaluated multiple photosynthetic parameters for *ics1-1* mutant and wild-type siblings to see if the loss of phylloquinone in *ics1-1* mutants disrupted photosynthesis. Compared to wildtype, *ics1-1* mutants had increased non-photochemical quenching (NPQ; Figure 4.7A), indicating that *ics1-1* mutants cannot utilize light as efficiently as wild-type plants. In addition, the *ics1-1* mutants had decreased operating and maximum quantum efficiencies of PSII ($\Phi$PSII and $F_v/F_m$; Figures 4.7B and 4.7D), and linear electron transport rate (ETR; Figure 4.7C) compared to wild-type plants, demonstrating lower photosynthetic efficiency in *ics1-1* mutants. The oxidation state of the plastoquinone (PQ) pool was also much lower in *ics1-1* mutants than in wild-type controls (Figure 4.7F).

Given phylloquinone's role as an electron carrier in PSI, I evaluated how the loss of phylloquinone alters PSI electron transport in *ics1-1* mutants by measuring the rate of re-reduction of the reaction center P700$^+$ chlorophyll in *ics1-1* mutants and wild-type plants (Figure 4.7G). Plastoquinone can occupy PSI in the absence of phylloquinone in both *Synechocystis sp.* PCC 6803 (Semenov et al., 2000) and *Chlamydomonas reinhardtii* (Lefebvre-Legendre et al., 2007). The replacement of phylloquinone with plastoquinone reduces the free energy gap to the $F_x$ iron-sulfur cluster in PSI, resulting in a faster P700 dark re-reduction due to a backflow of electrons from plastoquinone to P700$^+$ (Johnson et al., 2000; Shinkarev et al., 2002). The dark re-reduction of the P700$^+$ complex was faster in *ics1-1* mutants than in wild-type controls, indicating that forward electron transport through PSI is altered in *ics1-1* mutants (Figure 4.7G). These findings are consistent with an electron carrier with a more positive midpoint potential, such as plastoquinone, replacing phylloquinone in PSI in *ics1-1* mutants. The amount of plastoquinone in leaves of *ics1-1* mutants is half that of wild-type samples (Figure 4.6B); however, the 2-fold

90

reduction of plastoquinone and the 8.4-fold reduction of phylloquinone in *ics1-1* mutants compared to wild-type samples results in the relative ratio of plastoquinone to phylloquinone changing from 1:1.1 in wild-type plants to 4.8:1 in *ics1-1* mutants (Figure 4.6C). Therefore, despite a decrease in plastoquinone levels in *ics1-1* mutants, plastoquinone is 4.8-times more abundant than phylloquinone in these mutants which may facilitate plastoquinone replacing phylloquinone in PSI. Like the maize *ics1-1* mutant, the *Arabidopsis ics1; ics2* double mutants also reduced plastoquinone accumulation compared to wildtype (Gross et al., 2006), which indicates that plastoquinone biosynthesis has a yet-to-be characterized requirement for ICS.

Finally, I evaluated how disruption of *ics1* alters the stoichiometric ratios of PSII and PSI. On a per chlorophyll basis, *ics1-1* mutants have about 2-times more PSII (Figure 4.8A) and about 2.7-times less PSI (Figure 4.8B) than wild-type plants. This results in a shift in the ratio of PSII:PSI from 1:2 in wild-type plants to 2.7:1 in *ics1-1* mutants (Figure 4.8C). Since chlorophyll levels in *ics1-1* mutants are about half the level in wild-type plants (Figure 4.7E),the total amount of PSII in *ics1-1* mutants and wild-type plants is similar but the amount of PSI in *ics1-1* mutants is approximately 5.3-times less than wild type. This is similar to the observations and interpretation of phylloquinone loss mutants of *Chlamydomonas reinhardtii* (Sakuragi et al., 2002) Thus, the altered stoichiometry between PSII and PSI in *ics1-1* mutants is driven by the loss of PSI.

### 4.4.4   *ics1* is required for hypersensitive response-induced SA biosynthesis in maize

Disruption of *ICS* in plants blocks the biosynthesis of phylloquinone and SA (Figure 4.6A; Wildermuth et al., 2001; Gross et al., 2006; Garcion et al., 2008; Qin et al., 2019). In addition, loss of ICS activity indirectly leads to changes in the levels of other metabolites, such as lower levels of plastoquinone (Figure 4.6B; Gross et al., 2006) and chlorophyll (Figure 4.7E). To investigate the metabolic consequences of disrupting *ics1* in maize leaves, I performed a liquid-chromatography/mass-spectrometry (LC/MS) untargeted analysis of methanol-soluble metabolites separated by reverse phase chromatography. This analysis efficiently detects SA and multiple SA-derivatives while also enabling the analysis of thousands of additional metabolic features. In addition to the *ics1-1* mutant, I also included the *Rp1-D21#4/+* mutant in our metabolite analysis. *Rp1-D21#4* encodes a weak intragenic suppressor allele of *Rp1-D21* derived by ethyl methanesulfonate (EMS) mutagenesis that still displays constitutively active HR, but has a less severe phenotype and greater fertility than *Rp1-D21* (Wang and Balint-Kurti, 2015; Karre

et al., 2021). Also included in this metabolite analysis were *Rp1-D21#4/+; ics1-1* double mutants, which permitted evaluation of both basal and HR-responsive SA biosynthesis and analysis of how other HR-responsive metabolites are affected by disruption of *ics1*.

The material used for this untargeted metabolite analysis was from the sibling progeny of a cross of +/+; *ics1-1/+* with *Rp1-D21#4/+; ics1-1/+* that segregated phenotypically 3:3:1:1 for wildtype, *Rp1-D21#4*, *ics1-1*, and *Rp1-D21#4; ics1-1* (58:54:20:10, $\chi^2$= 4.10, df = 3, $p$ = 0.25). The untargeted metabolomics analysis of this tissue detected 7,094 mass features that were reproducibly detectable in all replicates (four for wild type and *Rp1-D21#4/+*, three for *ics1-1*, and five for *Rp1-D21#4/+; ics1-1*) of at least one of the four genotypes. Peak areas for all features were extracted using XCMS (Smith et al., 2006), and the average peak area of each feature was calculated for each of the four genotypes and compared for compounds of interest. SA was identified in our analysis by comparison to an authentic standard. Both the SA parent ion (M137.024_T538; mass to charge ratio in negative ionization mode_retention time in seconds) and spontaneous decarboxylation fragment (M93.034_T538) were detected by MS with the decarboxylated fragment being the more abundant feature. Consistent with earlier reports of *Rp1-D21/+* mutants (Ge et al., 2021), SA accumulation was 4.5 times greater in *Rp1-D21#4/+* mutants compared to wild-type samples (Figure 4.9A). SA accumulation in *ics1-1* mutants and *Rp1-D21#4/+; ics1-1* double mutants was not significantly different from accumulation in wild-type samples indicating that *ics1-1* was epistatic to *Rp1-D21#4* for induced SA accumulation. The requirement for ICS1 was also observed for SA catabolites. SA-glucoside (Figure 4.9B, M299.07_T317), 2,5-DHBA glucoside (Figure 4.9C M315.072_T186), and 2,3-DHBA glucoside (Figure 4.9D, M315.072_T244; See methods for means of compound identification) are all compounds synthesized from SA in plants (Figure 4.1). All three accumulated in *Rp1-D21#4/+* mutants and were not significantly different between the *Rp1-D21#4/+; ics1-1* double mutants and wild-type controls. The two DHBA glucosides were also reduced in *ics1-1* mutants as compared to wild-type controls. Taken together, these findings demonstrate that *ics1* is required for *Rp1-D21#4*-induced SA accumulation.

Previously, SA accumulation and HR severity were measured in *Rp1-D21/+* mutants crossed to different genetic backgrounds (Ge et al., 2021). I calculated the correlation between SA accumulation and lesion severity in these *Rp1-D21/+* mutants. Lesion severity was positively correlated with both free SA ($r$ = 0.72, $p$ = 0.01) and total SA ($r$ = 0.92, $p$ = 4.5E-5) levels (Figure

4.10). The suppression of SA accumulation during *Rp1-D21#4*-induced HR by *ics1-1* allowed us to test whether SA accumulation was necessary for lesion formation during HR in maize. Lesion formation in *Rp1-D21#4/+; ics1-1* double mutants was visually indistinguishable from *Rp1-D21#4/+* single mutants (Figures 4.5B and 4.5C) demonstrating that SA accumulation was a response to lesion formation and increased accumulation of SA was not required for lesion formation during HR in maize.

The biosynthetic steps that comprise an ICS-dependent pathway to SA were recently elucidated in Arabidopsis (Rekhter et al., 2019; Torrens-Spence et al., 2019). Isochorismate is first conjugated with glutamate by PBS3 to form the intermediate isochorismoyl-glutamate which spontaneously fragments or is enzymatically cleaved by EPS1 to produce SA (Figure 4.1). Isochorismoyl-glutamate was readily detectable in 50% methanol extracts from Arabidopsis at an *m/z* [M-H] = 354.083 in negative ionization mode (Rekhter et al., 2019; Torrens-Spence et al., 2019). Despite analyzing mutants that accumulated SA using similar extraction and chromatography as the Arabidopsis studies, I did not detect any mass features that could be isochorismoyl-glutamate in any of our maize genotypes. It is possible that this pathway exists in maize, but the intermediate does not accumulate or that a different amino acid conjugation is used. I calculated the expected *m/z* values for isochorismate conjugated with the other 19 amino acids and searched the untargeted mass feature list for any mass matches. Of all the matches, only one mass feature, with the predicted mass of a conjugate with threonine (M326.088_T171), increased in accumulation in *Rp1-D21#4/+* mutants. I used linear modeling to test the interaction between *Rp1-D21#4* and *ics1-1* to determine if accumulation of this feature was dependent on *ics1-1*. The M326.088_T171 feature accumulation in *Rp1-D21#4* was partially dependent on *ics1-1* and *Rp1-D21#4 ics1-1* double mutants accumulated less of this feature than the *Rp1-D21#4* single mutant (Summarized in Table 4.1). The failure to detect isochorismoyl-glutamate, especially in *Rp1-D21#4* mutant plants that accumulate SA, suggests that this pathway is not responsible for induced SA accumulation in maize.

### 4.4.5   SA can be synthesized from phenylalanine in maize

Genetic evidence suggests that the PAL-dependent SA biosynthetic pathway may contribute as much as 50% of total SA biosynthesis in maize (Yuan et al., 2019); however, this has never been demonstrated biochemically. To test if SA can be synthesized from phenylalanine in maize,

I performed stable isotopic labeling of *Rp1-D21/+* mutants and wild-type controls with phenylalanine or $^{13}$C-ring-labeled phenylalanine via roots. Soluble metabolites were extracted from developing shoots and analyzed using the same untargeted metabolomics analysis described above. Compounds synthesized from exogenously supplied $^{13}$C ring-labeled phenylalanine will co-elute with their unlabeled counterparts but differ in *m/z* by 6.020 amu. Pools of the SA derivatives, SA glucoside (M299.077_T326), 2,5-DHBA glucoside (M315.072_T190), and 2,3-DHBA glucoside (M315.072_T295) were all labeled by $^{13}$C-phenylalanine by 1-2%. The labeled forms of these compounds were detected in plants fed $^{13}$C-ring-labeled phenylalanine and not in any plants fed non-labeled phenylalanine (Figures 4.11 and 4.12). Although labeled conjugated SA was detected, labeled free SA was not detected as either the parent ion (Figure 4.13) or decarboxylation fragment (Figure 4.14) in any of the three *Rp1-D21*/+ replicates fed $^{13}$C-ring labeled phenylalanine. Taken together, the presence of labeled SA derivatives from fed $^{13}$C-ring-labeled phenylalanine suggests that SA can be produced from phenylalanine in maize.

### 4.4.6 Disruption of *ics1* suppressed PAL activity, increased tryptophan and phenylalanine accumulation, and decreased accumulation of phenylalanine-derived compounds

To evaluate if disrupting *ics1* affects chorismate-derived metabolism, I compared the accumulation of L-tryptophan and L-phenylalanine, two products derived from chorismate (Figure 4.1), in wildtype, *Rp1-D21#4/+* mutants, *ics1-1* mutants, and *Rp1-D21#4/+; ics1-1* double mutants using data generated from our untargeted metabolomics data. Phenylalanine (M164.072_103) and tryptophan (M203.038_T192) were identified by comparison to an authentic standard. Both amino acids accumulated to higher levels in *ics1-1* mutants compared to wild type (Figures 4.15A and 4.15B). In addition, *Rp1-D21#4/+; ics1-1* double mutants accumulated significantly higher levels of each amino acid compared to *ics1-1* mutants (Figures 4.15A and 4.15B Thus, disrupting *ics1* resulted in an increased accumulation of chorismate-derived amino acids (Figure 4.1) consistent with increased substrate availability.

Evidence of regulatory cross talk between the ICS-dependent and PAL-dependent SA biosynthetic pathways was previously observed in Arabidopsis. The combined decrease in SA accumulation of Arabidopsis *pal1/pal2/pal3/pal4* quadruple mutants and *ics1* mutants relative to wild-type samples exceeds 100% (Huang et al., 2010). Since disruption of ICS and PAL pathways each led to a greater than 50% reduction in SA accumulation in Arabidopsis, I propose that the

ICS1 and PAL pathways are co-regulated. If this co-regulation is conserved in maize, then the requirement of *ics1* for SA accumulation in *Rp1-D21#4* might result from both a disruption of ICS-dependent SA biosynthesis and an indirect reduction of the PAL-dependent SA biosynthetic pathway.

To determine if disrupting *ics1* affects phenylalanine-derived metabolism, I compared the accumulation of phenylalanine-derived compounds in *Rp1-D21#4/+*, *ics1-1*, and the *Rp1-D21#4/+; ics1-1* double mutant using our untargeted metabolomics data. Features derived from phenylalanine were identified by matching the masses and retention times from our ^{13}C-phenylalanine feeding experiment to our 7,094-feature list from our untargeted analysis. This identified 124 phenylalanine-derived features in our untargeted metabolite profiling. Three of these features corresponded to phenylalanine or fragments of it (M164.072_T116, M164.072_T103, and M147.045_T103) and were not considered further in this analysis. To evaluate how the remaining 121 features were affected by genotype, I performed a linear model analysis that considered how *Rp1-D21#4*, *ics1-1*, and the interaction of *Rp1-D21#4* and *ics1-1* affect metabolite accumulation. The coefficients for *Rp1-D21#4* and *ics1-1* indicate the direction (positive: higher accumulating; negative: lower accumulating) and magnitude of change in mass feature accumulation in each genotype relative to the wild-type value. The coefficient for the *Rp1-D21#4* by *ics1-1* interaction indicates the direction and magnitude of how the accumulation of a mass feature deviates from the predicted additive effect of *Rp1-D21#4* and *ics1-1* in the *Rp1-D21#4/+; ics1-1* double mutant samples. For features where *Rp1-D21#4* and *ics1-1* affected accumulation in the same direction, I also considered in which genotype the magnitude of the affect was larger. Features were grouped by coefficient significance and the direction of the coefficients for *Rp1-D21#4*, *ics1-1*, and their interaction for all 121 features are presented in Table 4.2. Despite *ics1-1* mutants accumulating 5.1 times wild-type phenylalanine levels (Figure 4.15A), only 7 of the 121 features accumulated to significantly higher levels in *ics1-1* mutants compared to wild-type controls, whereas 28 features accumulated to significantly lower levels. Of the 121 features, 48 accumulated to significantly higher levels in *Rp1-D21#4/+* mutants than in wild-type controls. These findings are consistent with a previous RNA-seq analysis, which found that transcripts encoding steps in the phenylpropanoid pathway were increased in abundance in *Rp1-D21* mutants (Olukolu et al., 2014). Of these 48 features, 37 (77%) have a significant negative

95

interaction effect, indicating *ics1-1* suppresses most *Rp1-D21#4*-induced phenylalanine-derived metabolite accumulation in *Rp1-D21#4/+; ics1-1* double mutants.

The increase in phenylalanine and decrease in phenylalanine-derived compounds in *ics1-1* mutants could be explained if maize PAL activity was reduced. To test if PAL activity is reduced in *ics1-1* mutants, I grew progeny segregating for wild type, *Rp1-D21#4/+*, *ics1-1*, and *Rp1-D21#4/+; ics1-1* and tested PAL activity in protein extracts from leaves of these four genotypes (Figure 4.15C). The *Rp1-D21#4/+* mutants had 22.2-fold higher PAL activity than wild-type siblings, consistent with the accumulation of many phenylalanine-derived compounds in *Rp1-D21#4/+* mutants. The *ics1-1* mutants had 8.2-fold less PAL activity than wild-type siblings. Consistent with the suppression of phenylalanine-derived metabolism in *ics1-1* mutants, PAL activity of the *Rp1-D21#4/+; ics1-1* double mutant was more than 5-fold less than that of *Rp1-D21#4/+* mutants. The reduction in PAL activity combined with the accumulation of phenylalanine and decrease in phenylalanine-derived compounds in the *ics1-1* mutant suggests that phenylalanine network metabolism is coordinately linked to isochorismate metabolism.

### 4.4.7 Disruption of *ics1* suppresses HR-responsive metabolism in *Rp1-D21#4* mutants

To discern if *ics1-1* is epistatic to *Rp1-D21#4* for metabolites other than those derived from phenylalanine, I utilized the same linear model analysis and applied it to all 7,094 features and again assessed how *Rp1-D21#4*, *ics1-1*, and the interaction of *Rp1-D21#4* and *ics1-1* affect metabolite accumulation I used a false discovery rate (FDR) corrected (Benjamini and Hochberg, 1995) cutoff of $p < 0.05$ which retained 3,881 features whose accumulation was under genetic control. Features were grouped by coefficient significance and the direction of the coefficients for *Rp1-D21#4*, *ics1-1*, and their interaction for all 3,881 features are presented in Table 4.3.

There were 847 features that accumulated to significantly higher levels (positive coefficient; $p < 0.05$) in *Rp1-D21#4/+* mutants and 1,061 features that accumulated to significantly higher levels in *ics1-1* mutants. Only 34 features accumulated to significantly higher levels in both genotypes, indicating that *Rp1-D21#4* and *ics1-1* predominantly lead to changes in the accumulation of different metabolites. The metabolites that were significantly decreased in abundance in either genotype did not show this pattern. Of the 694 and 1,113 features that accumulated to significantly lower levels in *Rp1-D21#4/+* and *ics1-1* mutants, respectively, 464 features accumulated to significantly lower levels in both mutants. Thus, *Rp1-D21#4* and *ics1-1*

induced the accumulation of distinct metabolite sets but tended to decrease the abundance of a similar set of metabolites.

We next evaluated the interaction effects between *Rp1-D21#4* and *ics1-1*. There were 79 features that had significant and opposite effects of *Rp1-D21#4* and i*cs1-1* and significant interaction effects. In all 79 instances, *Rp1-D21#4* increased, and *ics1-1* decreased feature accumulation (Table 4.3). For all 79 features, *ics1-1* was epistatic to *Rp1-D21#4,* and the directions of their interaction effects were always in the same direction as the main effects for *ics1-1* (Table 4.3).

The epistatic interactions between *ics1-1* to *Rp1-D21#4* were further explored by analyzing the directions of genetic effects for all mass features affected by *Rp1-D21#4*. Of the 847 features that accumulated to significantly higher levels in *Rp1-D21#4*, 601 features (71%) had a significant negative interaction coefficient and only 1 feature (0.1%) had a significant positive interaction coefficient (Table 4.3). Thus, *ics1* was required to accumulate *Rp1-D21#4*-induced metabolites. Since only 79 of these 601 features had a main effect for *ics1-1*, these findings indicate that disruption of *ics1* suppressed *Rp1-D21#4*-induced metabolism despite not detectably altering basal accumulation of these features.

Consistent with *ics1-1* acting epistatically to *Rp1-D21#4* for many metabolite features (Table 4.3), the overall metabolic consequences of *Rp1-D21#4/+; ics1-1* double mutants were very similar to those of *ics1-1* mutants and not similar to *Rp1-D21#4/+* mutants. I calculated the $log_2$ fold-change accumulation of each of the 3,881 features for each of the three genotypes in relation to the wild-type controls and performed a linear regression analysis. The correlation coefficient between *Rp1-D21#4/+; ics1-1* and *ics1-1* was 0.93 ($p < 10^{-200}$) while the correlation coefficient between *Rp1-D21#4/+; ics1-1* and *Rp1-D21#4/+* was only 0.15 ($p = 8\times10^{-22}$).

### 4.4.8 Foliar application of SA does not restore most HR-responsive metabolism in *Rp1-D21#4/+; ics1-1* double mutants

SA is a known disease signaling molecule in plants, and suppression of HR-responsive metabolic perturbations by *ics1-1* in *Rp1-D21#4/+; ics1-1* double mutants may be the result of a failure to accumulate SA. To test if increasing SA levels in *Rp1-D21#4/+; ics1-1* double mutants could restore *Rp1-D21#4*-responsive metabolism, I first determined the effects of SA application on maize metabolism. Seedlings of the inbred B73 were sprayed 10 d after sowing with 0.1 mM

SA, 1 mM SA, 5 mM SA, or mock solution every 24 h for 3 d. 72 hours after the first treatment, I performed an untargeted metabolite analysis on leaf samples. Measurements of free SA (decarboxylated fragment at M93.035_T643; Figure 4.16A) likely included SA accumulated on the leaf surface from the spray treatment. To better estimate the uptake and utilization of SA, I examined the derivatives SA-glucoside (M299.078_T412; Figure 4.16B) 2,5-DHBA glucoside (M315.073_T235; Figure 4.16C), and 2,3-DHBA glucoside (M315.072_T325; Figure 4.16D). Levels of these three SA-derivatives increased in a dose-dependent manner. The 1 mM and 5 mM treatments accumulated levels of these metabolites comparable to or higher than those observed in *Rp1-D21/+* mutants (Figure 4.16). Leaves were damaged and browned on plants treated with 5 mM SA, but not 1 mM, (Figure 4.17), indicating that a high concentration of SA was toxic. Thus, the 1 mM SA spray was used in subsequent treatments.

Families segregating for wildtype, *Rp1-D21#4/+*, *ics1-1*, and *Rp1-D21#4/+; ics1-1* were grown for 14 days and then sprayed with control solution or 1 mM SA once every 24 hours for 3 days. After the third day, I performed an untargeted metabolomic analysis of leaves. In this analysis, I detected 6,676 mass features that were present in all replicates of at least one genotype/treatment combination. Consistent with our prior SA treatments, the levels of SA (M93.035_T642), SA glucoside (M299.078_T411), 2,5-DHBA glucoside (315.073_T248), and 2,3-DHBA glucoside (M315.072_T323) were higher in all four genotypes in treated compared to non-treated samples (Figure 4.18).

Metabolite features differentially affected by SA application were identified in these samples. Foliar application of 1 mM SA affected the levels of 308 features in wild-type samples (Student's t-test, SA-treated vs. mock-treated, $p < 0.05$). Of these 308 features, 234 and 74 features showed increased and decreased accumulation respectively in wild-type plants after SA treatment. A greater number of metabolites, 505, were affected by 1 mM SA application to *ics1-1* mutants. Of these 505 features, 311 and 194 features showed increased and decreased accumulation respectively in *ics1-1* mutants after SA treatment. There were 74 features affected by SA treatment of both wild-type plants and *ics1-1* mutants. Of these 74 features, the SA-induced change in metabolite accumulation was in the same direction for 58 features and the opposite direction for 16 features (Chi-squared deviation from 1:1, $p < 10^{-7}$). I next evaluated how the SA-responsive metabolites are affected by disruption of *ics1*. Of the 308 features affected by 1 mM SA supplementation in wild-type plants, the effect of *ics1-1* was in the same direction as the SA-

treatment effect for 142 features and in the opposite direction for 166 features (Chi-squared deviation from 1:1, $p > 0.05$). These findings indicate that SA supplementation of wild-type plants did not predict the effect of disruption of *ics1*. Of the 505 features affected by 1 mM SA application to *ics1-1* mutants, the main effect of *ics1-1* was in the same direction as the SA-effect for 199 features and in the opposite direction for 306 features (Chi squared deviation from 1:1 p value$< 10^{-9}$). Thus, the loss of *ics1-1* and supplementation of *ics1-1* mutants with SA had opposing effects for more metabolites than expected by chance, indicating SA supplementation was able to counteract the metabolic consequences of *ics1-1*.

If a lack of SA is the cause of the suppression of *Rp1-D21#4*-induced metabolite features in *Rp1-D21#4/+; ics1-1* double mutants, then features that accumulate in *Rp1-D21#4/+* and not in *Rp1-D21#4/+; ics1-1* double mutants should show increased accumulation in samples treated with SA. I again utilized a linear model to analyze the genetic effects of and interactions between *Rp1-D21#4/+* and *ics1-1* on metabolite features in the mock-treated samples (Table 4.4). Of the 6,676 mass features detected, 1239 mass features accumulated to higher levels in *Rp1-D21#4/+,* and 901 (73%) of these were suppressed by the interaction of *ics1-1* and *Rp1-D21#4*. Of these 901 features, only 42 (5%) were significantly higher in *Rp1-D21#4/+; ics1-1* double mutants treated with 1 mM SA than mock-treated double mutants (Table 4.5). The 42 features included SA (decarboxylation fragment- M93.035_T642) and masses consistent with SA derivatives including methyl salicylate (M151.04_T611), SA glucoside (Parent- M299.078_T411, aglucone fragment- M137.025_T411, decarboxylation fragment- M93.035_T409, SA-glucoside dimer- M599.162_T406), 2,3-DHBA glucoside (M315.072_T323), amino SA (Parent- M152.012_T257, decarboxylation fragment- M108.022_T257), and methyl amino SA (M166.027_T336). In addition to the putative amino SA and decarboxylation fragment, eight differentially accumulated metabolite features co-elute from 254-258 seconds, suggesting they are either artifacts generated by the putative amino SA or derive from a co-eluting unknown compound. These features included a mass consistent with catechol (M109.029_T256), suggesting an additional unknown compound with a dihydroxy benzene moiety that is also derived from SA co-elutes at this time. Taken together, this experiment demonstrates that SA was not sufficient to restore the accumulation of most of the *Rp1-D21#4*-responsive metabolites that are suppressed in *Rp1-D21#4/+; ics1-1* double mutants. Of the features restored by SA treatment, many are likely derived directly from SA indicating that

the addition of SA provided substrate for their synthesis and did not induce the accumulation of these metabolites through signaling.

### 4.4.9  Loss of chlorophyll by *Oy1-N1989* does not suppress *Rp1-D21#4*-induced metabolism

If the loss of photosynthetic capacity in *ics1-1*, and not a specific requirement for a downstream isochorismate-derived metabolite(s), is responsible for the suppression of *Rp1-D21#4*-induced metabolism, any mutant with impaired photosynthesis should also be epistatic to *Rp1-D21#4*. To test this, I used the *Oy1-N1989* mutant, a semi-dominant allele of subunit I of the Magnesium Chelatase enzyme in the chlorophyll pathway. Chlorophyll levels of *Oy1-N1989/+* mutants are only 10% of wild-type siblings early in development (Khangura et al., 2019). In addition, *Oy1-N1989* mutants have decreased $CO_2$ assimilation and decreased maximum quantum yield of PSII (Fv/Fm; Khangura et al., 2020). I crossed *Oy1-N1989/+* mutants as a pollen parent onto *Rp1-D21#4/+* mutant ears to generate material segregating phenotypically for wild type*, Rp1-D21#4, Oy1-N1989,* and *Rp1-D21#4; Oy1-N1989* double mutants. The same untargeted metabolomic profiling described above was performed to determine what effect loss of chlorophyll and reduced photosynthesis had on metabolite accumulation in these leaf samples. This analysis detected 1,927 mass features that were reproducibly detectable in all replicates (n=4) in at least one of the four genotypes.

Like the *Rp1-D21#4/+* and *Rp1-D21#4/+; ics1-1* siblings, there were little to no distinguishable differences in the lesion phenotypes of *Rp1-D21#4/+* and *Rp1-D21#4/+; Oy1-N1989/+* siblings (Figure 4.19). Unlike the *Rp1-D21#4/+; ics1-1* double mutants, the metabolite response of *Rp1-D21#4/+; Oy1-N1989/+* double mutants closely resembled that of *Rp1-D21#4/+* mutants. I calculated the $\log_2$ fold-change accumulation of all 1,927 features for each genotype relative to the wild-type controls and performed a linear regression analysis. The correlation coefficient between *Rp1-D21#4/+* and the *Rp1-D21#4/+; Oy1-N1989/+* double mutants was 0.73 ($p < 10^{-200}$) while the correlation coefficient between *Oy1-N1989/+* and *Rp1-D21#4/+; Oy1-N1989/+* was only 0.39 ($p < 10^{-69}$). Thus, most of the *Rp1-D21#4*-responsive metabolites are still affected in *Rp1-D21#4/+; Oy1-N1989/+* double mutants. In addition, the *Rp1-D21#4*-induced increased accumulation of SA, SA glucoside, 2,5-DHBA glucoside, and 2,3-DHBA glucoside was also observed for *Rp1-D21#4/+; Oy1-N1989/+* double mutants (Figures 20A-D). Taken together, these findings, along with the insufficiency of SA supplementation to restore *Rp1-D21#4*-induced

metabolism in *Rp1-D21#4/+; ics1-1* double mutants suggest that *ics1-1* blocks *Rp1-D21#4-*induced metabolism by a mechanism independent of SA biosynthesis or photosynthetic limitation.

## 4.5 Discussion, Conclusions, and Future Directions

In this work I describe a loss-of-function mutant of maize *ics1*. The *ics1-1* allele resulted in a ~90% reduction in phylloquinone biosynthesis (Figure 4.6A). While not quite as severe, the *ics1-1* mutants phenotypically more closely resemble *ics1 ics2* double mutants of Arabidopsis than single mutants of either gene (Wildermuth et al., 2001; Gross et al., 2006; Garcion et al., 2008). The two Arabidopsis *ICS* genes do not equally contribute to ICS activity (Garcion et al., 2008), and single mutants of *ics1* are often used for studying the role of ICS in SA production (Wildermuth et al., 2001; Huang et al., 2010). Despite producing only 33% of wild-type phylloquinone levels and about half of wild-type SA levels under control conditions, Arabidopsis *ics1* mutants are morphologically similar to wild-type plants (Garcion et al., 2008) and do not present any stunted growth or leaf yellowing. In contrast, maize *ics1-1*, which produced ~10% of wild-type phylloquinone levels had severe growth and chlorophyll defects (Figures 4.5 and 4.7E). This suggests that plants can sustain normal growth and coloration with reduced phylloquinone, and that growth and pigmentation defects manifest when phylloquinone drops below a critical level. The viability of the strong hypofunctional *ics1-1* allele allowed us to examine the role of ICS in phenomena that occur as plants develop and mature, such as the formation of lesions during the hypersensitive response.

### 4.5.1 Reduction in photosynthesis was insufficient to block Rp1-D21#4-induced metabolism

Of the photosynthetic parameters that have been measured for both *Oy1-N1989/+* and *ics1-1* mutants, photosynthesis is reduced more by *Oy1-N1989/+* than by *ics1-1* mutants. Compared to wild-type controls, chlorophyll levels were reduced 89% and the maximum efficiency of PSII photochemistry (Fv/Fm) was decreased 41% in *Oy1-N1989/+*:B73 mutants (Khangura et al., 2019, 2020). These decreases are greater than the 50% drop in chlorophyll (Figure 4.7E) and 16% drop in Fv/Fm (Figure 4.7D) in chlorophyll levels and Fv/Fm measured in *ics1-1* mutants. Yet, *Oy1-*mediated loss of photosynthesis did not suppress *Rp1-D21#4*-induced metabolite accumulation (Figure 4.20). Thus, energy limitation per se is an unlikely mechanism for suppressing HR-induced

metabolism in *Rp1-D21#4;ics1-1* double mutants. It is possible that the way photosynthesis is altered in *ics1-1* but not *Oy1-N1989* can suppress specialized metabolism. PSII and PSI stoichiometry, the levels of phylloquinone and plastoquinone, and the PSI electron transport rate are unknown in *Oy1-N1989/+* mutants. If these are unaffected by *Oy1-N1989*, it is possible that the shift in PSII and PSI stoichiometry (Figure 4.8), the loss of phylloquinone or plastoquinone (Figure 4.6), or the decrease rate of forward electron flow through PSI in *ics1-1* mutants (Figure 4.7) leads to suppression of and HR-induced metabolism. Inhibiting phylloquinone biosynthesis in *Rp1-D21#4/+* mutants by targeting enzymes in the phylloquinone biosynthetic pathway downstream of ICS (Widhalm and Rhodes, 2016) would provide a test of whether a loss of phylloquinone and photosynthetic deficiencies lead to suppression of HR-induced metabolism.

### 4.5.2   The two known pathways of SA biosynthesis in plants are not independent

In plants, SA can be synthesized from both the ICS-dependent and PAL-dependent pathways (Figure 4.1). In this work, I have provided evidence for the existence of both pathways in maize. *ics1* was required for SA accumulation (Figure 4.9), and SA-derivatives can be labeled by $^{13}$C-phenylalanine (Figures 4.11 and 4.12). One unexpected finding is that derivatives of the phenylpropanoid pathway and PAL activity both require *ics1* (Table 4.2 and Figure 4.15C). This result entangles the two known plant SA biosynthetic pathways and complicates the interpretation of the loss of SA in *ics* mutants in maize and possibly all plants. Because SA can be made from phenylalanine via PAL, and PAL activity was suppressed in the *ics1-1* mutant (Figure 4.15C), the loss of SA in the *ics1-1* mutant could result, at least in part, from the suppression of PAL. Thus, I cannot regard the requirement of *ics1* for SA accumulation during *Rp1-D21*-mediated HR as evidence that SA is predominantly derived from isochorismate. A retrospective assessment of the literature suggests this is unlikely restricted to maize. For example, previous work in Arabidopsis found that SA was reduced by 90% in *ics1* mutants and 50% in a *pal1/2/3/4* quadruple mutant (Huang et al., 2010). Similar results were obtained in soybean where SA accumulation was decreased by 90% when ICS was knocked down by virus-induced gene silencing (VIGS) and 95% when PAL was knocked down by VIGS (Shine et al., 2016). If both pathways additively contribute to SA accumulation, then the single pathway knockdowns should add up to 100%, perhaps even less if the loss of one pathway is compensated for by increased flux through the other. Instead, these prior studies and ours indicate that these two pathways require each other in some previously

unrecognized manner. Since disruption of *ICS* suppresses PAL activity, our results, and any of the prior genetic experiments are not sufficient to estimate the relative contribution of the two pathways to SA accumulation. Metabolic flux analyses with labeled phenylalanine and labeled isochorismate are required to determine how much each pathway contributes to SA biosynthesis. In our labeling experiment I did not detect phenylalanine-derived labeled free SA. The relative counts of SA were much lower than SA glucoside, 2,5-DHBA glucoside, and 2,3-DHBA glucoside in *Rp1-D21#4/+* mutants (Figure 4.9). The detection of the more abundant derivatives, and failure to detect labeled SA may be due to hyperconversion of SA to these derivatives. Metabolic flux analyses of SA biosynthesis and catabolism will likely require optimizing SA detection or monitoring of SA-derived products as presented here.

We did not detect the intermediates in the recently described ICS-dependent SA biosynthetic pathway from Arabidopsis (Rekhter et al., 2019; Torrens-Spence et al., 2019) in maize. This failure to detect included *Rp1-D21* mutants which accumulated 9-fold more SA and as much as 99-fold more SA-glucoside. I used similar extraction and chromatography methods as used in the studies of Arabidopsis, so this failure is unlikely to owe to technical variation in the methods. The maize genome encodes a number of genes in the *Gretchen Hagen3* enzyme family, one or more of which may catalyze the same or similar reaction as PBS3, but I did not find any metabolite features with the *m/z* values for isochorismate conjugated with any amino acid that was ICS-dependent. It may be that the PBS3 pathway is taxonomically restricted. PBS3 is a member of a group of the *Gretchen Hagen3* enzyme family which is present in Arabidopsis but not maize and no clear PBS ortholog is encoded by the maize genome (Feng et al., 2014). Consistent with this, *EPS1*, the second step in the Arabidopsis ICS-dependent SA pathway, is restricted to the *Brassicaceae* . This enzyme is unlikely to be strictly required for this pathway as isochorismoyl-glutamate can spontaneously convert to SA (Rekhter et al., 2019; Torrens-Spence et al., 2019). The presence of EPS1 in the *Brassicaceae* may indicate that the ICS-dependent pathway is the predominant route for induced SA synthesis in that plant family. This is further evidenced in the correlation of *ICS* expression and SA accumulation in Arabidopsis (Wildermuth et al., 2001). Further work is needed to demonstrate the generality of this pathway. In tobacco, despite accumulating high levels of SA, *ICS* expression was unchanged following pathogen infection and instead PAL transcripts were increased (Ogawa et al., 2006). In pathogen-infected soybean and *Rp1-D21* mutants, which both accumulate increased levels of SA, ICS transcript accumulation is

significantly decreased, and PAL transcripts were increased (Olukolu et al., 2014; Shine et al., 2016) inconsistent with the ICS pathway contributing to the induced accumulation of SA. Thus, in multiple experiments outside the Brassicaceae, including *Rp1-D21*-induced gene expression in maize, *PAL* expression is corelated with SA accumulation and *ICS* expression was not.

### 4.5.3 Increased accumulation of SA is not required for Rp1-D21#4-induced HR lesion formation

Accumulation of SA is a hallmark of HR and many autoimmune lesion-forming mutants (Morris et al., 1998; Bruggeman et al., 2015; Radojičić et al., 2018). In this work, I demonstrated that increased SA accumulation is not required for the initiation or progression of lesions caused by *Rp1-D21#4*. The *Rp1-D21#4/+*; *ics1-1* double mutants, which accumulated approximately four-fold less SA than *Rp1-D21#4/+* single mutants (Figure 4.9), has a similar lesion phenotype as *Rp1-D21#4/+* (Figure 4.5). In addition, foliar application of SA that increased SA concentration by almost 300-fold compared to mock-treated plants and 17-fold compared to *Rp1-D21/+* (Figure 4.16) did not induce HR-like lesions formation 72 h after treatment. Likewise, SA treatment neither induced the accumulation of HR-induced metabolites, nor rescued the *Rp1-D21*-induced metabolites from the epistatic suppression by *ics1-1* (Table 4.5). These findings demonstrate that SA is neither necessary nor sufficient for lesion formation during HR in maize. These findings indicate a difference in signaling between maize and Arabidopsis. In Arabidopsis, conversion of SA to catechol by overexpression of the *NahG* SA hydroxylase suppressed lesion formation and cell death in autoimmune lesion-forming mutants (Weymann et al., 1995; Rate et al., 1999; Brodersen et al., 2005; Huang et al., 2018). HR and cell death can also be triggered in Arabidopsis via supplemental treatment with SA (Dietrich et al., 1994).

SA can be converted to 2,5-DHBA and 2,3-DHBA, which are rapidly glycosylated (Huang et al., 2018). In Arabidopsis, overexpression of *UGT76D1*, which glycosylates 2,5-DHBA and 2,3-DHBA, resulted in increased cell death (Huang et al., 2018), indicating these DHBAs may function in lesion formation during HR. I demonstrated that both 2,5-DHBA glucoside and 2,3-DHBA glucoside accumulated in *Rp1-D21#4/+* mutants (Figure 4.9) and both compounds accumulated in a concentration-dependent manner after foliar spray with SA (Figures 4.16 and 4.18). Neither 2,5-DHBA glucoside nor 2,3-DHBA glucoside accumulated in *Rp1-D21#4/+*; *ics1-1* mutants (Figure 4.9). Given that none of these treatments altered lesion formation, 2,5-DHBA and 2,3-

DHBA were also not required for HR lesion formation in maize. Similarly, I expect that other isochorismate-derived products, like phylloquinone and the pathway intermediate 1,4-dihydroxy-2-naphthoic acid (DHNA) which were proposed to be involved in triggering programmed cell death in Arabidopsis (Brodersen et al., 2005) are also not involved in HR lesion formation in maize.

### 4.5.4 Suppression of Rp1-D21#4-induced metabolism in Rp1-D21#4/+; ics1-1 is not dependent on SA

Our untargeted metabolite analysis demonstrated suppression of *Rp1-D21#4*-induced metabolism in *Rp1-D21#4/+; ics1-1* double mutants (Tables 4.3 and 4.4). PAL activity was decreased in *ics1-1* mutants (Figure 4.15C), and of the 46 phenylalanine-derived *Rp1-D21#4*-induced compounds, 37 were reduced in accumulation in the double mutants (Table 4.2). Just as for SA, these findings indicate that accumulation of these phenylalanine-derived compounds was not required for *Rp1-D21#4*-induced lesion formation. Phenylalanine-derived features accounted for only 5% of those induced by *Rp1-D21#4* and suppressed by the interaction of *Rp1-D21#4* and *ics1-1*. Thus, disrupting *ics1* suppressed multiple *Rp1-D21#4*-induced metabolic pathways. These effects were not rescued by the addition of SA, demonstrating that SA accumulation is neither the trigger nor a modulator of HR-induced metabolic perturbations in this system.       Despite evidence that phenylpropanoids are unnecessary for HR-induced lesions, the phenylpropanoid pathway has been linked to HR suppression. Two enzymes likely involved in phenylpropanoid metabolism, a hydroxycinnamoyl transferase paralog  and caffeoyl CoA *O*-methyltransferase paralog, physically interact with the *Rp1-D21* protein and suppress HR and lesion formation in response to *Rp1-D21* (Wang et al., 2015a; Wang and Balint-Kurti, 2016). Mutations of conserved residues required for the catalytic functions of these enzymes did not interfere with HR suppression indicating that suppression is likely mediated by protein-protein interaction and does not require a phenylalanine-derived product.

That the loss of ICS suppressed most *Rp1-D21#4*-induced metabolites and did not block lesion formation suggests that many of the metabolic changes are consequences of a programmed response rather than the effects of oxidation during cell death. The presence of lesions in the double mutants also demonstrates that HR initiation and progression are not dependent on the soluble metabolites suppressed by *ics1-1*. The 29% of the *Rp1-D21#4*-induced features that are not suppressed by the interaction of *Rp1-D21#4/+*; *ics1-1* contain the remaining candidates for HR

induction signaling along with features that accumulate because of cell death. Further experimentation is necessary to determine if these metabolites act in a signaling capacity.

## 4.6    Declaration of collaborative work

The ordering of *isc1-1* mutants and designing of genotyping primers were performed by Dr. Ross Zhan (Purdue University) and Dr. Gurmukh Johal (Purdue University). All photosynthetic parameter measurements and photosystem quantifications were performed by Dr. Iskander Ibrahim (Purdue University) and Sujith Puthiyaveetil (Purdue University). Phylloquinone and plastoquinone measurements were performed by Dr. Rachel McCoy (Purdue University). Stable isotope feedings were performed by Dr. Jeff Simpson (Purdue University). The PAL assay was performed with Dr. Fabiola Muro-Villanueva (Purdue University). Interpretation of results and written preparations were completed either by or with consult from the people who performed experiments and contributions from Dr. Brian Dilkes (Purdue University), Dr. Clint Chapple (Purdue University), and Dr. Joshua Widhalm (Purdue University).

## 4.7  Figures and Tables
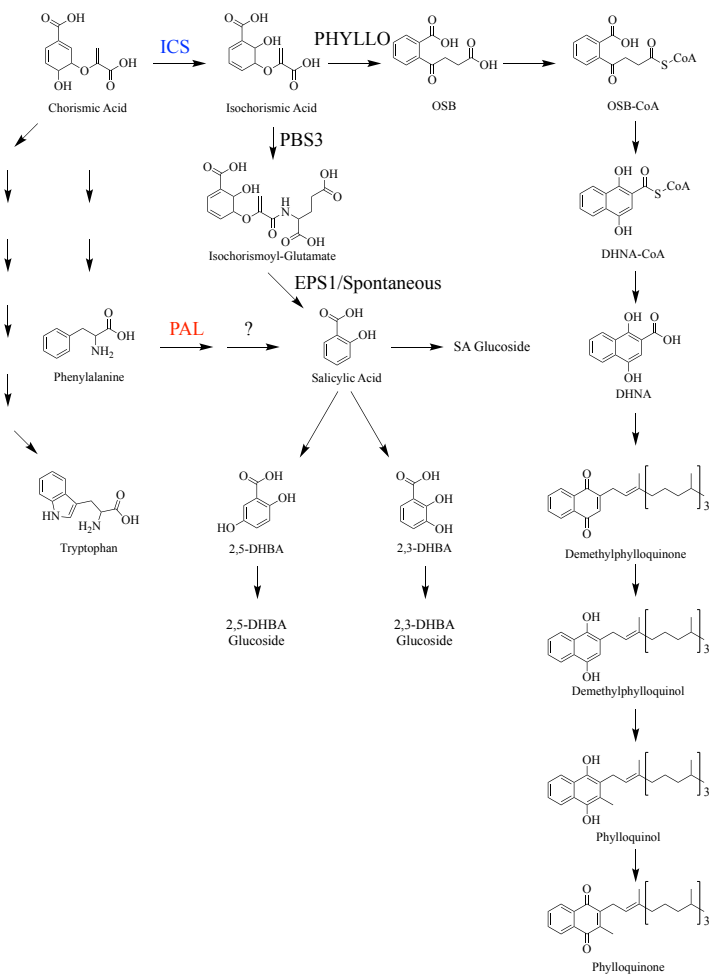


**Figure 4.1: Biosynthetic pathways of phylloquinone and salicylic acid in plants.**
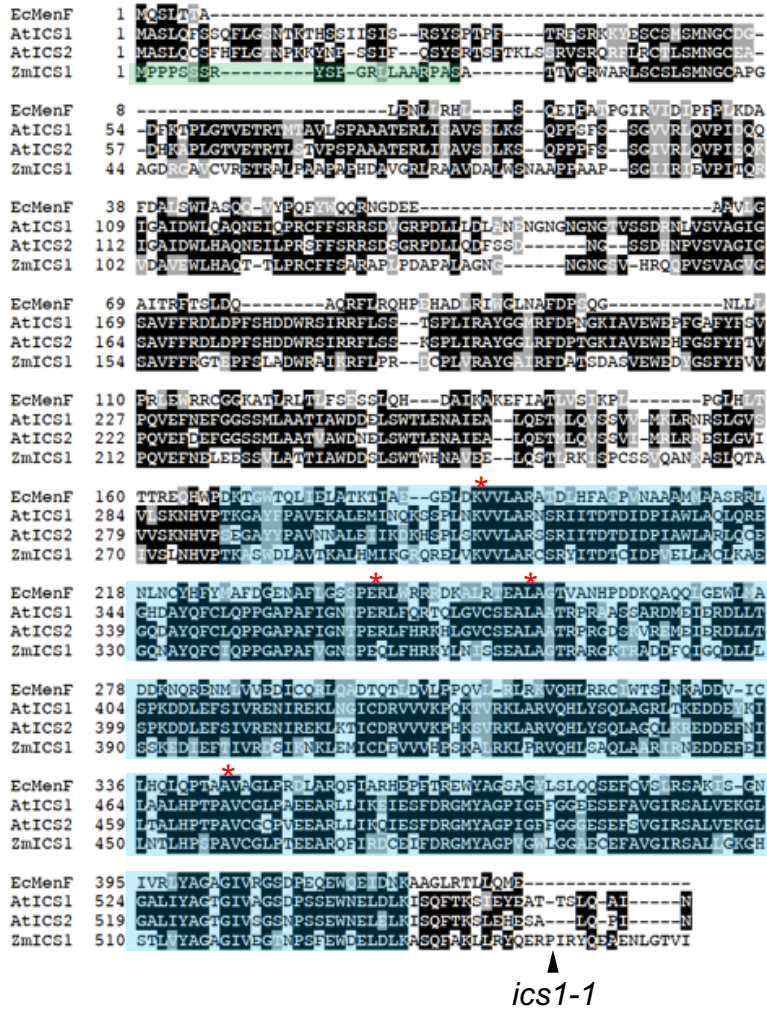
**Figure 4.2: Zea mays encodes a single isochorismate synthase gene.**

Sequence alignment of the amino acid sequence of *Escherichia coli* MenF, *Arabidopsis thaliana* ICS1 and ICS2, and *Zea mays* ICS1. Conserved lysine (*E. coli* K190), glutamic acid *(E. coli* E240)*, leucine *(E. coli* L255)*, and alanine (*E. coli* A344) residues required for ICS activity are denoted by red stars(Kolappan et al., 2007). The highly conserved chorismate binding domain (Pfam accession no. PF00425) is shaded in blue. The putative 21 amino acids that make up the maize ICS1 chloroplast targeting peptide are highlighted in green. Mutator insertion position for *ics1-1,* relative to the *Z. mays* ICS1 amino acid sequence, is labeled by a black arrowhead.
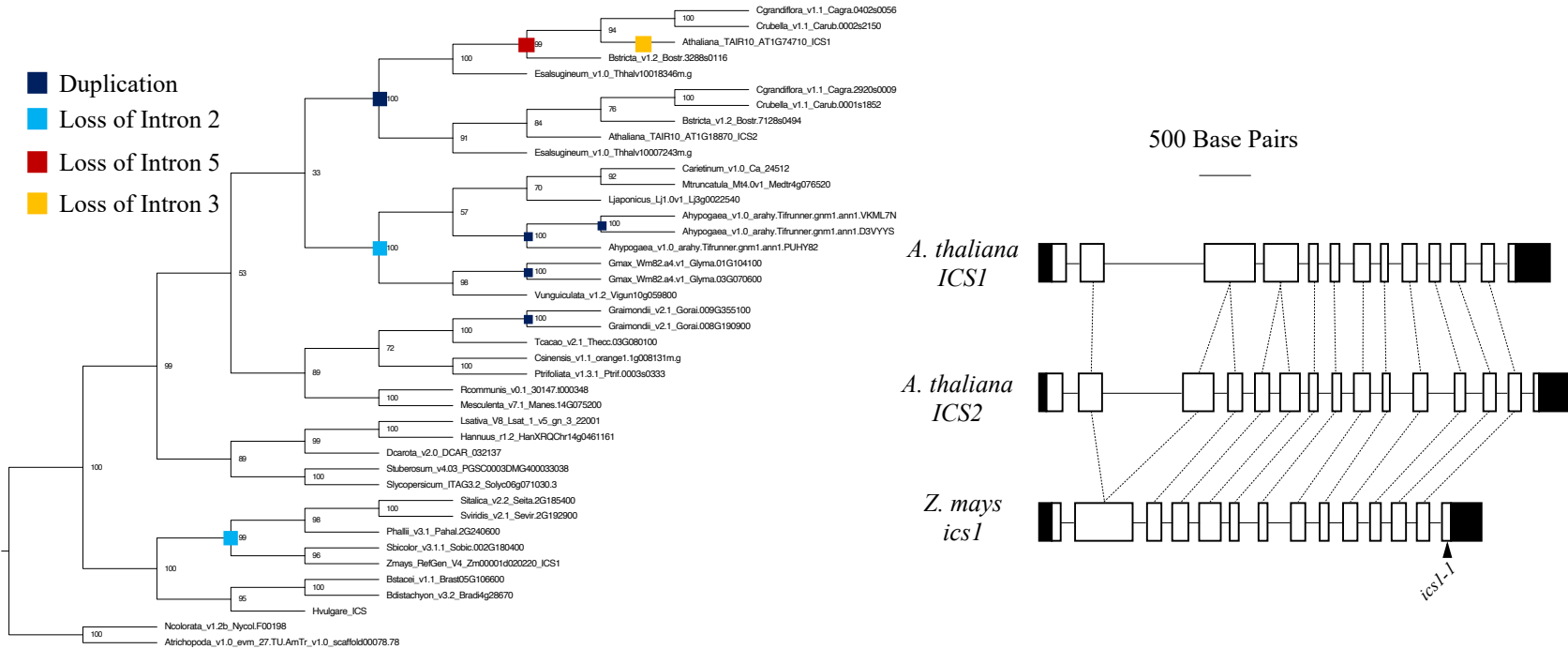
**Figure 4.3: Phylogeny and structures of angiosperm isochorismate synthases.**

All gene names are from Phytozome v13 except for *Hordeum vulgare.* Bootstrap values are out of 100 iterations. Colored squares represent points of gene duplication or loss of introns 2, 3, or 5 as depicted by the exon intron diagrams (right) for Arabidopsis *ICS1* and *ICS2* and maize *ics1*. Exons are denoted by empty white boxes and introns by thin black lines. Shaded boxes represent the 5'- and 3'-UTR. Exons connected by dotted lines denote regions of high sequence similarity. Mutator insertion position for *ics1-1* relative to the maize *ics1* gene structure is labeled by a black arrowhead.
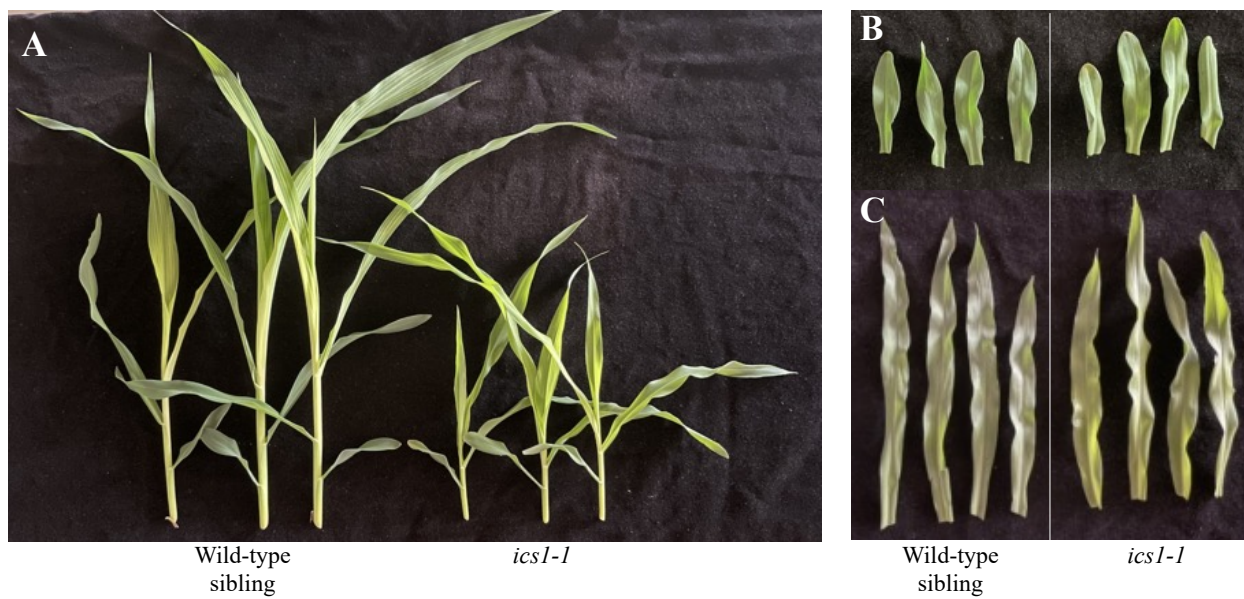
**Figure 4.4: Phenotypic severity of *ics1-1* mutants.**

Representative photos of (A) whole seedlings, (B) first leaves, and (C) second leaves from 14-day old *ics1-1* mutants and wild-type siblings.

**Figure 4.5: *ics1-1* mutants are stunted and pale, and *Rp1-D21#4/+; ics1-1* have a similar lesion severity as *Rp1-D21#4/+* mutants.**

A) Field grown wild-type, *Rp1-D21#4/+*, *ics1-1*, and *Rp1-D21#4/+; ics1-1* plants ~50 days after planting. Representative B) first and C) second leaves from wildtype, *Rp1-D21#4/+* mutants, *ics1-1* mutants, and *Rp1-D21#4/+; ics1-1* double mutants grown under greenhouse conditions 16-days after sowing.
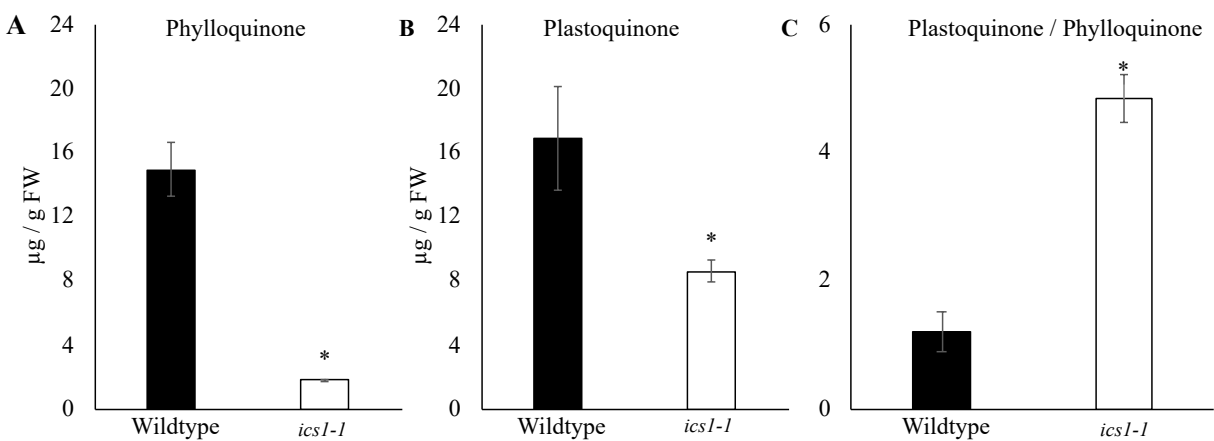
**Figure 4.6: Phylloquinone and plastoquinone accumulation is reduced in the _ics1-1_ mutant.**

(A) Phylloquinone and (B) plastoquinone amounts and (C) and the relative ratio of plastoquinone/phylloquinone in wild-type and _ics1-1_ siblings. Data presented are mean $\pm$ S.E. (n = 4). Stars above bars represent statistically different measurements between wildtype and _ics1-1_ (Student's T-test, $p < 0.05$).
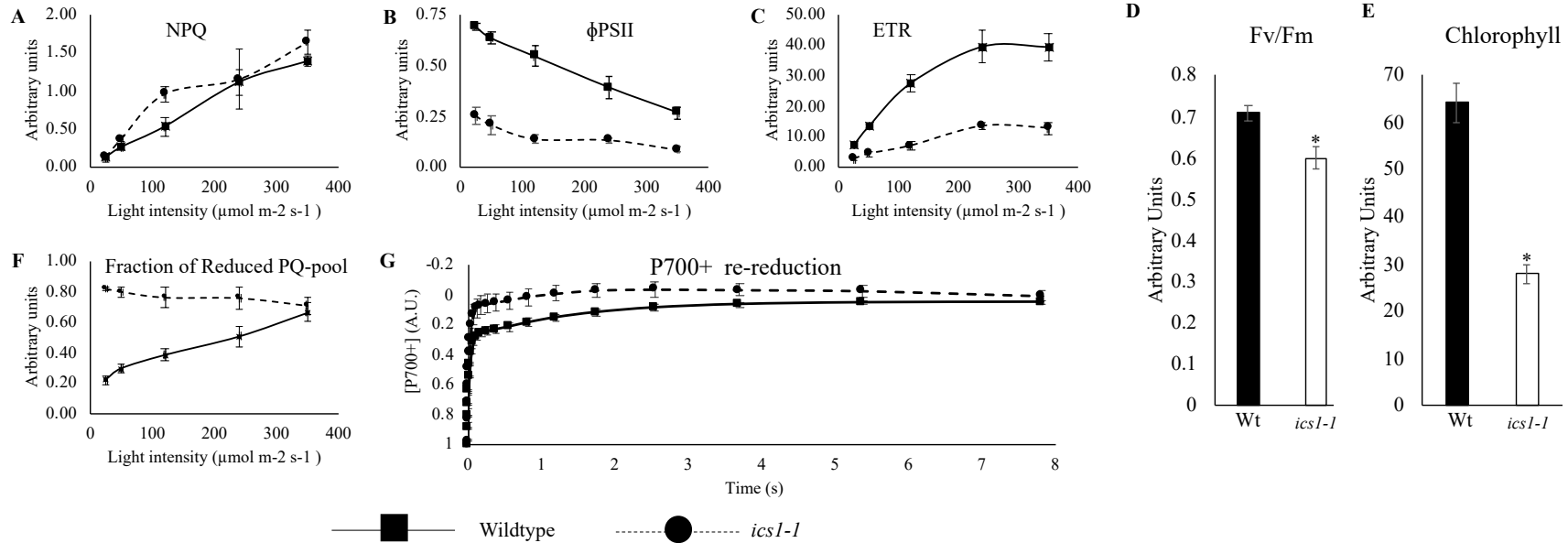
**Figure 4.7: *ics1-1* mutants have decreased photosynthetic efficiency and impaired electron transport.**

A) Non-photochemical quenching (NPQ), (B) PSII efficiency (ΦPSII), (C) electron transport rate (ETR), (D) Maximum efficiency of PSII photochemistry (Fv/Fm), (E) relative chlorophyll content, and (F) fraction of reduced PQ-pool in wild-type and *ics1-1* siblings. Data presented are means ± S.E. (n ≥ 5). Asterix indicate a statistically significant difference between wild-type and *ics1-1* samples (Student's T-test, $p < 0.05$). (G) Re-reduction of P700$^+$ complexes in wild-type and *ics1-1* siblings over time after transfer from light to dark. Data for each timepoint represents the means ± S.E. (n ≥ 5).
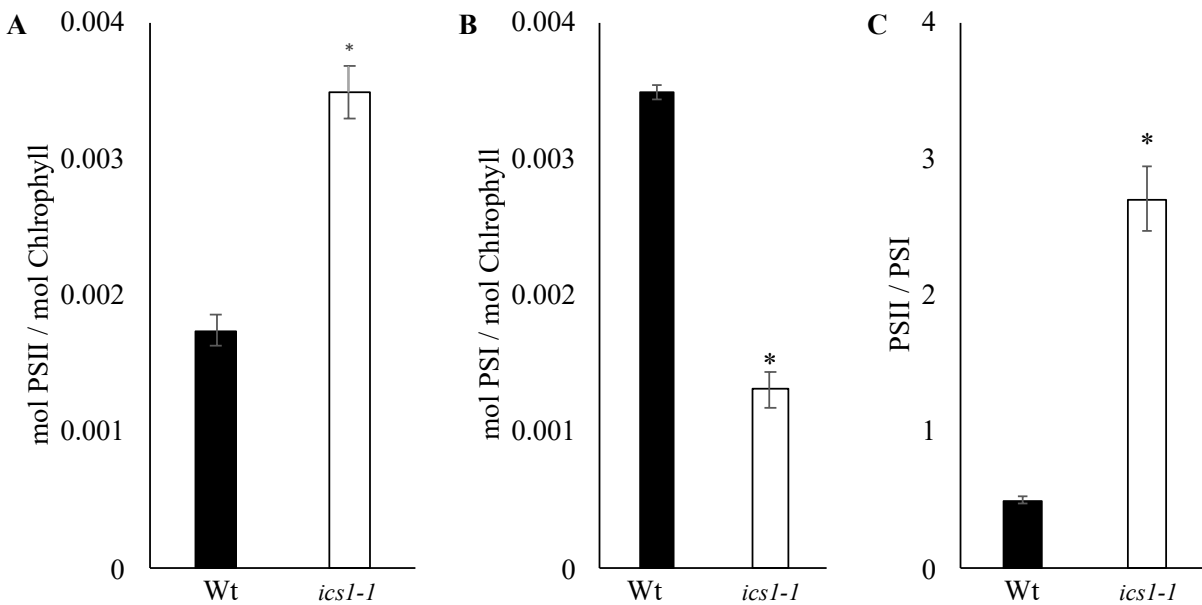
**Figure 4.8: There is loss of photosystem I in *ics1-1* mutants.**

(A) Amount of photosystem II and (B) photosystem I relative to chlorophyll and (C) the relative ratios of photosystem II and I in Wt and *ics1-1* siblings. Data presented are means $\pm$ S.E. (n = 4). Stars above bars represent statistically different measurements between Wt and *ics1-1* (Student's T-test, $p < 0.05$).
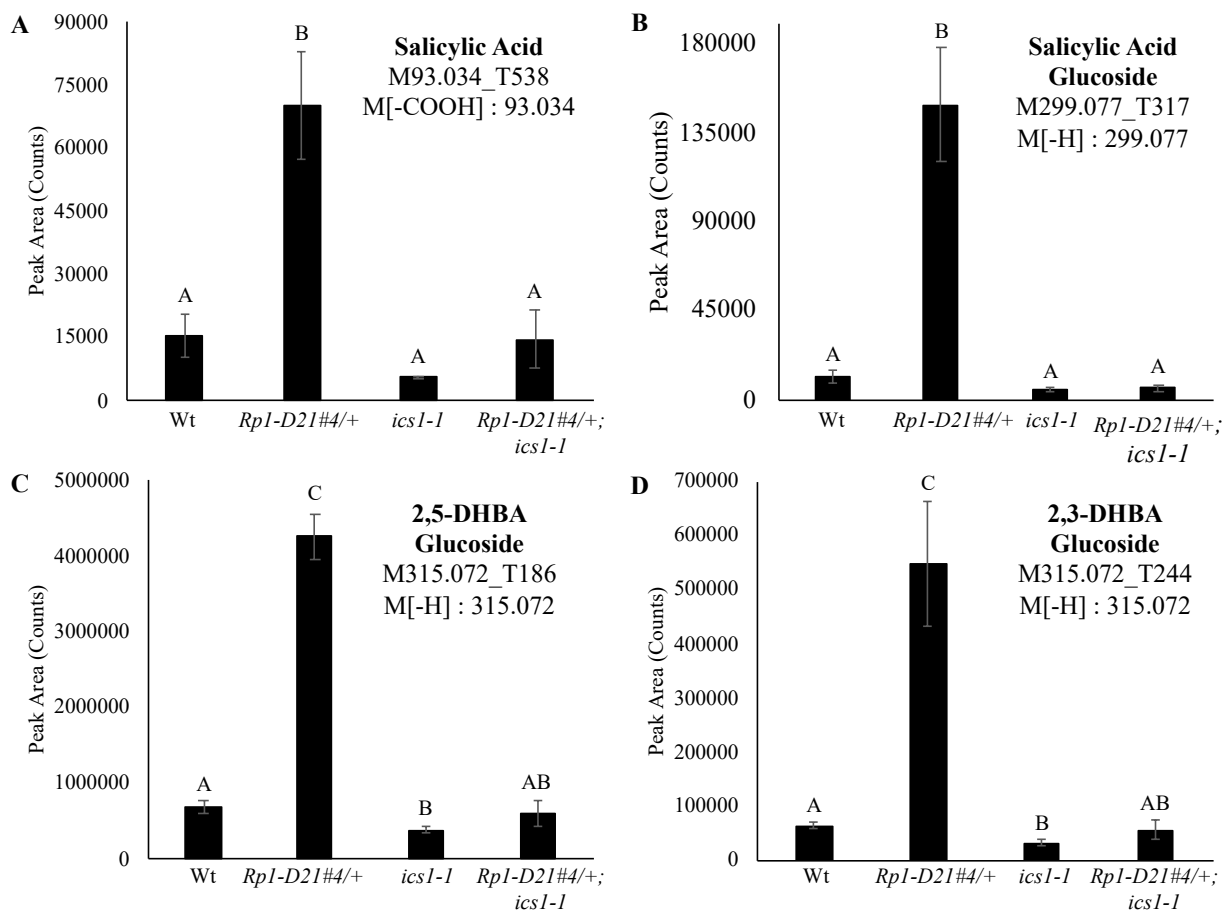
**Figure 4.9: *ics1* is required for *Rp1-D21#4*-induced SA accumulation.**

Integrated peak areas of (A) salicylic acid, (B) salicylic acid glucoside, (C) 2,5-DHBA glucoside, and (D) 2,3-DHBA glucoside from leaves of Wt, *Rp1-D21#4/+, ics1-1,* and *Rp1-D21#4/+; ics1-1*. Metabolites were analyzed in negative ionization mode. For salicylic acid, the integrated values are of the major decarboxylation fragment M[-COOH]. For salicylic acid glucoside, 2,5-DHBA glucoside, and 2,3-DHBA glucoside the values are integrations of the parent ion. Data presented are the mean values $\pm$ S.E. (n $\geq$ 3). Letters above bars represent statistically different measurements (paired sample Student's T-test $p < 0.05$).

| *Rp1-D21/+* X | Total SA Bar height (mm) | Free SA Bar height (mm) | Lesion severity |
|---|---|---|---|
| B73 | 7 | 1.5 | 3 |
| Mo17 | 14 | 4 | 6 |
| H95 | 9 | 1 | 4 |
| B97 | 2 | 0.5 | 2 |
| NC350 | 24 | 5 | 9 |
| M162W | 13 | 6 | 8 |
| M37W | 18 | 7 | 8 |
| Tx303 | 28 | 21 | 9 |
| Oh7b | 2 | 1.5 | 3 |
| Oh43 | 4 | 2 | 3 |
| Ky21 | 6 | 4 | 5 |
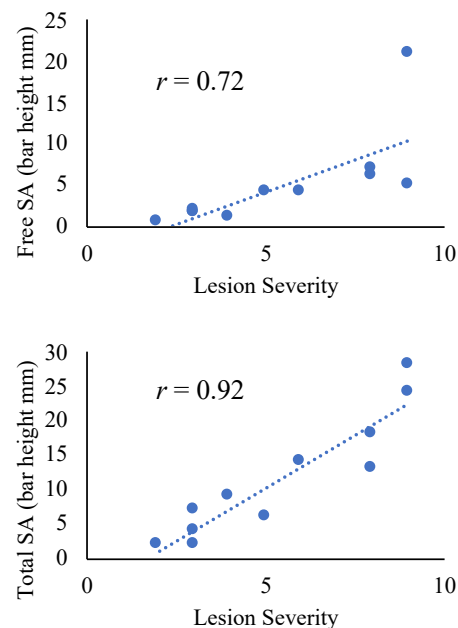


**Figure 4.10: *Rp1-D21/+* lesion severity is positively correlated with levels of salicylic acid.**

SA levels and Lesion severity scores are from Ge et a. 2021(Ge et al., 2021). Linear regression comparing lesion severity of the different *Rp1-D21/+* mutants and (top) free SA and (bottom) total SA levels.

**Table 4.1: Accumulation of putative isochorismoyl-amino acids in *Rp1-D21#4/+*, *ics1-1*, and *Rp1-D21#4/+; ics1-1***

| Amino Acid | Predicted *m/z* isochorismate [M-H) | Mass Matches | Intercept coefficient | *Rp1-D21#4* coefficient | *ics1-1* coefficient | Interaction coefficient |
|---|---|---|---|---|---|---|
| Glycine | 282.062 | M282.062_T174 | 3357.8 | 566.32 | 56245.91 | 9098.134 |
| Alanine | 296.077 | M296.082_T251 | 6016.29 | -47.115 | 2052.4833 | 769.6657 |
| Serine | 312.072 | M312.073_T124 | 18600.43 | 11062.1 | 5479.857 | 2718.653 |
| | | M312.073_T163 | 21719.907 | 7813.723 | 4186.959 | -3597.417 |
| | | M312.073_T194 | 986.155 | 3132.792 | 26986.752* | 7180.751 |
| | | M312.073_T238 | 3161.145 | 726.645 | 61202.578* | -46540.766 |
| Proline | 322.092 | M322.09_T445 | 12759.8 | 7123.21 | 11009.11* | -4606.286 |
| | | M322.093_T513 | 2004.0475 | 237.11 | 723.1258 | 312.5087 |
| Threonine | 326.087 | M326.088_T171 | 23360.472 | 32908.92* | -6366.596 | -33660.709* |
| | | M326.088_T394 | 107215.04 | 17851.64 | 44432.23 | 5784.69 |
| | | M326.087_T408 | 34566.05 | 18301.3 | 31727.66 | -25300.02 |
| | | M326.088_T155 | 11183.1075 | 693.4725 | 2807.6058 | -3751.8318 |
| | | M326.088_T593 | 1566.48 | -64.565 | 3445.327 | 5558.292 |
| Cysteine | 328.049 | M328.045_T84 | 1703.73 | 1995.512 | 134836.793 | -87544.748 |
| Aspartic Acid | 340.067 | M340.068_T181 | 5384.895 | 3492.385 | 7428.178* | -3309.49 |
| | | M340.067_T239 | 4387.925 | -428.55 | 81024.985* | -63728.13 |
| Phenylalanine | 372.108 | M372.108_T520 | 88580.81 | -59293.18* | -61800.06* | 40811.26 |
| Arginine | 381.141 | M381.14_T192 | 11659.065 | 1295.97 | -294.0483 | -2459.7747 |
| Aspartic Acid | 340.067 | M340.068_T181 | 5384.895 | 3492.385 | 7428.178* | -3309.49 |
| | | M340.067_T239 | 4387.925 | -428.55 | 81024.985* | -63728.13 |
| Phenylalanine | 372.108 | M372.108_T520 | 88580.81 | -59293.18* | -61800.06* | 40811.26 |
| Arginine | 381.141 | M381.14_T192 | 11659.065 | 1295.97 | -294.0483 | -2459.7747 |

\* Values are significantly different than the intercept ($p < 0.05$)
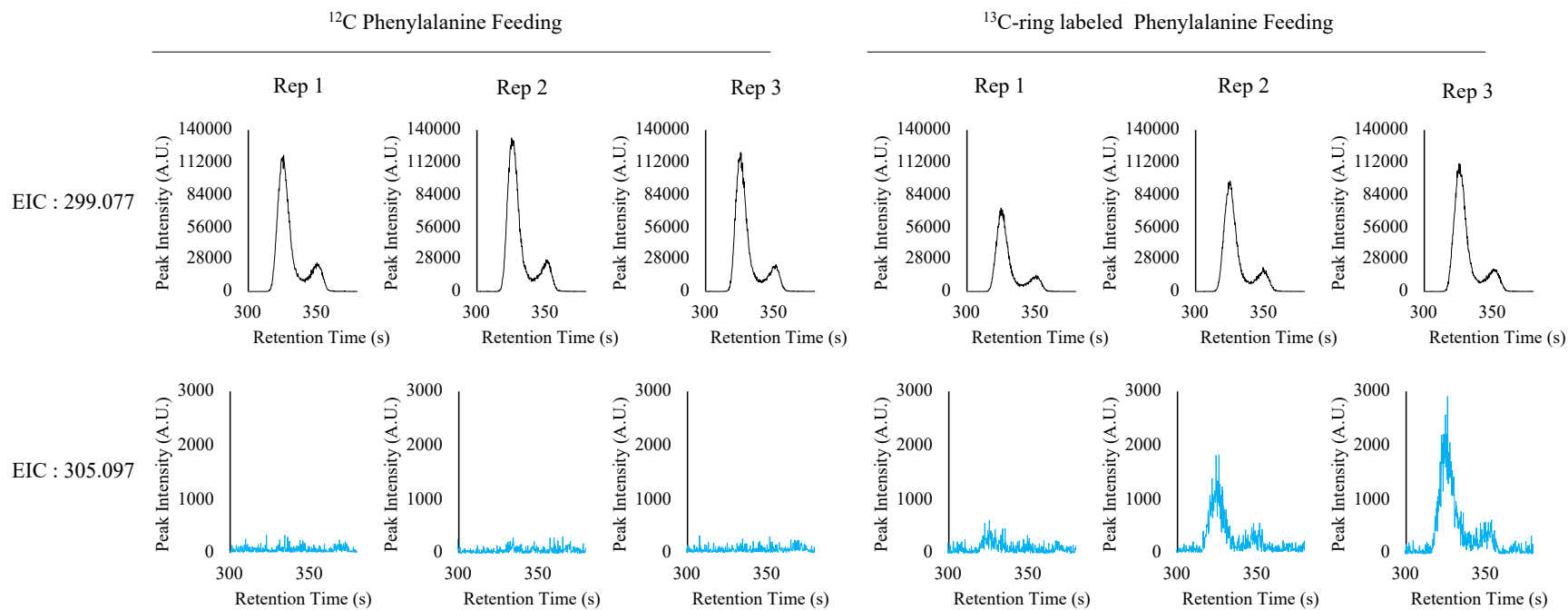
**Figure 4.11: Salicylic acid glucoside can be synthesized from phenylalanine in maize.**

Extracted ion chromatograms for (top) SA-glucoside ($m/z$[-H] = 299.077) and (bottom) $^{13}$C-ring labeled SA-glucoside ($m/z$[-H] = 305.097) for *Rp1-D21-ref* mutants fed (left) non-labeled phenylalanine or (right) $^{13}$C-ring labeled phenylalanine.
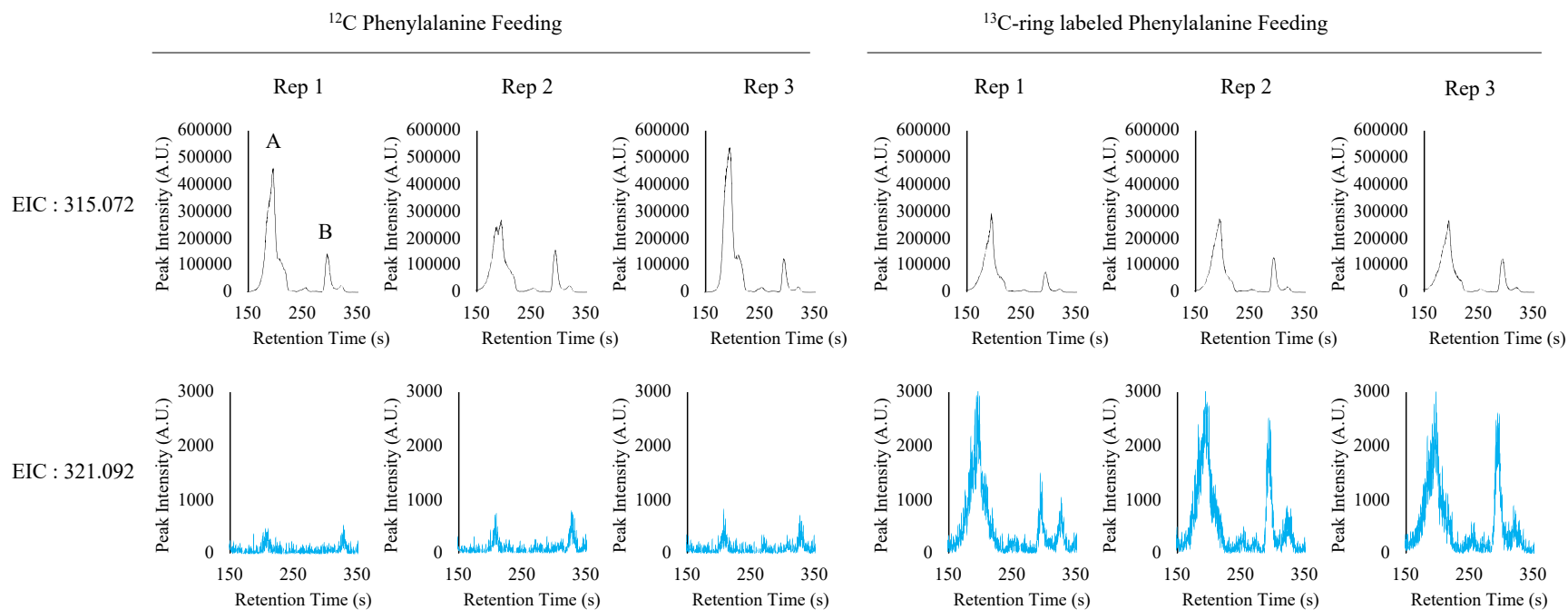
**Figure 4.12: 2,5-DHBA glucoside and 2,3-DHBA glucoside can be synthesized from phenylalanine in maize.**

Extracted ion chromatograms for (top) 2,5-DHBA glucoside (A) and 2,3-DHBA glucoside (B) ($m/z$[-H] = 315.072) and (bottom) $^{13}$C-ring labeled 2,5-DHBA glucoside and 2,3-DHBA glucoside ($m/z$[-H] = 321.092) for *Rp1-D21/+* mutants fed (left) non-labeled phenylalanine or (right) $^{13}$C-ring labeled phenylalanine.
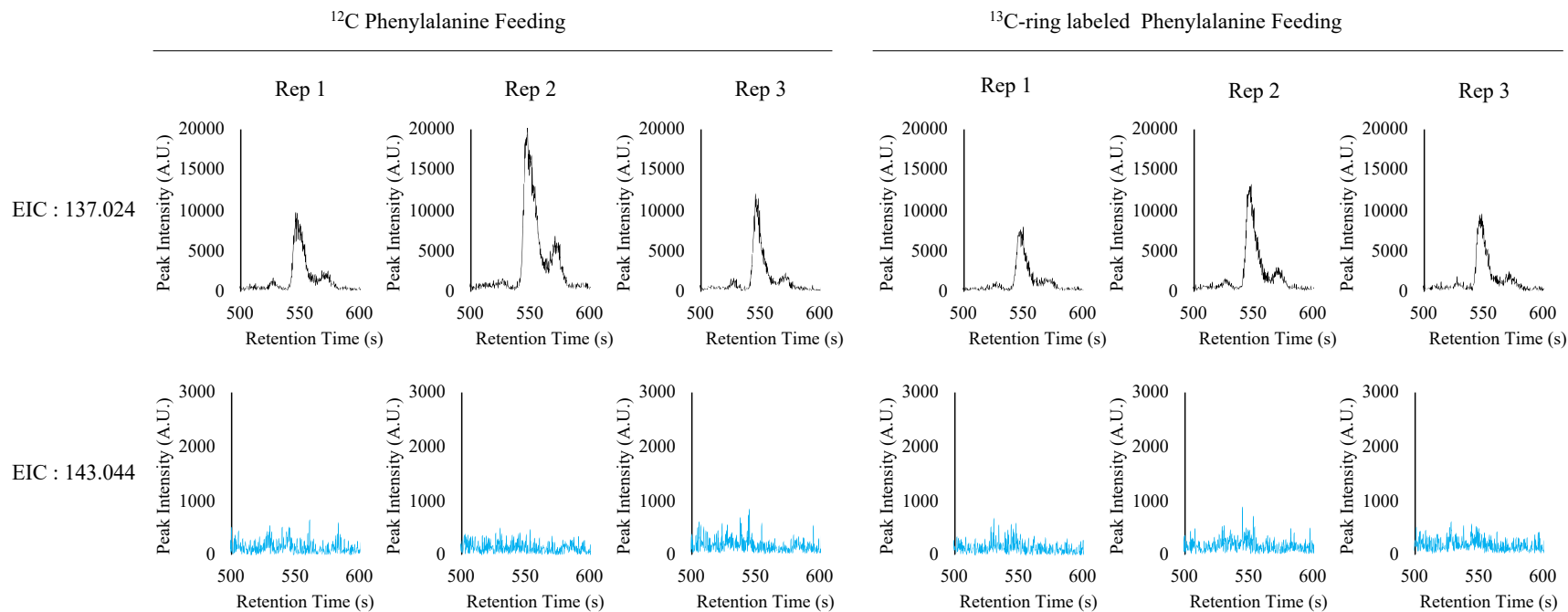
**Figure 4.13: Ring-labeled parent ion of SA was not detected after feeding with 13C-ring labeled phenylalanine.**

Extracted ion chromatograms for (top) SA ($m/z$[-H] = 137.024) and (bottom) $^{13}$C-ring labeled SA ($m/z$[-H] = 143.044) for *Rp1-D21/+* mutants fed (left) non-labeled phenylalanine or (right) $^{13}$C-ring labeled phenylalanine.
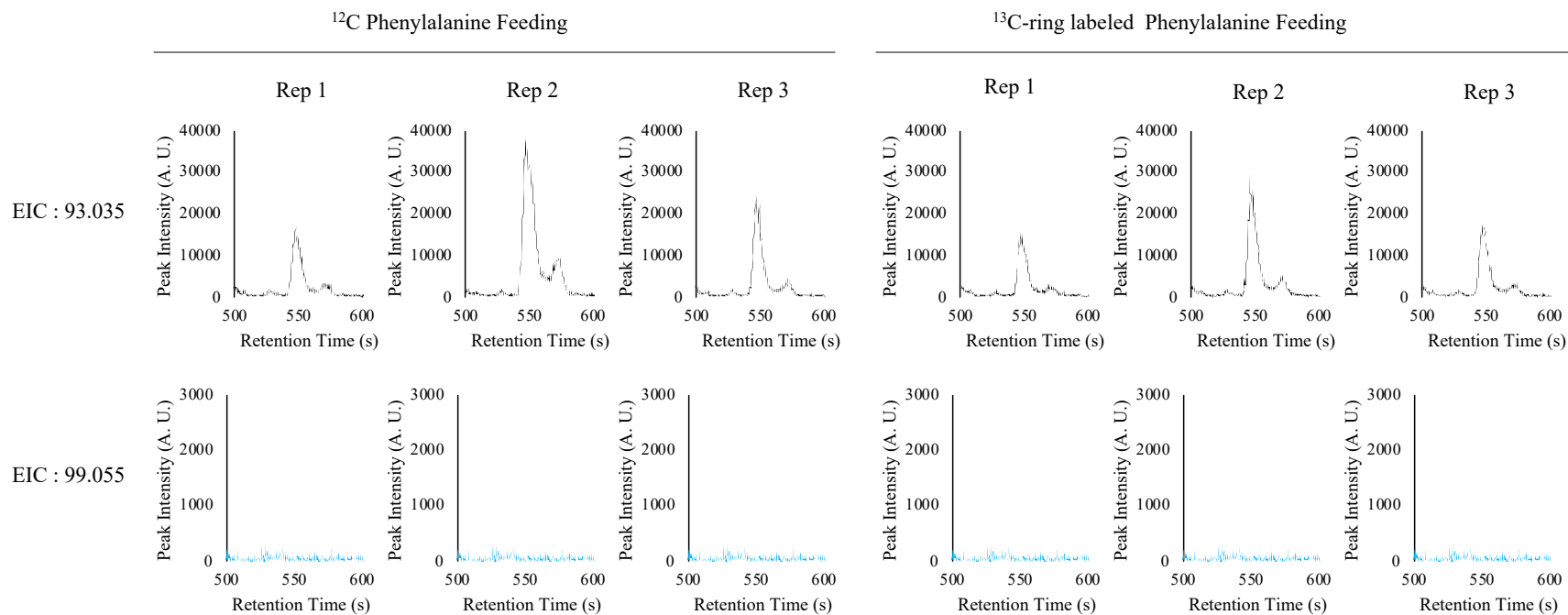
**Figure 4.14: Ring-labeled decarboxylated fragment of SA was not detected after feeding with 13C-ring labeled phenylalanine.**

Extracted ion chromatograms for (top) the decarboxylation fragment of SA ($m/z$[-COOH] = 93.035) and (bottom) ^{13}C-ring labeled decarboxylation fragment of SA ($m/z$[-COOH] = 99.055) for *Rp1-D21/+* mutants fed (left) non-labeled phenylalanine or (right) ^{13}C-ring labeled phenylalanine.
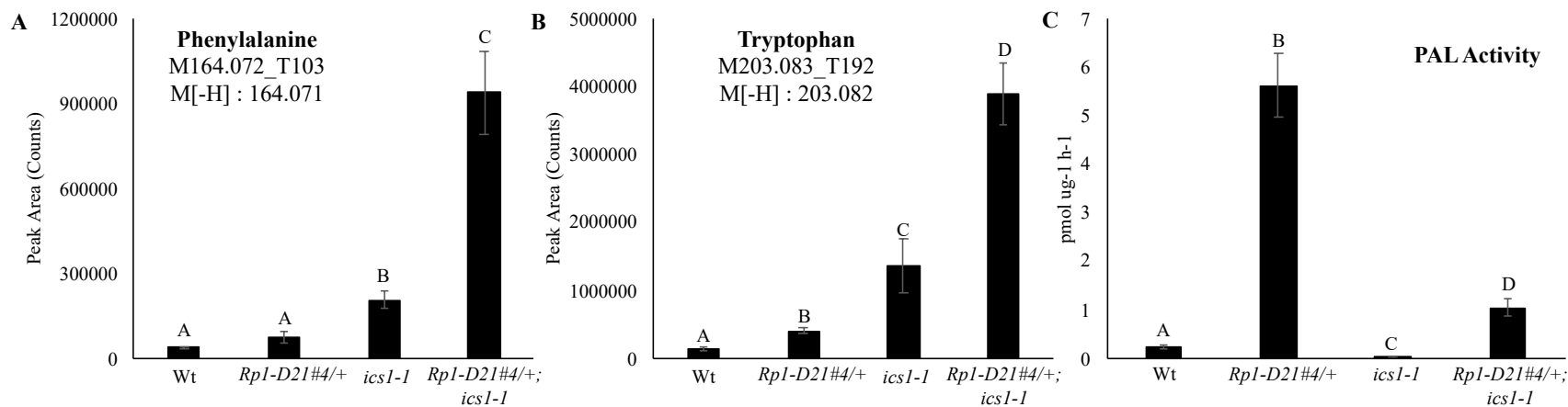
**Figure 4.15: *ics1-1* mutants have decreased PAL activity coinciding with increased accumulation of phenylalanine and tryptophan.**

Integrated peak areas of (A) phenylalanine and (B) tryptophan, and (C) PAL activity in Wt, *Rp1-D21#4/+, ics1-1,* and *Rp1-D21#4/+; ics1-1* samples. Metabolites were analyzed in negative ionization mode and the integrated values are of the major parent ion. Data presented are the mean values ± S.E. (n ≥ 3). Letters above bars represent statistically different measurements (paired sample Student's T-tests, $p < 0.05$).

**Table 4.2: Disruption of *ics1* suppresses phenylalanine-derived metabolism.**

| *Rp1-D21#4* coefficient | *ics1-1* coefficient | Interaction coefficient | Rp1-D21#4 > ics1-1 | All[a] | *Rp1-D21#4*[b] | *ics1-1*[c] | *Rp1-D21#4*[b] *ics1-1*[c] | *Rp1-D21#4* [b] Interaction[d] | *ics1-1*[c] Interaction[d] | *Rp1-D21#4*[b] *ics1-1*[c] Interaction[d] |
|---|---|---|---|---|---|---|---|---|---|---|
| + | + | + | Yes | 0 | 0 | 0 | 0 | 0 | 0 | 0 |
|  |  |  | No | 8 | 0 | 3 | 0 | 0 | 1 | 0 |
| + | + | - | Yes | 5 | 4 | 1 | 1 | 3 | 1 | 1 |
|  |  |  | No | 5 | 0 | 2 | 0 | 0 | 0 | 0 |
| + | - | + | Yes | 2 | 1 | 0 | 0 | 0 | 0 | 0 |
| + | - | - | Yes | 64 | 41 | 18 | 7 | 34 | 7 | 7 |
| - | + | + | No | 7 | 1 | 3 | 0 | 1 | 1 | 0 |
| - | + | - | No | 3 | 1 | 1 | 1 | 0 | 0 | 0 |
| - | - | + | Yes | 15 | 1 | 5 | 1 | 0 | 0 | 0 |
|  |  |  | No | 7 | 5 | 4 | 4 | 1 | 1 | 1 |
| - | - | - | Yes | 4 | 0 | 1 | 0 | 0 | 0 | 0 |
|  |  |  | No | 1 | 0 | 0 | 0 | 0 | 0 | 0 |

[a]All 121 phenylalanine derived features, [b]Phenylalanine derived features whose accumulation was significantly affected by *Rp1-D21#4* ($p < 0.05$), [c]Phenylalanine derived features whose accumulation was significantly affected by *ics1-1* ($p < 0.05$), [d]Phenylalanine derived features whose accumulation was significantly affected by the interaction of *Rp1-D21#4* and *ics1-1* ($p < 0.05$). Columns with multiple headings represent features who meet all criteria as described above

**Table 4.3: *Rp1-D21#4*-responsive metabolism is suppressed in *Rp1-D21#4; ics1-1* double mutants.**

| *Rp1-D21#4* coefficient | *ics1-1* coefficient | Interaction coefficient | Rp1-D21#4 > ics1-1 | All[a] | FDR[b] | FDR[b] *Rp1-D21#4*[c] | FDR[b] *ics1-1*[d] | FDR[b] *Rp1-D21#4*[c] *ics1-1*[d] | FDR[b] *Rp1-D21#4*[c] Interaction[e] | FDR[b] *ics1-1*[d] Interaction[e] | FDR[b] *Rp1-D21#4*[c] *ics1-1*[d] Interaction[e] |
|---|---|---|---|---|---|---|---|---|---|---|---|
| + | + | + | Yes | 108 | 30 | 4 | 1 | 1 | 0 | 0 | 0 |
| | | | No | 672 | 506 | 3 | 275 | 2 | 0 | 47 | 0 |
| + | + | - | Yes | 520 | 183 | 177 | 10 | 10 | 136 | 9 | 9 |
| | | | No | 776 | 337 | 21 | 333 | 21 | 10 | 89 | 10 |
| + | - | + | Yes | 210 | 39 | 4 | 24 | 0 | 1 | 0 | 0 |
| + | - | - | Yes | 1417 | 966 | 638 | 318 | 115 | 455 | 82 | 79 |
| - | + | + | No | 846 | 528 | 54 | 206 | 10 | 13 | 38 | 0 |
| - | + | - | No | 580 | 267 | 22 | 236 | 6 | 0 | 48 | 0 |
| - | - | + | Yes | 986 | 566 | 300 | 553 | 300 | 153 | 160 | 153 |
| | | | No | 675 | 313 | 300 | 162 | 162 | 102 | 81 | 81 |
| - | - | - | Yes | 183 | 112 | 2 | 76 | 2 | 0 | 3 | 0 |
| | | | No | 92 | 34 | 16 | 0 | 0 | 0 | 0 | 0 |

[a]All 7,094 features, [b]Features with an FDR-adjusted model p value $< 0.05$, [c]Features whose accumulation was significantly affected by *Rp1-D21#4* ($p < 0.05$), [d]Features whose accumulation was significantly affected by *ics1-1* ($p < 0.05$), [e]Features whose accumulation was significantly affected by the interaction of *Rp1-D21#4* and *ics1-1* ($p < 0.05$). Columns with multiple headings represent features who meet all criteria as described above
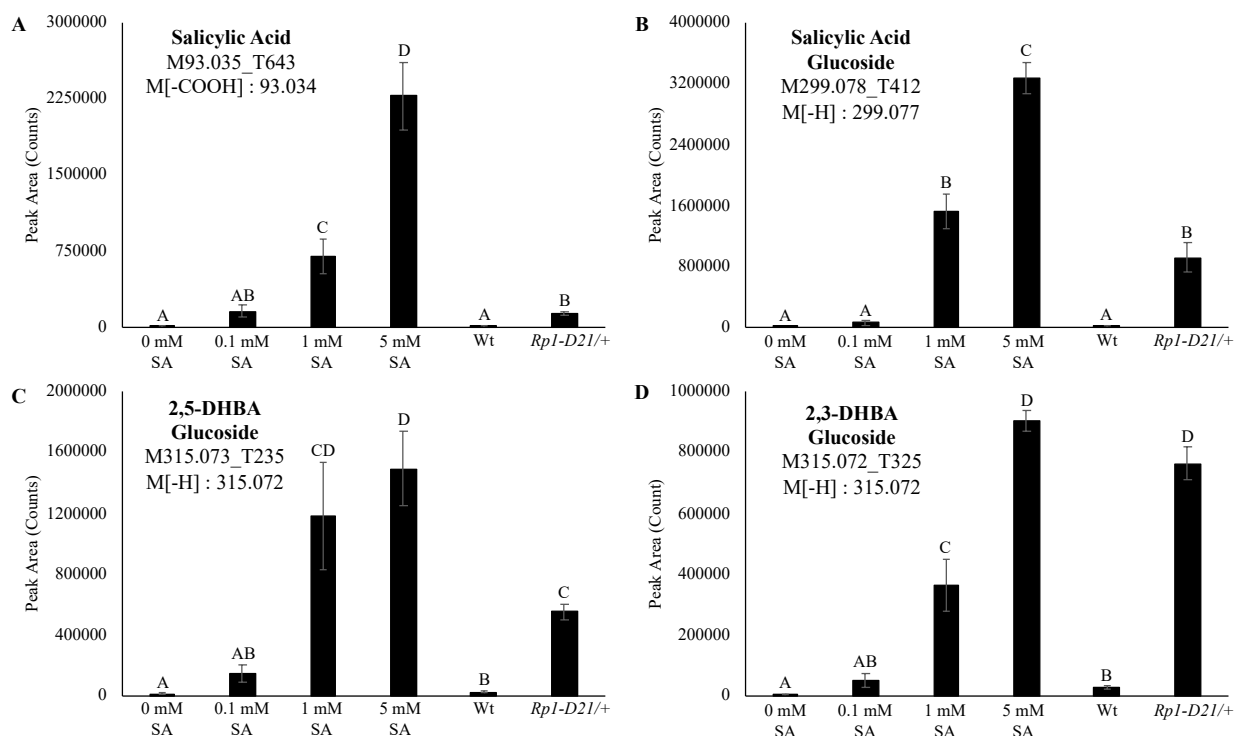
**Figure 4.16: Foliar application of SA to maize leaves results in increased accumulation of SA and SA-derived compounds.**

Integrated peak areas of (A) salicylic acid, (B) salicylic acid glucoside, (C) 2,5-DHBA glucoside, and (D) 2,3-DHBA glucoside from same aged leaves of untreated *Rp1-D21/+* and its wildtype sibling and B73 wildtype plants treated with 0 mM, 0.1 mM, 1 mM, and 5 mM SA every 24 hours four three days. Metabolites were analyzed in negative ionization mode. For salicylic acid, the integrated values are of the major decarboxylation fragment M[-COOH]. For salicylic acid glucoside, 2,5-DHBA glucoside, and 2,3-DHBA glucoside the values are integrations of the parent ion. Data presented are the mean values $\pm$ S.E. (n = 3). Letters above bars represent statistically different measurements (paired sample Student's T-test $p < 0.05$).
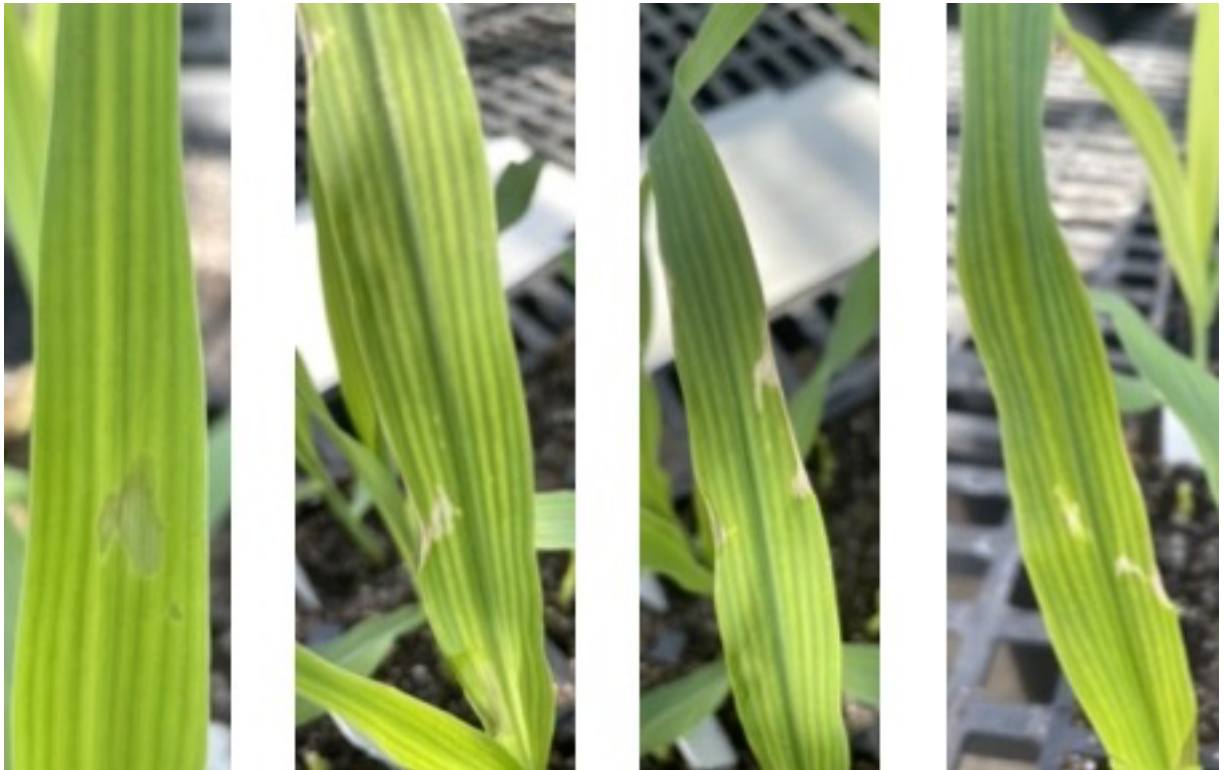
**Figure 4.17: Foliar application of high concentrations of SA causes chemical damage to leaves.**

Representative leaves of B73 plants after 3-days of spray-treatment with 5 mM SA. Chemical damage was only visible after the third day of application and was present on ~50% of treated plants. No chemical damage was visible on leaves of plants treated with mock solution, 0.1 mM SA, or 1 mM SA.
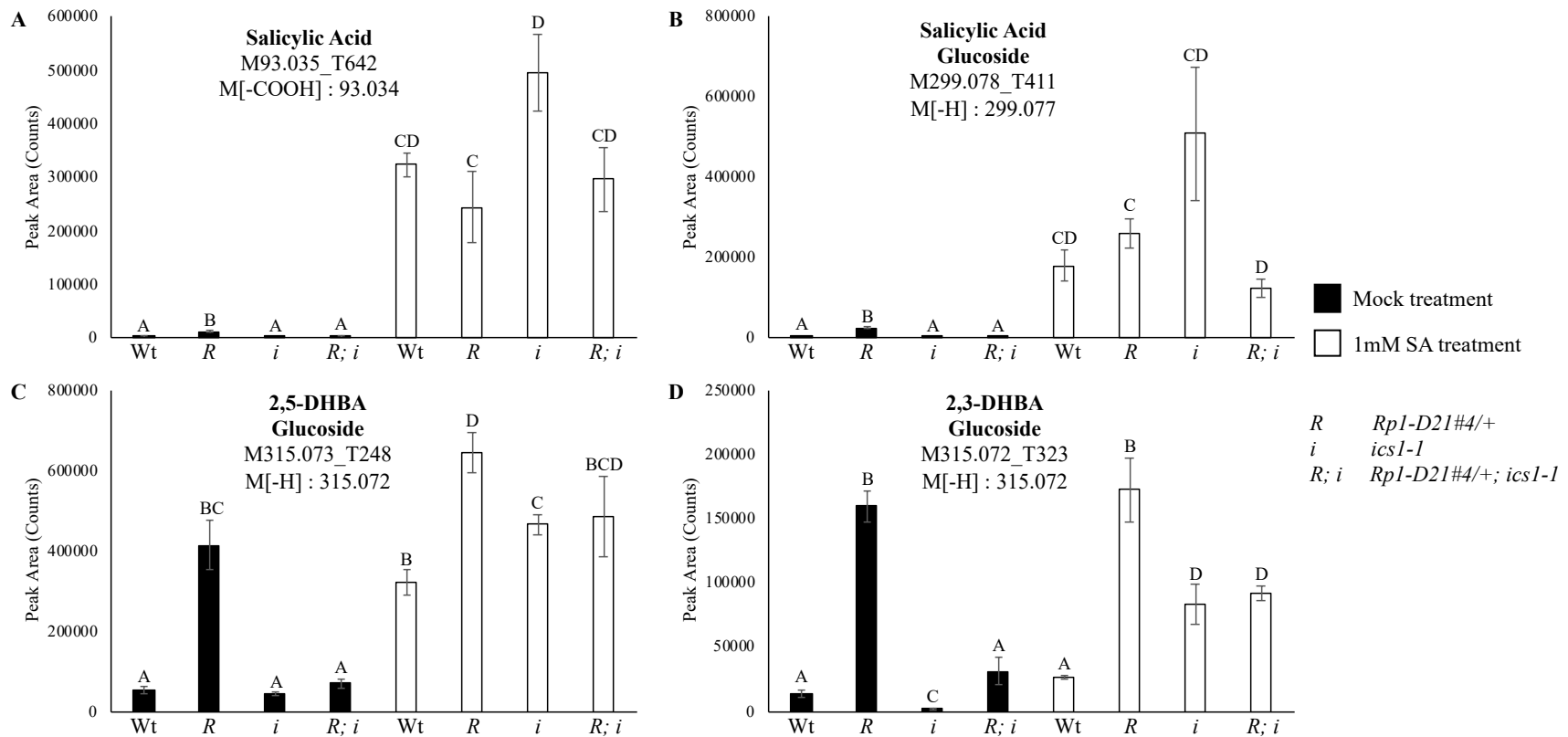
**Figure 4.18: Foliar application of SA to maize leaves results in increased accumulation of SA and SA-derived compounds.**

Integrated peak areas of (A) salicylic acid, (B) salicylic acid glucoside, (C) 2,5-DHBA glucoside, and (D) 2,3-DHBA glucoside for wt, *Rp1-D21#4/+*, *ics1-1* and *Rp1-D21#4/+; ics1-1* plants treated with 0 mM, 0.1 mM, 1 mM, and 5 mM SA every 24 hours four three days. Metabolites were analyzed in negative ionization mode. For salicylic acid, the integrated values are of the major decarboxylation fragment M[-COOH]. For salicylic acid glucoside, 2,5-DHBA glucoside, and 2,3-DHBA glucoside the values are integrations of the parent ion. Data presented are the mean values $\pm$ S.E. (n = 3). Letters above bars represent statistically different measurements (paired sample Student's T-test $p < 0.05$).

**Table 4.4: Reproducible finding that *Rp1-D21#4* responsive metabolism is suppressed in *Rp1-D21#4; ics1*-1 double mutants.**

| *Rp1-D21#4* coefficient | *ics1-1* coefficient | Interaction coefficient | Rp1-D21#4 > ics1-1 | All[a] | FDR[b] | FDR[b] *Rp1-D21#4*[c] | FDR[b] *ics1-1*[d] | FDR[b] *Rp1-D21#4*[c] *ics1-1*[d] | FDR[b] *Rp1-D21#4*[c] Interaction[e] | FDR[b] *ics1-1*[d] Interaction[e] | FDR[b] *Rp1-D21#4*[c] *ics1-1*[d] Interaction[e] |
|---|---|---|---|---|---|---|---|---|---|---|---|
| + | + | + | Yes | 77 | 10 | 5 | 1 | 1 | 0 | 0 | 0 |
| | | | No | 352 | 211 | 3 | 181 | 3 | 0 | 6 | 0 |
| + | + | - | Yes | 579 | 305 | 303 | 32 | 32 | 227 | 23 | 23 |
| | | | No | 673 | 358 | 51 | 358 | 51 | 26 | 57 | 26 |
| + | - | + | Yes | 219 | 61 | 4 | 57 | 1 | 0 | 0 | 0 |
| + | - | - | Yes | 1375 | 1094 | 873 | 414 | 240 | 648 | 166 | 166 |
| - | + | + | No | 838 | 477 | 99 | 317 | 39 | 25 | 25 | 6 |
| - | + | - | No | 481 | 287 | 4 | 282 | 3 | 0 | 16 | 0 |
| - | - | + | Yes | 1335 | 855 | 433 | 853 | 433 | 250 | 257 | 250 |
| | | | No | 604 | 189 | 184 | 111 | 111 | 134 | 86 | 86 |
| - | - | - | Yes | 99 | 35 | 0 | 30 | 0 | 0 | 0 | 0 |
| | | | No | 42 | 2 | 0 | 0 | 0 | 0 | 0 | 0 |

[a]All 6,676 features, [b]Features with an FDR-adjusted model p value $< 0.05$, [c]Features whose accumulation was significantly affected by *Rp1-D21#4* ($p < 0.05$), [d]Features whose accumulation was significantly affected by *ics1-1* ($p < 0.05$), [e]Features whose accumulation was significantly affected by the interaction of *Rp1-D21#4* and *ics1-1* ($p < 0.05$). Columns with multiple headings represent features who meet all criteria as described above

**Table 4.5: Most of the *Rp1-D21#4*-induced metabolites that are suppressed in *Rp1-D21#4; ics1-1* double mutants do not respond to SA treatment.**

| *Rp1-D21#4 coefficient* | *ics1-1 coefficient* | *Interaction coefficient* | Rp1-D21#4 > ics1-1 | All[a] | FDR[b] | FDR[b] Rp1-D21#4[c] | FDR[b] Rp1-D21#4[c] Interaction[d] | FDR[b] Rp1-D21#4[c] Interaction[d] Respond Up to SA[e] | FDR[b] Rp1-D21#4[c] Interaction[d] Respond down to SA[f] |
|---|---|---|---|---|---|---|---|---|---|
| + | + | + | Yes | 77 | 10 | 5 | 0 | 0 | 0 |
| | | | No | 352 | 211 | 3 | 0 | 0 | 0 |
| + | + | - | Yes | 579 | 305 | 303 | 227 | 12 | 4 |
| | | | No | 673 | 358 | 51 | 26 | 1 | 2 |
| + | - | + | Yes | 219 | 61 | 4 | 0 | 0 | 0 |
| + | - | - | Yes | 1375 | 1094 | 873 | 648 | 29 | 4 |
| - | + | + | No | 838 | 477 | 99 | 25 | 0 | 0 |
| - | + | - | No | 481 | 287 | 4 | 0 | 0 | 0 |
| - | - | + | Yes | 1335 | 855 | 433 | 250 | 2 | 5 |
| | | | No | 604 | 189 | 184 | 134 | 1 | 2 |
| - | - | - | Yes | 99 | 35 | 0 | 0 | 0 | 0 |
| | | | No | 42 | 2 | 0 | 0 | 0 | 0 |

[a]All 6,676 features, [b]Features with an FDR-adjusted model p value $< 0.05$, [c]Features whose accumulation was significantly affected by *Rp1-D21#4* ($p < 0.05$), [d]Features whose accumulation was significantly affected by the interaction of *Rp1-D21#4* and *ics1-1* ($p < 0.05$), [e]Feaatures whose accumulation was significantly higher in *Rp1-D21#4; ics1-1* treated with 1mM SA as compared to untreated *Rp1-D21#4; ics1-1* samples ($p < 0.05$), [f]Feaatures whose accumulation was significantly lower in *Rp1-D21#4; ics1-1* treated with 1mM SA as compared to untreated *Rp1-D21#4; ics1-1* samples ($p < 0.05$). Columns with multiple headings represent features who meet all criteria as described above
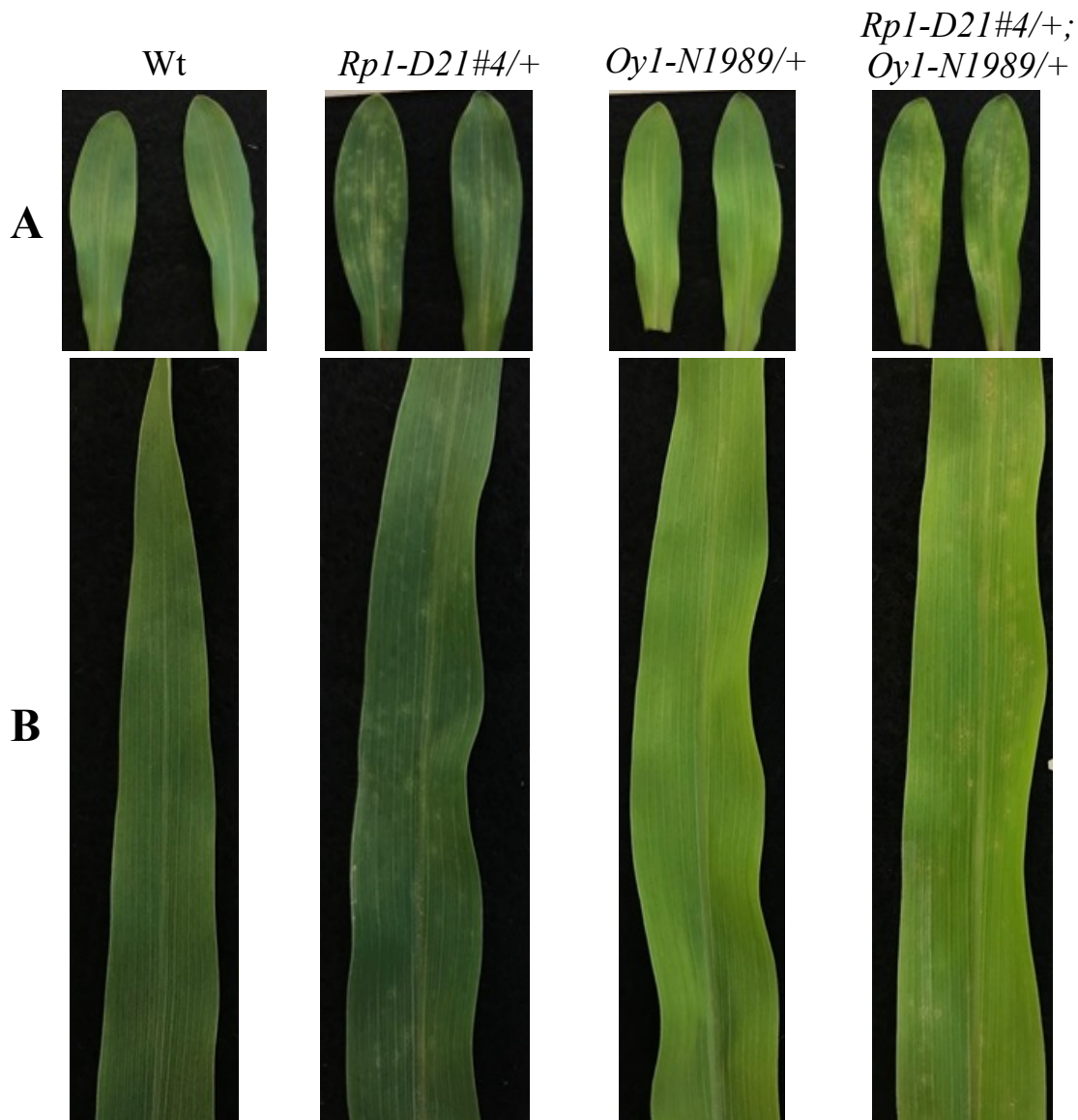
**Figure 4.19: *Rp1-D21#4/+; Oy1N-1989/+* double mutants have a similar lesion severity as *Rp1-D21#4/+* mutants.**

Representative A) first and B) second leaves from Wt, *Rp1-D21#4/+* mutants, *Oy1-N1989/+* mutants, and *Rp1-D21#4/+; Oy1-N1989/+* double mutants grown under greenhouse conditions 14-days after sowing.
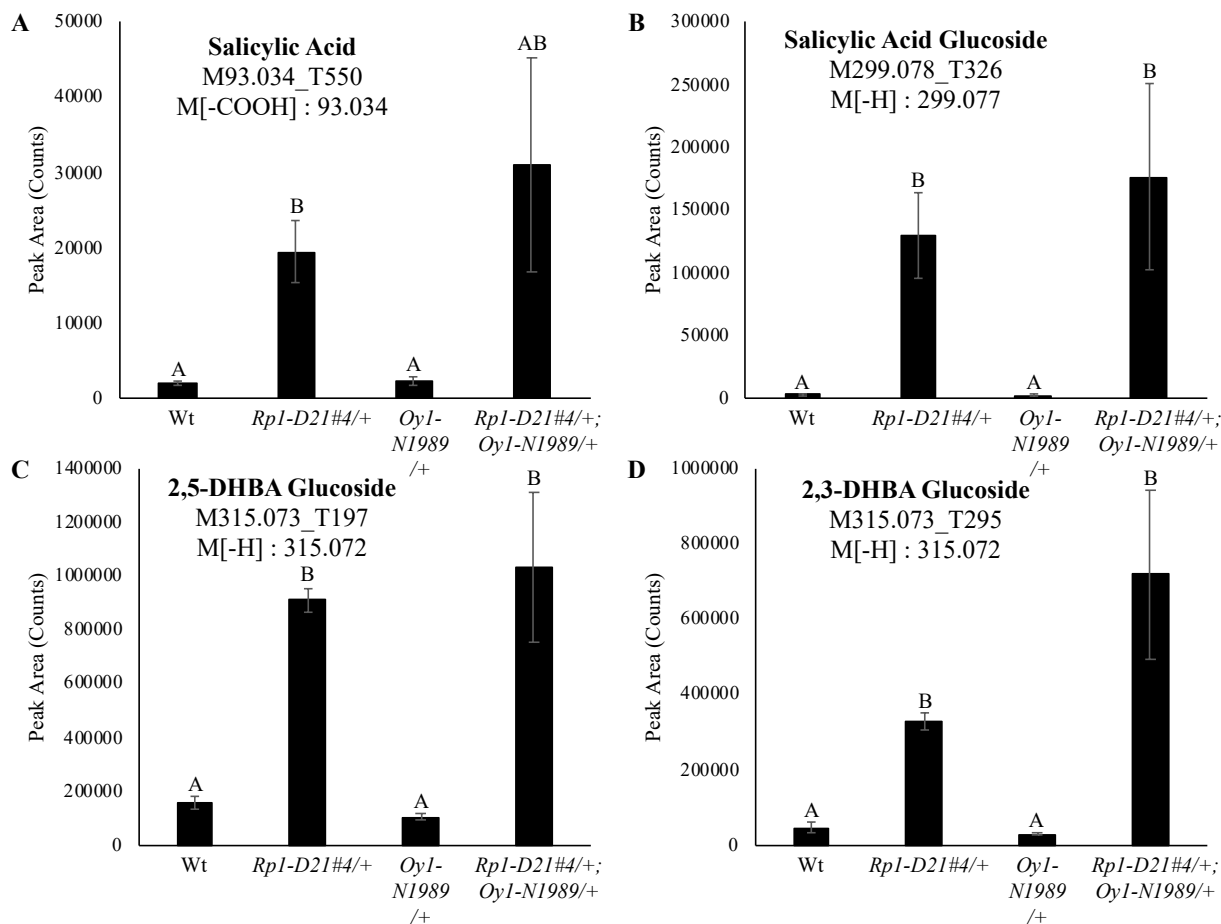
**Figure 4.20: Disruption of photosynthesis does not suppress *Rp1-D21#4*-induced accumulation of SA or SA-derived compounds.**

Integrated peak areas of (A) salicylic acid, (B) salicylic acid glucoside, (C) 2,5-DHBA glucoside, and (D) 2,3-DHBA glucoside from leaves of Wt, *Rp1-D21#4/+, Oy1-N1989/+,* and *Rp1-D21#4/+; Oy1-N1989/+*. Metabolites were analyzed in negative ionization mode. For salicylic acid, the integrated values are of the major decarboxylation fragment M[-COOH]. For salicylic acid glucoside, 2,5-DHBA glucoside, and 2,3-DHBA glucoside the values are integrations of the parent ion. Data presented are the mean values $\pm$ S.E. (n = 4). Letters above bars represent statistically different measurements (paired sample Student's T-test $p < 0.05$).

# CHAPTER 5.  CONCLUSIONS AND FUTURE DIRECTIONS

## 5.1  Conclusion

In this dissertation, I have presented three projects centered around the genetic and molecular characterization of the plant hypersensitive response. The first project (Chapter 2) showed that untargeted metabolomics could be used as a high throughput means to identify lesion mimic mutants that have HR-like metabolic syndromes and identified a subset of mutants that are likely mutated in genes involved in the HR or defense response. The second project (Chapter 3) presented phenotypic characterizations of *Les10,* which is one of the mutants with an HR-like metabolic syndrome. In Chapter 3, I have demonstrated that *Les10* is a dominant mutant and proposed a gene candidate that may modify *Les10* phenotypic severity. Chapter 4 demonstrated that SA is neither necessary nor sufficient for the HR in maize and that the ICS-dependent and PAL-dependent SA biosynthetic pathways are interdependent.

## 5.2  Remaining questions and future directions

In Chapter 2, I have identified four mutants with similar metabolic syndromes as the known HR-mutant *Rp1-D21*; however, it still remains unknown what the genetic causes of those mutants are. The only mutant that has been characterized is *Bf1*, which is encoded by a yet-to-be characterized glutamate receptor (Khangura et al., unpublished). As depicted in Chapter 3, I have begun characterization of *Les10*. The whole genome sequencing results of *Les10/Les10* homozygous mutants and the *Les10/+* wild-type revertant sectors will be combined with genetic fine-mapping to identify a list of gene candidates encoding *Les10*. Depending on the size of this list, transient expression of allele candidates in tobacco and monitoring for the lesion phenotype can be used to test and validate the causative gene. The experiments described for *Les10* in Chapter 3 and in this discussion could be utilized to characterize the other unknown LMMs.

*Bf1* is mutated in a glutamate receptor which is known to be involved in defense response; therefore, so far, none of the mutants that cluster with *Rp1-D21* have violated the hypothesis that they are all involved in the HR or defense response. Determining the cause of *Les10*, *Les17* and *Les23-like* will each act as an individual test of this hypothesis. Furthermore, determining the cause of any of the mutants that do not cluster with *Rp1-D21* will also test this hypothesis. If there are

any LMMs mutated in genes involved in defense response that do not cluster with *Rp1-D21*, this would indicate the clustering analysis, as performed, is not robust enough to identify all the defense response-like mutants.

In Chapter 4, I have shown that the ICS-dependent and PAL-dependent SA biosynthetic pathways in maize are interdependent (Figure 4.15C). There is genetic evidence that this interdependency is also present in Arabidopsis (Huang et al., 2010) and soybean (Shine et al., 2016). The *ics1*; *ics2* double mutants have been developed in Arabidopsis (Garcion et al., 2008) and an *ics* mutant exists in barley (Qin et al., 2019); therefore, a test of the interdependency between these two pathways can be completed in these systems using the aforementioned mutants and the methodology described here.

It still remains enigmatic why *Rp1-D21#4*-induced metabolism is suppressed in *Rp1-D21#4; ics1-1* double mutants (Table 4.2). I have shown that this suppression is independent of SA levels (Table 4.5), and I was unable to replicate this suppression by using a mutant with decreased photosynthetic capacity (Figure 4.20) indicating energy limitation is likely also not a contributing factor. It is possible that additional deficiencies of *ics1-1* mutants, such as decreased accumulation of phylloquinone (Figure 4.6) or lower levels of PSI (Figure 4.8), which are two parameters that are unknown for *Oy1-N1989/+* mutants may be responsible for this suppression. Generating *Rp1-D21#4/+* mutants that are also deficient in phylloquinone biosynthesis by targeting another enzyme in the pathway downstream from ICS and performing a similar untargeted metabolomics experiment as described here would answer if the suppression is caused by loss of phylloquinone or a subsequent affect from having reduced levels of phylloquinone.

There is a lack of characterization of SA biosynthesis outside of angiosperms. As such, the hypothesis of Gross et al. that the origin of an *ICS* gene allowed for isochorismate-derived synthesis of SA remains largely untested. Can all Viridiplantae produce SA? If so, is that SA synthesized from phenylalanine, isochorismate, or both? In addition, are there alternative SA biosynthetic pathways in plants that have yet-to-be discovered? Answering these questions will rely on multiple scientific efforts screening for SA accumulation and using genetic manipulation and enzymatic assays to test for SA biosynthesis pathways across multiple plant systems.

# REFERENCES

**Akira, S.** (2009). Pathogen recognition by innate immunity and its signaling. Proc. Jpn. Acad. Ser. B **85**: 143–156.

**Balint-Kurti, P.** (2019). The plant hypersensitive response: concepts, control and consequences. Mol. Plant Pathol. **20**: 1163–1178.

**Baxter, I.** (2020). We aren't good at picking candidate genes, and it's slowing us down. Curr. Opin. Plant Biol. **54**: 57–60.

**Benjamini, Y. and Hochberg, Y.** (1995). Controlling the False Discovery Rate: A Practical and Powerful Approach to Multiple Testing. J. R. Stat. Soc. Ser. B Methodol. **57**: 289–300.

**Bent, A.** (1996). Plant Disease Resistance Genes: Function Meets Structure. Plant Cell **8**: 1757–1771.

**Berghold, J., Müller, T., Ulrich, M., Hörtensteiner, S., and Kräutler, B.** (2006). Chlorophyll Breakdown in Maize: On the Structure of Two Nonfluorescent Chlorophyll Catabolites. Monatshefte Für Chem. - Chem. Mon. **137**: 751–763.

**Bisgrove, S.R., Simonich, M.T., Smith, N.M., Sattler, A., and Innes, R.W.** (1994). A disease resistance gene in Arabidopsis with specificity for two different pathogen avirulence genes. Plant Cell **6**: 927–933.

**Block, A., Fristedt, R., Rogers, S., Kumar, J., Barnes, B., Barnes, J., Elowsky, C.G., Wamboldt, Y., Mackenzie, S.A., Redding, K., Merchant, S.S., and Basset, G.J.** (2013). Functional modeling identifies paralogous solanesyl-diphosphate synthases that assemble the side chain of plastoquinone-9 in plastids. J. Biol. Chem. **288**: 27594–27606.

**Block, A., Widhalm, J.R., Fatihi, A., Cahoon, R.E., Wamboldt, Y., Elowsky, C., Mackenzie, S.A., Cahoon, E.B., Chapple, C., Dudareva, N., and Basset, G.J.** (2014). The Origin and Biosynthesis of the Benzenoid Moiety of Ubiquinone (Coenzyme Q) in *Arabidopsis*. Plant Cell **26**: 1938–1948.

**Bradford, M.M.** (1976). A rapid and sensitive method for the quantitation of microgram quantities of protein utilizing the principle of protein-dye binding. Anal. Biochem. **72**: 248–254.

**Brodersen, P., Malinovsky, F.G., Hématy, K., Newman, M.-A., and Mundy, J.** (2005). The Role of Salicylic Acid in the Induction of Cell Death in Arabidopsis *acd11*. Plant Physiol. **138**: 1037–1045.

**Bruggeman, Q., Raynaud, C., Benhamed, M., and Delarue, M.** (2015). To die or not to die? Lessons from lesion mimic mutants. Front. Plant Sci. **6**.

**Bukowski, R. et al.** (2018). Construction of the third-generation Zea mays haplotype map. GigaScience **7**.

**Chandra-Shekara, A.C., Gupte, M., Navarre, D., Raina, S., Raina, R., Klessig, D., and Kachroo, P.** (2006). Light-dependent hypersensitive response and resistance signaling against Turnip Crinkle Virus in Arabidopsis. Plant J. Cell Mol. Biol. **45**: 320–334.

**Chintamanani, S., Hulbert, S.H., Johal, G.S., and Balint-Kurti, P.J.** (2010). Identification of a Maize Locus That Modulates the Hypersensitive Defense Response, Using Mutant-Assisted Gene Identification and Characterization. Genetics **184**: 813–825.

**Coquoz, J.-L., Buchala, A., and Métraux, J.-P.** (1998). The Biosynthesis of Salicylic Acid in Potato Plants. Plant Physiol. **117**: 1095–1101.

**Danecek, P., Auton, A., Abecasis, G., Albers, C.A., Banks, E., DePristo, M.A., Handsaker, R.E., Lunter, G., Marth, G.T., Sherry, S.T., McVean, G., and Durbin, R.** (2011). The variant call format and VCFtools.: 3.

**Dangl, J.L. and Jones, J.D.G.** (2001). Plant pathogens and integrated defence responses to infection. Nature **411**: 826–833.

**Danilevskaya, O.N., Yu, G., Meng, X., Xu, J., Stephenson, E., Estrada, S., Chilakamarri, S., Zastrow-Hayes, G., and Thatcher, S.** (2019). Developmental and transcriptional responses of maize to drought stress under field conditions. Plant Direct **3**: e00129.

**David Hoisington** (1987). Les10, a new lesion mutant located near v4 on chromosome 2L. Maize Newsl. **61**: 48–49.

**DebRoy, S., Thilmony, R., Kwack, Y.-B., Nomura, K., and He, S.Y.** (2004). A family of conserved bacterial effectors inhibits salicylic acid-mediated basal immunity and promotes disease necrosis in plants. Proc. Natl. Acad. Sci. **101**: 9927–9932.

**Delaney, T.P., Uknes, S., Vernooij, B., Friedrich, L., Weymann, K., Negrotto, D., Gaffney, T., Gut-Rella, M., Kessmann, H., Ward, E., and Ryals, J.** (1994). A central role of salicylic Acid in plant disease resistance. Science **266**: 1247–1250.

**Delledonne, M., Zeier, J., Marocco, A., and Lamb, C.** (2001). Signal interactions between nitric oxide and reactive oxygen intermediates in the plant hypersensitive disease resistance response. Proc. Natl. Acad. Sci. **98**: 13454–13459.

**Dietrich, R.A., Delaney, T.P., Uknes, S.J., Ward, E.R., Ryals, J.A., and Dangl, J.L.** (1994). Arabidopsis mutants simulating disease resistance response. Cell **77**: 565–577.

**Ding, Y., Sun, T., Ao, K., Peng, Y., Zhang, Y., Li, X., and Zhang, Y.** (2018). Opposite Roles of Salicylic Acid Receptors NPR1 and NPR3/NPR4 in Transcriptional Regulation of Plant Immunity. Cell **173**: 1454-1467.e15.

**Ellis, J., Dodds, P., and Pryor, T.** (2000). Structure, function and evolution of plant disease resistance genes. Curr. Opin. Plant Biol. **3**: 278–284.

**Elvin Stakman** (1915). Relation Between Puccinia Graminis and Plants highly resistant to its attack. J. Agric. Res. **IV**: 193–200.

**Emanuelsson, O., Nielsen, H., and von Heijne, G.** (1999). ChloroP, a neural network-based method for predicting chloroplast transit peptides and their cleavage sites. Protein Sci. Publ. Protein Soc. **8**: 978–984.

**Emonds-Alt, B., Coosemans, N., Gerards, T., Remacle, C., and Cardol, P.** (2017). Isolation and characterization of mutants corresponding to the MENA, MENB, MENC and MENE enzymatic steps of 5′-monohydroxyphylloquinone biosynthesis in Chlamydomonas reinhardtii. Plant J. **89**: 141–154.

**Enyedi, A.J., Yalpani, N., Silverman, P., and Raskin, I.** (1992). Localization, conjugation, and function of salicylic acid in tobacco during the hypersensitive reaction to tobacco mosaic virus. Proc. Natl. Acad. Sci. **89**: 2480–2484.

**Flint-Garcia, S.A., Thuillet, A.-C., Yu, J., Pressoir, G., Romero, S.M., Mitchell, S.E., Doebley, J., Kresovich, S., Goodman, M.M., and Buckler, E.S.** (2005). Maize association population: a high-resolution platform for quantitative trait locus dissection: High-resolution maize association population. Plant J. **44**: 1054–1064.

**Flor, H.H.** (1971). Current Status of the Gene-For-Gene Concept. Annu. Rev. Phytopathol. **9**: 275–296.

**G. H. Elder and A. G. Robers** (1995). Uroporphyrinogen decarboxylase. J. Bioenerg. Biomembr. **27**: 8.

**Gaffney, T., Friedrich, L., Vernooij, B., Negrotto, D., Nye, G., Uknes, S., Ward, E., Kessmann, H., and Ryals, J.** (1993). Requirement of Salicylic Acid for the Induction of Systemic Acquired Resistance. Science **261**: 754–756.

**Gallavotti, A., Malcomber, S., Gaines, C., Stanfield, S., Whipple, C., Kellogg, E., and Schmidt, R.J.** (2011). BARREN STALK FASTIGIATE1 Is an AT-Hook Protein Required for the Formation of Maize Ears. Plant Cell **23**: 1756–1771.

**Garcion, C., Lohmann, A., Lamodière, E., Catinot, J., Buchala, A., Doermann, P., and Métraux, J.-P.** (2008). Characterization and Biological Function of the ISOCHORISMATE SYNTHASE2 Gene of Arabidopsis. Plant Physiol. **147**: 1279–1287.

**Ge, C., Wang, Y.-G., Lu, S., Zhao, X.Y., Hou, B.-K., Balint-Kurti, P.J., and Wang, G.-F.** (2021). Multi-Omics Analyses Reveal the Regulatory Network and the Function of ZmUGTs in Maize Defense Response. Front. Plant Sci. **12**: 738261.

**Gerald Neuffer** (1994). Dominant lesion mutants on chromosome 2 and designation of les18 and les19. Maize Newsl. **68**: 29.

**Gertz, E.M., Yu, Y.-K., Agarwala, R., Schäffer, A.A., and Altschul, S.F.** (2006). Composition-based statistics and translated nucleotide searches: Improving the TBLASTN module of BLAST. BMC Biol. **4**: 41.

**Gibson, C.M.** (1904). Notes on Infection Experiments with Various Uredineae. New Phytol. **3**: 184–191.

**Goodstein, D.M., Shu, S., Howson, R., Neupane, R., Hayes, R.D., Fazo, J., Mitros, T., Dirks, W., Hellsten, U., Putnam, N., and Rokhsar, D.S.** (2012). Phytozome: a comparative platform for green plant genomics. Nucleic Acids Res. **40**: D1178–D1186.

**Govrin, E.M., Rachmilevitch, S., Tiwari, B.S., Solomon, M., and Levine, A.** (2006). An Elicitor from Botrytis cinerea Induces the Hypersensitive Response in Arabidopsis thaliana and Other Plants and Promotes the Gray Mold Disease. Phytopathology® **96**: 299–307.

**Gray, J., Close, P.S., Briggs, S.P., and Johal, G.S.** (1997). A Novel Suppressor of Cell Death in Plants Encoded by the Lls1 Gene of Maize. Cell **89**: 25–31.

**Greenberg, J.T. and Ausubel, F.M.** (1993). Arabidopsis mutants compromised for the control of cellular damage during pathogenesis and aging. Plant J. Cell Mol. Biol. **4**: 327–341.

**Greenberg, J.T., Silverman, F.P., and Liang, H.** (2000). Uncoupling salicylic acid-dependent cell death and defense-related responses from disease resistance in the Arabidopsis mutant acd5. Genetics **156**: 341–350.

**Greene, E.A., Codomo, C.A., Taylor, N.E., Henikoff, J.G., Till, B.J., Reynolds, S.H., Enns, L.C., Burtner, C., Johnson, J.E., Odden, A.R., Comai, L., and Henikoff, S.** (2003). Spectrum of chemically induced mutations from a large-scale reverse-genetic screen in Arabidopsis. Genetics **164**: 731–740.

**Gross, J., Cho, W.K., Lezhneva, L., Falk, J., Krupinska, K., Shinozaki, K., Seki, M., Herrmann, R.G., and Meurer, J.** (2006). A Plant Locus Essential for Phylloquinone (Vitamin K $_1$) Biosynthesis Originated from a Fusion of Four Eubacterial Genes. J. Biol. Chem. **281**: 17189–17196.

**Hashimoto, Y. and Shudo, K.** (1996). Chemistry of biologically active benzoxazinoids. Phytochemistry **43**: 551–559.

**Hostetler, A.N., Khangura, R.S., Dilkes, B.P., and Sparks, E.E.** (2021). Bracing for sustainable agriculture: the development and function of brace roots in members of Poaceae. Curr. Opin. Plant Biol. **59**: 101985.

**Hu, G., Richter, T.E., Hulbert, S.H., and Pryor, T.** (1996). Disease Lesion Mimicry Caused by Mutations in the Rust Resistance Gene rp1. Plant Cell **8**: 1367–1376.

**Hu, G., Yalpani, N., Briggs, S.P., and Johal, G.S.** (1998). A Porphyrin Pathway Impairment Is Responsible for the Phenotype of a Dominant Disease Lesion Mimic Mutant of Maize. Plant Cell **10**: 1095–1105.

**Huang, J., Gu, M., Lai, Z., Fan, B., Shi, K., Zhou, Y.-H., Yu, J.-Q., and Chen, Z.** (2010). Functional Analysis of the Arabidopsis PAL Gene Family in Plant Growth, Development, and Response to Environmental Stress. Plant Physiol. **153**: 1526–1538.

**Huang, M., Slewinski, T.L., Baker, R.F., Janick-Buckner, D., Buckner, B., Johal, G.S., and Braun, D.M.** (2009). Camouflage Patterning in Maize Leaves Results from a Defect in Porphobilinogen Deaminase. Mol. Plant **2**: 773–789.

**Huang, X., Zhu, G., Liu, Q., Chen, L., Li, Y., and Hou, B.** (2018). Modulation of Plant Salicylic Acid-Associated Immune Responses via Glycosylation of Dihydroxybenzoic Acids. Plant Physiol. **176**: 3103–3119.

**Jiao, Y. et al.** (2017). Improved maize reference genome with single-molecule technologies. Nature **546**: 524–527.

**Johal, G.S. and Briggs, S.P.** (1992). Reductase activity encoded by the HM1 disease resistance gene in maize. Science **258**: 985–987.

**Johal, G.S., Hulbert, S.H., and Briggs, S.P.** (1995). Disease lesion mimics of maize: A model for cell death in plants. BioEssays **17**: 685–692.

**Johnson, T.W., Shen, G., Zybailov, B., Kolling, D., Reategui, R., Beauparlant, S., Vassiliev, I.R., Bryant, D.A., Jones, A.D., Golbeck, J.H., and Chitnis, P.R.** (2000). Recruitment of a Foreign Quinone into the A1 Site of Photosystem I. J. Biol. Chem. **275**: 8523–8530.

**Jubic, L.M., Saile, S., Furzer, O.J., El Kasmi, F., and Dangl, J.L.** (2019). Help wanted: helper NLRs and plant immune responses. Curr. Opin. Plant Biol. **50**: 82–94.

**Karre, S., Kim, S.-B., Kim, B.-S., Khangura, R.S., Sermons, S.M., Dilkes, B., Johal, G., and Balint-Kurti, P.** (2021). Maize Plants Chimeric for an Autoactive Resistance Gene Display a Cell-Autonomous Hypersensitive Response but Non–Cell Autonomous Defense Signaling. Mol. Plant-Microbe Interactions®: MPMI-04-20-0091.

**Karrer, E.E., Beachy, R.N., and Holt, C.A.** (1998). Cloning of tobacco genes that elicit the hypersensitive response.: 10.

**Keller, H., Pamboukdjian, N., Ponchet, M., Poupet, A., Delon, R., Verrier, J.-L., Roby, D., and Ricci, P.** (1999). Pathogen-Induced Elicitin Production in Transgenic Tobacco Generates a Hypersensitive Response and Nonspecific Disease Resistance. Plant Cell **11**: 223–235.

**Khangura, R.S., Marla, S., Venkata, B.P., Heller, N.J., Johal, G.S., and Dilkes, B.P.** (2019). A Very Oil Yellow1 Modifier of the Oil Yellow1-N1989 Allele Uncovers a Cryptic Phenotypic Impact of Cis-regulatory Variation in Maize. G3 GenesGenomesGenetics **9**: 375–390.

**Khangura, R.S., Venkata, B.P., Marla, S.R., Mickelbart, M.V., Dhungana, S., Braun, D.M., Dilkes, B.P., and Johal, G.S.** (2020). Interaction Between Induced and Natural Variation

at oil yellow1 Delays Reproductive Maturity in Maize. G3 GenesGenomesGenetics **10**: 797–810.

**Kim, S.-B., Karre, S., Wu, Q., Park, M., Meyers, E., Claeys, H., Wisser, R., Jackson, D., and Balint-Kurti, P.** (2020). Multiple insertions of COIN, a novel maize Foldback transposable element, in the Conring gene cause a spontaneous progressive cell death phenotype. Plant J. **104**: 581–595.

**Klämbt, H.D.** (1962). Conversion in Plants of Benzoic Acid to Salicylic Acid and its βd-Glucoside. Nature **196**: 491.

**Klempien, A. et al.** (2012). Contribution of CoA Ligases to Benzenoid Biosynthesis in Petunia Flowers. Plant Cell **24**: 2015–2030.

**Kolappan, S., Zwahlen, J., Zhou, R., Truglio, J.J., Tonge, P.J., and Kisker, C.** (2007). Lysine 190 Is the Catalytic Base in MenF, the Menaquinone-Specific Isochorismate Synthase from *Escherichia coli* : Implications for an Enzyme Family [†]. Biochemistry **46**: 946–953.

**Kourelis, J. and van der Hoorn, R.A.L.** (2018). Defended to the Nines: 25 Years of Resistance Gene Cloning Identifies Nine Mechanisms for R Protein Function. Plant Cell **30**: 285–299.

**Kremling, K.A.G., Chen, S.-Y., Su, M.-H., Lepak, N.K., Romay, M.C., Swarts, K.L., Lu, F., Lorant, A., Bradbury, P.J., and Buckler, E.S.** (2018). Dysregulation of expression correlates with rare-allele burden and fitness loss in maize. Nature **555**: 520–523.

**Kulich, I., Pečenková, T., Sekereš, J., Smetana, O., Fendrych, M., Foissner, I., Höftberger, M., and Zárský, V.** (2013). Arabidopsis exocyst subcomplex containing subunit EXO70B1 is involved in autophagy-related transport to the vacuole. Traffic Cph. Den. **14**: 1155–1165.

**Lacombe, S., Rougon-Cardoso, A., Sherwood, E., Peeters, N., Dahlbeck, D., van Esse, H.P., Smoker, M., Rallapalli, G., Thomma, B.P.H.J., Staskawicz, B., Jones, J.D.G., and Zipfel, C.** (2010). Interfamily transfer of a plant pattern-recognition receptor confers broad-spectrum bacterial resistance. Nat. Biotechnol. **28**: 365–369.

**Lawton, K., Weymann, K., Friedrich, L., Vernooij, B., Uknes, S., and Ryals, J.** (1995). Systemic Acquired Resistance in Arabidopsis Salicylic Acid but not Ethylene. Mol. Plant. Microbe Interact. **8**: 863–870.

**Lefebvre-Legendre, L., Rappaport, F., Finazzi, G., Ceol, M., Grivet, C., Hopfgartner, G., and Rochaix, J.-D.** (2007). Loss of Phylloquinone in Chlamydomonas Affects Plastoquinone Pool Size and Photosystem II Synthesis *. J. Biol. Chem. **282**: 13250–13263.

**Li, X., Svedin, E., Mo, H., Atwell, S., Dilkes, B.P., and Chapple, C.** (2014). Exploiting Natural Variation of Secondary Metabolism Identifies a Gene Controlling the Glycosylation Diversity of Dihydroxybenzoic Acids in Arabidopsis thaliana. Genetics **198**: 1267–1276.

**Lo Presti, L., Lanver, D., Schweizer, G., Tanaka, S., Liang, L., Tollot, M., Zuccaro, A., Reissmann, S., and Kahmann, R.** (2015). Fungal effectors and plant susceptibility. Annu. Rev. Plant Biol. **66**: 513–545.

**Lu, H., Rate, D.N., Song, J.T., and Greenberg, J.T.** (2003). ACD6, a Novel Ankyrin Protein, Is a Regulator and an Effector of Salicylic Acid Signaling in the Arabidopsis Defense Response. Plant Cell **15**: 2408–2420.

**Mach, J.M., Castillo, A.R., Hoogstraten, R., and Greenberg, J.T.** (2001). The Arabidopsis-accelerated cell death gene ACD2 encodes red chlorophyll catabolite reductase and suppresses the spread of disease symptoms. Proc. Natl. Acad. Sci. U. S. A. **98**: 771–776.

**Malamy, J., Carr, J.P., Klessig, D.F., and Raskin, I.** (1990). Salicylic Acid: a likely endogenous signal in the resistance response of tobacco to viral infection. Science **250**: 1002–1004.

**Mateo, A., Mühlenbock, P., Rustérucci, C., Chang, C.C.-C., Miszalski, Z., Karpinska, B., Parker, J.E., Mullineaux, P.M., and Karpinski, S.** (2004). LESION SIMULATING DISEASE 1 is required for acclimation to conditions that promote excess excitation energy. Plant Physiol. **136**: 2818–2830.

**McCarty, D.R., Latshaw, S., Wu, S., Suzuki, M., Hunter, C.T., Avigne, W.T., and Koch, K.E.** (2013). Mu-seq: Sequence-Based Mapping and Identification of Transposon Induced Mutations. PLoS ONE **8**: e77172.

**McCoy, R.M., Utturkar, S.M., Crook, J.W., Thimmapuram, J., and Widhalm, J.R.** (2018). The origin and biosynthesis of the naphthalenoid moiety of juglone in black walnut. Hortic. Res. **5**: 67.

**McKenzie, S.D., Ibrahim, I.M., Aryal, U.K., and Puthiyaveetil, S.** (2020). Stoichiometry of protein complexes in plant photosynthetic membranes. Biochim. Biophys. Acta BBA - Bioenerg. **1861**: 148141.

**Menden, B., Kohlhoff, M., and Moerschbacher, B.M.** (2007). Wheat cells accumulate a syringyl-rich lignin during the hypersensitive resistance response. Phytochemistry **68**: 513–520.

**Mestre, P. and Baulcombe, D.C.** (2006). Elicitor-Mediated Oligomerization of the Tobacco N Disease Resistance Protein. Plant Cell **18**: 491–501.

**Mohr, T.J., Mammarella, N.D., Hoff, T., Woffenden, B.J., Jelesko, J.G., and McDowell, J.M.** (2010). The Arabidopsis downy mildew resistance gene RPP8 is induced by pathogens and salicylic acid and is regulated by W box cis elements. Mol. Plant-Microbe Interact. MPMI **23**: 1303–1315.

**Morris, S.W., Vernooij, B., Titatarn, S., Starrett, M., Thomas, S., Wiltse, C.C., Frederiksen, R.A., Bhandhufalck, A., Hulbert, S., and Uknes, S.** (1998). Induced Resistance Responses in Maize. Mol. Plant-Microbe Interactions® **11**: 643–658.

**Morrison, T.A. and Buxton, D.R.** (1993). Activity of Phenylalanine Ammonia-Lyase, Tyrosine Ammonia-Lyase, and Cinnamyl Alcohol Dehydrogenase in the Maize Stalk. Crop Sci. **33**: cropsci1993.0011183X003300060030x.

**Mu, X., Li, J., Dai, Z., Xu, L., Fan, T., Jing, T., Chen, M., and Gou, M.** (2021). Commonly and Specifically Activated Defense Responses in Maize Disease Lesion Mimic Mutants Revealed by Integrated Transcriptomics and Metabolomics Analysis. Front. Plant Sci. **12**.

**Murtagh, Fionn** (2014). Ward's Hierarchical Agglomerative Clustering Method: Which Algorithms Implement Ward's Criterion? J. Classif. **31**: 274–295.

**Negeri, A., Wang, G.-F., Benavente, L., Kibiti, C.M., Chaikam, V., Johal, G., and Balint-Kurti, P.** (2013). Characterization of temperature and light effects on the defense response phenotypes associated with the maize Rp1-D21autoactive resistance gene. BMC Plant Biol. **13**: 106.

**Neuffer, M.G. and Calvert, O.H.** (1975). Dominant Disease Lesion Mimics in Maize. J. Hered. **66**: 265–270.

**Ogawa, D., Nakajima, N., Seo, S., Mitsuhara, I., Kamada, H., and Ohashi, Y.** (2006). The phenylalanine pathway is the main route of salicylic acid biosynthesis in Tobacco mosaic virus-infected tobacco leaves. Plant Biotechnol. **23**: 395–398.

**Olukolu, B.A. et al.** (2014). A Genome-Wide Association Study of the Maize Hypersensitive Defense Response Identifies Genes That Cluster in Related Pathways. PLoS Genet. **10**: e1004562.

**Orcheski, B., Parker, R., and Brown, S.** (2015). Pale green lethal disorder in apple (Malus) is caused by a mutation in the PHYLLO gene which is essential for phylloquinone (vitamin K1) biosynthesis. Tree Genet. Genomes **11**: 131.

**Pallas, J.A., Paiva, N.L., Lamb, C., and Dixon, R.A.** (1996). Tobacco plants epigenetically suppressed in phenylalanine ammonia-lyase expression do not develop systemic acquired resistance in response to infection by tobacco mosaic virus. Plant J. **10**: 281–293.

**Papadopoulos, J.S. and Agarwala, R.** (2007). COBALT: constraint-based alignment tool for multiple protein sequences. Bioinformatics **23**: 1073–1079.

**Park, S.-W., Kaimoyo, E., Kumar, D., Mosher, S., and Klessig, D.F.** (2007). Methyl Salicylate Is a Critical Mobile Signal for Plant Systemic Acquired Resistance. Science **318**: 113–116.

**Qin, Y., Torp, A.M., Glauser, G., Pedersen, C., Rasmussen, S.K., and Thordal-Christensen, H.** (2019). Barley isochorismate synthase mutant is phylloquinone-deficient, but has normal basal salicylic acid level. Plant Signal. Behav. **14**.

**Radojičić, A., Li, X., and Zhang, Y.** (2018). Salicylic Acid: A Double-Edged Sword for Programed Cell Death in Plants. Front. Plant Sci. **9**.

**Rate, D.N., Cuenca, J.V., Bowman, G.R., Guttman, D.S., and Greenberg, J.T.** (1999). The Gain-of-Function Arabidopsis acd6 Mutant Reveals Novel Regulation and Function of the Salicylic Acid Signaling Pathway in Controlling Cell Death, Defenses, and Cell Growth. Plant Cell **11**: 1695–1708.

**Rekhter, D., Lüdke, D., Ding, Y., Feussner, K., Zienkiewicz, K., Lipka, V., Wiermer, M., Zhang, Y., and Feussner, I.** (2019). Isochorismate-derived biosynthesis of the plant stress hormone salicylic acid. Science **365**: 498–502.

**Rollins Adams Emerson** (1923). The inheritance of blotched leaf in maize. Cornell Univ. Mem. **70**: 3–16.

**Romay, M.C. et al.** (2013). Comprehensive genotyping of the USA national maize inbred seed bank. Genome Biol. **14**: R55.

**Rossi, M., Goggin, F.L., Milligan, S.B., Kaloshian, I., Ullman, D.E., and Williamson, V.M.** (1998). The nematode resistance gene Mi of tomato confers resistance against the potato aphid. Proc. Natl. Acad. Sci. U. S. A. **95**: 9750–9754.

**Sakuragi, Y., Zybailov, B., Shen, G., Jones, A.D., Chitnis, P.R., van der Est, A., Bittl, R., Zech, S., Stehlik, D., Golbeck, J.H., and Bryant, D.A.** (2002). Insertional inactivation of the menG gene, encoding 2-phytyl-1,4-naphthoquinone methyltransferase of Synechocystis sp. PCC 6803, results in the incorporation of 2-phytyl-1,4-naphthoquinone into the A(1) site and alteration of the equilibrium constant between A(1) and F(X) in photosystem I. Biochemistry **41**: 394–405.

**Semenov, A.Yu., Vassiliev, I.R., van der Est, A., Mamedov, M.D., Zybailov, B., Shen, G., Stehlik, D., Diner, B.A., Chitnis, P.R., and Golbeck, J.H.** (2000). Recruitment of a Foreign Quinone into the A$_1$ Site of Photosystem I: ALTERED KINETICS OF ELECTRON TRANSFER IN PHYLLOQUINONE BIOSYNTHETIC PATHWAY MUTANTS STUDIED BY TIME-RESOLVED OPTICAL, EPR, AND ELECTROMETRIC TECHNIQUES. J. Biol. Chem. **275**: 23429–23438.

**Shine, M.B., Yang, J.-W., El-Habbak, M., Nagyabhyru, P., Fu, D.-Q., Navarre, D., Ghabrial, S., Kachroo, P., and Kachroo, A.** (2016). Cooperative functioning between phenylalanine ammonia lyase and isochorismate synthase activities contributes to salicylic acid biosynthesis in soybean. New Phytol. **212**: 627–636.

**Shinkarev, V.P., Zybailov, B., Vassiliev, I.R., and Golbeck, J.H.** (2002). Modeling of the P700+ Charge Recombination Kinetics with Phylloquinone and Plastoquinone-9 in the A1 Site of Photosystem I. Biophys. J. **83**: 2885–2897.

**Sievers, F., Wilm, A., Dineen, D., Gibson, T.J., Karplus, K., Li, W., Lopez, R., McWilliam, H., Remmert, M., Söding, J., Thompson, J.D., and Higgins, D.G.** (2011). Fast, scalable generation of high-quality protein multiple sequence alignments using Clustal Omega. Mol. Syst. Biol. **7**: 539.

**Simmons, C., Hantke, S., Grant, S., Johal, G.S., and Briggs, S.P.** (1998). The Maize Lethal Leaf Spot 1 Mutant Has Elevated Resistance to Fungal Infection at the Leaf Epidermis. Mol. Plant. Microbe Interact. **11**: 1110–1118.

**Simpson, J.P., Olson, J., Dilkes, B., and Chapple, C.** (2021a). Identification of the Tyrosine- and Phenylalanine-Derived Soluble Metabolomes of Sorghum. Front. Plant Sci. **12**: 1733.

**Simpson, J.P., Wunderlich, C., Li, X., Svedin, E., Dilkes, B., and Chapple, C.** (2021b). Metabolic source isotopic pair labeling and genome-wide association are complementary tools for the identification of metabolite–gene associations in plants. Plant Cell **33**: 492–510.

**Sindhu, A., Janick-Buckner, D., Buckner, B., Gray, J., Zehr, U., Dilkes, B.P., and Johal, G.S.** (2018). Propagation of cell death in dropdead1, a sorghum ortholog of the maize lls1 mutant. PLOS ONE **13**: e0201359.

**Smith, C.A., Want, E.J., O'Maille, G., Abagyan, R., and Siuzdak, G.** (2006). XCMS: Processing Mass Spectrometry Data for Metabolite Profiling Using Nonlinear Peak Alignment, Matching, and Identification. Anal. Chem. **78**: 779–787.

**Song, J.T., Koo, Y.J., Seo, H.S., Kim, M.C., Choi, Y.D., and Kim, J.H.** (2008). Overexpression of AtSGT1, an Arabidopsis salicylic acid glucosyltransferase, leads to increased susceptibility to Pseudomonas syringae. Phytochemistry **69**: 1128–1134.

**Strauch, R.C., Svedin, E., Dilkes, B., Chapple, C., and Li, X.** (2015). Discovery of a novel amino acid racemase through exploration of natural variation in *Arabidopsis thaliana*. Proc. Natl. Acad. Sci. **112**: 11726–11731.

**Takahashi, A., Kawasaki, T., Henmi, K., Shii, K., Kodama, O., Satoh, H., and Shimamoto, K.** (1999). Lesion mimic mutants of rice with alterations in early signaling events of defense. Plant J. **17**: 535–545.

**Tang, Y., Liu, X., Wang, J., Li, M., Wang, Q., Tian, F., Su, Z., Pan, Y., Liu, D., Lipka, A.E., Buckler, E.S., and Zhang, Z.** (2016). GAPIT Version 2: An Enhanced Integrated Tool for Genomic Association and Prediction. Plant Genome **9**: plantgenome2015.11.0120.

**The Arabidopsis Genome Initiative** (2000). Analysis of the genome sequence of the flowering plant Arabidopsis thaliana. Nature **408**: 796–815.

**Tipton, C.L., Ming-Chung, W., Tsao, F.H.-C., Chang-chu, L.T., and Husted, R.R.** (1973). Biosynthesis of 1,4-benzoxazin-3-ones in Zea mays. Phytochemistry **12**: 347–352.

**Todesco, M., Kim, S.-T., Chae, E., Bomblies, K., Zaidem, M., Smith, L.M., Weigel, D., and Laitinen, R.A.E.** (2014). Activation of the Arabidopsis thaliana Immune System by Combinations of Common ACD6 Alleles. PLOS Genet. **10**: e1004459.

**Torrens-Spence, M., Bobokalonova, Anastassia, Carballo, V., Glinkerman, C., Pluskal, T., Shen, A., and Weng, J.-K.** (2019). PBS3 and EPS1 Complete Salicylic Acid Biosynthesis from Isochorismate in Arabidopsis | Elsevier Enhanced Reader. Mol. Plant **12**: 1577–1586.

**Trifinopoulos, J., Nguyen, L.-T., von Haeseler, A., and Minh, B.Q.** (2016). W-IQ-TREE: a fast online phylogenetic tool for maximum likelihood analysis. Nucleic Acids Res. **44**: W232–W235.

**Undan, J.R. et al.** (2012). Mutation in OsLMS, a gene encoding a protein with two double-stranded RNA binding motifs, causes lesion mimic phenotype and early senescence in rice (Oryza sativa L.). Genes Genet. Syst. **87**: 169–179.

**Vlot, A.C., Dempsey, D.A., and Klessig, D.F.** (2009). Salicylic Acid, a Multifaceted Hormone to Combat Disease. Annu. Rev. Phytopathol. **47**: 177–206.

**Wang, G.-F. and Balint-Kurti, P.J.** (2015). Cytoplasmic and Nuclear Localizations Are Important for the Hypersensitive Response Conferred by Maize Autoactive Rp1-D21 Protein. Mol. Plant-Microbe Interactions® **28**: 1023–1031.

**Wang, G.-F. and Balint-Kurti, P.J.** (2016). Maize Homologs of CCoAOMT and HCT, Two Key Enzymes in Lignin Biosynthesis, Form Complexes with the NLR Rp1 Protein to Modulate the Defense Response. Plant Physiol. **171**: 2166–2177.

**Wang, G.-F., He, Y., Strauch, R., Olukolu, B., Nielsen, D., Li, X., and Balint-Kurti, P.** (2015a). Maize Homologs of HCT, a Key Enzyme in Lignin Biosynthesis, Bind the NLR Rp1 Proteins to Modulate the Defense Response. Plant Physiol.: pp.00703.2015.

**Wang, G.-F., Ji, J., EI-Kasmi, F., Dangl, J.L., Johal, G., and Balint-Kurti, P.J.** (2015b). Molecular and Functional Analyses of a Maize Autoactive NB-LRR Protein Identify Precise Structural Requirements for Activity. PLOS Pathog. **11**: e1004674.

**Wang, P., Guo, L., Jaini, R., Klempien, A., McCoy, R.M., Morgan, J.A., Dudareva, N., and Chapple, C.** (2018). A 13C isotope labeling method for the measurement of lignin metabolic flux in Arabidopsis stems. Plant Methods **14**: 51.

**Wang, Y., Bao, J., Wei, X., Wu, S., Fang, C., Li, Z., Qi, Y., Gao, Y., Dong, Z., and Wan, X.** (2022). Genetic Structure and Molecular Mechanisms Underlying the Formation of Tassel, Anther, and Pollen in the Male Inflorescence of Maize (Zea mays L.). Cells **11**: 1753.

**Ward, H.M.** (1902). On the Relations between Host and Parasite in the Bromes and their Brown Rust, Puccinia dispersa (Erikss.). Ann. Bot. **os-16**: 233–316.

**Weymann, K., Hunt, M., Uknes, S., Neuenschwander, U., Lawton, K., Steiner, H.-Y., and Ryals, J.** (1995). Suppression and Restoration of Lesion Formation in Arabidopsis Isd Mutants. **7**: 10.

**Widhalm, J.R. and Rhodes, D.** (2016). Biosynthesis and molecular actions of specialized 1,4-naphthoquinone natural products produced by horticultural plants. Hortic. Res. **3**: 16046.

**Wildermuth, M.C., Dewdney, J., Wu, G., and Ausubel, F.M.** (2001). Isochorismate synthase is required to synthesize salicylic acid for plant defence. Nature **414**: 562–565.

**Wu, C.-H., Abd-El-Haliem, A., Bozkurt, T.O., Belhaj, K., Terauchi, R., Vossen, J.H., and Kamoun, S.** (2017). NLR network mediates immunity to diverse plant pathogens. Proc. Natl. Acad. Sci. **114**: 8113–8118.

**Yalpani, N., LeÓn, J., and Lawton, M.A.** (1993). Pathway of Salicylic Acid Biosynthesis in Healthy and Virus-Inoculated Tobacco'. Plant Physiol. **103**: 7.

**Yuan, W., Jiang, T., Du, K., Chen, H., Cao, Y., Xie, J., Li, M., Carr, J.P., Wu, B., Fan, Z., and Zhou, T.** (2019). Maize phenylalanine ammonia-lyases contribute to resistance to Sugarcane mosaic virus infection, most likely through positive regulation of salicylic acid accumulation. Mol. Plant Pathol. **20**: 1365–1378.

**Yuan, Y., Chung, J.-D., Fu, X., Johnson, V.E., Ranjan, P., Booth, S.L., Harding, S.A., and Tsai, C.-J.** (2009). Alternative splicing and gene duplication differentially shaped the regulation of isochorismate synthase in Populus and Arabidopsis. Proc. Natl. Acad. Sci. **106**: 22020–22025.

**Zhang, K., Halitschke, R., Yin, C., Liu, C.-J., and Gan, S.-S.** (2013). Salicylic acid 3-hydroxylase regulates Arabidopsis leaf longevity by mediating salicylic acid catabolism. Proc. Natl. Acad. Sci. **110**: 14807–14812.

**Zhang, Y., Zhao, L., Zhao, J., Li, Y., Wang, J., Guo, R., Gan, S., Liu, C.-J., and Zhang, K.** (2017). S5H/DMR6 Encodes a Salicylic Acid 5-Hydroxylase That Fine-Tunes Salicylic Acid Homeostasis. Plant Physiol. **175**: 1082–1093.

**Zhang, Z., Guo, J., Zhao, Y., and Chen, J.** (2019). Identification and characterization of maize ACD6-like gene reveal ZmACD6 as the maize orthologue conferring resistance to Ustilago maydis. Plant Signal. Behav. **14**: e1651604.

**Zhou, S., Kremling, K.A., Bandillo, N., Richter, A., Zhang, Y.K., Ahern, K.R., Artyukhin, A.B., Hui, J.X., Younkin, G.C., Schroeder, F.C., Buckler, E.S., and Jander, G.** (2019). Metabolome-Scale Genome-Wide Association Studies Reveal Chemical Diversity and Genetic Control of Maize Specialized Metabolites. Plant Cell **31**: 937–955.

**Zipfel, C.** (2014). Plant pattern-recognition receptors. Trends Immunol. **35**: 345–351.